Towards a molecular understanding of centrosome integrity, function and organization in dendritic cells during T cell priming

Dissertation

zur

Erlangung des Doktorgrades (Dr. rer. nat.)

der

Mathematisch-Naturwissenschaftlichen Fakultät

der

Rheinischen Friedrich-Wilhelms-Universität Bonn

vorgelegt von

Isabel Katharina Stötzel

aus Neuss

Bonn, 2025

Angefertigt mit Genehmigung der Mathematisch-Naturwissenschaftlichen Fakultät der
Rheinischen Friedrich-Wilhelms-Universität Bonn

Gutachterin/Betreuerin: Prof. Dr. Eva Kiermaier

Gutachter: Prof. Dr. Sven Burgdorf

Tag der Promotion: 10.03.2026

Erscheinungsjahr: 2026

Table of Contents

Preliminary remarks

I hereby declare that I wrote this dissertation without sources other than indicated in the main text and without help from third parties. I have designed and conducted all the experiments described in this thesis, except for parts of the adoptive transfer experiments and mass spectrometry measurements. Assistance from other lab members or students under my supervision is indicated in the respective figure legends or methods sections.

Bonn,

_____

Isabel Stötzel

According to the common practice in English scientific writing, this thesis is written using the first-person plural narrator.

Parts of this dissertation have been published on a preprint server:

Isabel Stötzel, Ann-Kathrin Weier, Apurba Sarkar, Subhendu Som, Peter Konopka, Eliška Miková, Jan Böthling, Mirka Homrich, Laura Schaedel, Uli Kazmaier, Konstantinos Symeonidis, Zeinab Abdullah, Stefan Uderhardt, Miroslav Hons, Raja Paul, Heiko Rieger, Eva Kiermaier. Multiple clustered centrosomes in antigen-presenting cells foster T cell activation without MTOC polarization. bioRxiv 18.07.24 doi: 10.1101/2024.07.18.604057.

List of Abbreviations

°C	Degree Celsius
µ	Micro
2D	Two-dimensional
2N	Diploid
3D	Three-dimensional
4N	Tetraploid
ACK lysis	Ammonium-chloride-potassium lysis
ACN	Acetonitrile
ADP	Adenosine diphosphate
ANOVA	Analysis of variance
AP-1	Activator protein 1
APC	Antigen-presenting cell
APC/C	Anaphase-promoting complex or cyclosome
AU	Arbitrary unit
BM	Bone marrow
BMDCs	Bone marrow-derived dendritic cells
BSA	Bovine serum albumin
BTLA	B and T lymphocyte attenuator
Ca^{2+}	Calcium
CCR	C-C motif chemokine receptor
CD	Cluster of differentiation
Cdc42	Cell division control protein 42 homolog
CDK	Cyclin-dependent kinase
CDK5RAP2	CDK5 regulatory subunit-associated protein 2
CEP	Centrosomal protein
CETN2	Centrin 2
CFSE	Carboxyfluorescein succinimidyl ester
C-Nap1	Centrosomal Nek2-associated protein 1
CO_2	Carbon dioxide
CP	Center point
CPAP	Centrosomal P4.1-associated protein
cSMAC	central supramolecular activation cluster
ctrl	Control
CXCL	C-X-C motif chemokine ligand
DAG	Diacylglycerol
DAMP	Damage-associated molecular pattern
DAPI	4',6-diamidino-2-phenylindole
DC	Dendritic cell
$d_{CS\text{-}NS}$	Distance from centrosome to nuclear surface
DIC	Differential interference contrast
DMEM	Dulbecco's Modified Eagle Medium
DMSO	Dimethylsulfoxid
DNA	Deoxyribonucleic acid
d_{offset}	Offset of the nucleus from the cell center
Dox	Doxycycline
dSMAC	distal supramolecular activation cluster
Dyrk3	Dual-specificity tyrosine-(Y)-phosphorylation regulated kinase 3
E. coli	*Escherichia coli*

ECASP	Extra centrosome-associated secretory phenotype
EDTA	Ethylenediaminetetraacetic acid
ELISA	Enzyme-linked immunosorbent assay
ER	Endoplasmic reticulum
FACS	Fluorescence activated cell sorting
F-actin	Filamentous actin
FBS	Fetal bovine serum
FDR	False discovery rate
Flt3	FMS-like tyrosine kinase 3
FSC	Forward scatter
GFP	Green fluorescent protein
GM-CSF	Granulocyte-macrophage colony-stimulating factor
gMFI	Geometric mean fluorescence intensity
GTP	Guanosine triphosphate
h	Hour(s)
H_2O	Water
HBSS	Hank's Balanced Salt Solution
h_{CS}	Distance of the centrosome to the cell center
HEK293T	Human embryonic kidney cells
HEV	High endothelial venules
Hoxb8	Homeobox b8
ICAM1	Intercellular adhesion molecule 1
IFN	Interferon
IFT20	Intraflagellar transport 20
IL	Interleukin
IRF	Interferon regulatory factor
IS	Immune synapse
ITAM	Immunoreceptor tyrosine-based activation motif
KIFC1	Kinesin family member C1
LAT	Linker for activation of T cells
LB	Lysogeny broth
LFA1	Lymphocyte function-associated antigen 1
LINC	Linker of nucleoskeleton and cytoskeleton
LN	Lymph node
LPS	Lipopolysaccharide
LR reaction	Ligation-recombination reaction
LysC	Lysine C
M	Molar
m/z	Mass to charge ratio
MAP	Microtubule-associated proteins
MCCs	Multi-ciliated cells
MEM	Minimal essential medium
MFI	Mean fluorescence intensity
MHC	Major histocompatibility complex
min	Minute(s)
MLR	Mixed lymphocyte reaction
mRNA	Messenger RNA
MS	Mass spectrometry
MT	Microtubule
MTOC	Microtubule-organizing center
n	Nano

NEDD1	Neural precursor cell expressed, developmentally down-regulated 1
Nek2	NIMA-related kinase 2
NF-κB	Nuclear Factor kappa-light-chain-enhancer of activated B cells
NK cell	Natural killer cell
NLRP3	NOD-like receptor pyrin domain-containing protein 3
N_{MT}	MT number
Norm.	Normalized
ns	Non-significant
OVAp	Ovalbumin-peptide
PAC	Protein aggregation capture
PAMP	Pathogen-associated molecular pattern
PARP	Poly-ADP-ribose polymerase
PBS	Phosphate buffered saline
PCM	Pericentriolar material
PCNT	Pericentrin
PCR	Polymerase chain reaction
PFA	Paraformaldehyde
PLK	Polo-like kinase
pMHC	Peptide-MHC complex
pSMAC	peripheral supramolecular activation cluster
PTM	Post-translational modification
Rac1	Ras-related C3 botulinum toxin substrate 1
rCM1	Centrosomin motif originating from rat CDK5RAP2 protein sequence
$r_{CS\text{-}SP}$	Radius of imaginary sphere centered at the optimal centrosome position
RNA	Ribonucleic acid
ROI	Region of interest
ROS	Reactive oxygen species
RPE cells	Retinal pigment epithelial cells
rpm	Rounds per minute
RPMI	Roswell Park Memorial Institute
RT	Room temperature
rtTA	Reverse tetracycline-controlled transcriptional activator
s.d.	Standard deviation
SAS-6	Spindle assembly abnormal 6
SDC	Sodium deoxycholate
sec	Second(s)
siRNA	Small interfering RNA
SSC	Side scatter
SUN-1	Sad1 and UNC84 domain-containing protein 1
TAP	Transporter associated with antigen processing
TCR	T cell receptor
TF	Transcription factor
TFA	Trifluoracetic acid
T_{fh}	T follicular helper cells
TGFβ	Transforming growth factor β
Th	T helper cell
TLR	Toll-like receptor
TNF	Tumor necrosis factor
TRE	Tetracycline response element
T_{reg}	T regulatory cells
T_{search}	MT search time

UbC	Ubiquitin C
vs.	Versus
w/	With
w/o	Without
Wnt	Wingless-related integration site
ZYG-12	Zygote defective 12
β-ME	β-mercaptoethanol
γ-TuRC	γ-tubulin ring complex

List of Figures

1. Summary

The **centrosome**, nucleating microtubules (MTs) and serving as the primary microtubule-organizing center (MTOC), is a core component establishing eukaryotic cell architecture. It is composed of two centrioles, which are surrounded by pericentriolar material (PCM). The centrosome's major functions include enabling cell division, regulating intracellular organization, and facilitating cell polarity and signaling – several functions being important, for instance, in cells of the immune system. For the initiation of adaptive immune responses, **dendritic cells** (DCs), which are professional antigen-presenting cells (APCs), form specialized and highly dynamic cell-cell contacts with T cells. During **immune synapse** (IS) formation, interaction of surface molecules and the supply of soluble mediators instruct T cell activation and, importantly, centrosome polarization in T cells is critical for efficient T cell priming. However, surprisingly little is known about the **MT cytoskeleton** within DCs during IS formation.

In this study, we elaborated on the role of centrioles and MTs within DCs and their impact on cellular function, particularly in the context of the induction of $CD4^+$ T cell activation and proliferation. Through various drug treatments, we have uncovered that both components of the cytoskeleton – centrioles and MTs – are important for T cell priming.

While most non-proliferating cells contain two centrioles, previous research from our group has revealed that DCs acquire elevated numbers of centrioles (>2) upon immune activation. This phenomenon, although commonly observed in cancer cells, is rare in non-malignant cells. Functionally, extra centrioles form a single **over-active MTOC**, characterized by increased PCM recruitment and MT nucleation. Here, we showed that cells with multiple centrioles exhibit a higher capacity to activate T cells.

To understand the underlying processes, we visualized the **spatio-temporal dynamics** of centrioles in DCs upon antigen-specific T cell contacts. We observed that multiple centrioles **tightly cluster** during DC-T cell interactions. Additionally, unlike in T cells, MTOC polarization was absent in DCs. Instead, DC centrioles remained **centrally located** in the cell, in close proximity to the nucleus. Three-dimensional (3D) visualization of DC-T cell conjugates in peripheral lymph nodes (LNs) confirmed these findings *in vivo*. In further experiments, pharmacological perturbation of centriole clusters in DCs resulted in diminished T cell activation.

The secretion of soluble mediators has been described as intracellular process linked to the MT cytoskeleton. Thus, a comprehensive secretome analysis of DCs with distinct centriole numbers was performed. The results indicated that the **secretory profile of DCs** differs between cells with two and multiple centrioles. Given that DC secretion largely impacts the microenvironment of other immune

and non-immune cells, these findings provoke further questions regarding the response of surrounding cells.

Altogether, our results highlight the crucial role of centrosome integrity and proper MT array organization in DCs for T cell activation (summarized in **Figure 1.1**). The acquisition of multiple centrioles and their optimal spatial configuration and positioning within DCs facilitate the efficient initiation of adaptive immune responses. Future studies elucidating the impact of centrosome or MT array alterations will substantially advance our understanding of immune cell functionality and may facilitate the development of novel therapeutic strategies for example in the context of cancer treatment.

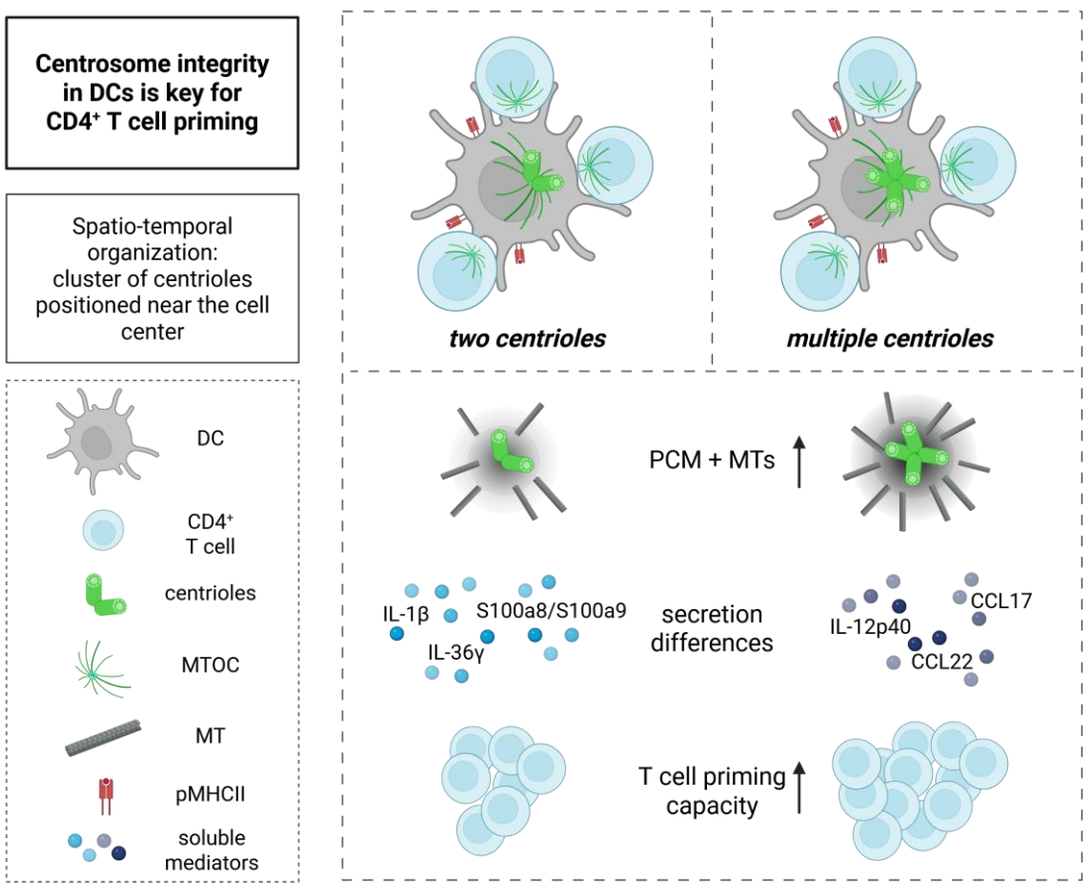

Figure 1.1 Graphical summary
Centrosome and MT integrity in DCs are key for CD4⁺ T cell priming. During antigen-specific T cell contacts, multiple centrioles in DCs cluster and localize in close proximity to the cell center. Moreover, DCs with multiple centrioles show an altered secretory phenotype and induce augmented T cell responses.

1.1. Zusammenfassung (German)

Das **Zentrosom**, welches Mikrotubuli (MT) nukleiert und als primäres Mikrotubuli-organisierendes Zentrum (MTOC) dient, ist eine wichtige Komponente für die Architektur eukaryotischer Zellen. Das Zentrosom besteht aus zwei Zentriolen, die von perizentriolärem Material (PCM) umgeben sind. Zu den wichtigsten Funktionen des Zentrosoms gehören die Ermöglichung der Zellteilung, die Regulation der intrazellulären Organisation und die Unterstützung der Zellpolarität und der Signalübertragung – einige Funktionen davon sind beispielsweise in Zellen des Immunsystems wichtig. Für die Ausbildung adaptiver Immunantworten bilden **dendritische Zellen** (DCs), die professionelle Antigen-präsentierende Zellen (APCs) sind, spezialisierte und hochdynamische Zell-Zell-Verbindungen mit T-Zellen aus. Während dieser Ausbildung der **Immunsynapse** (IS) leiten die Interaktion von Oberflächenmolekülen und die Versorgung mit löslichen Mediatoren die T-Zell Aktivierung ein und zudem ist eine Polarisation des Zentrosoms in T-Zellen entscheidend für effiziente T-Zell Aktivierung. Überraschenderweise ist jedoch nur wenig über das **MT Zytoskelett** in DCs während der Ausbildung der IS bekannt.

In diesem Projekt haben wir die Rolle von Zentriolen und MT in DCs und deren Einfluss auf die Zellfunktion, insbesondere im Zusammenhang mit der Induktion der Aktivierung und Proliferation von $CD4^+$ T-Zellen, näher untersucht. Durch das Verwenden verschiedener Wirkstoffe haben wir herausgefunden, dass beide Komponenten des Zytoskeletts – Zentriolen und MT – wichtig für T Zell Aktivierung sind.

Während die meisten nicht-proliferierenden Zellen zwei Zentriolen besitzen, haben vorherige Untersuchungen unserer Arbeitsgruppe gezeigt, dass DCs bei Immunaktivierung eine erhöhte Anzahl an Zentriolen (>2) erwerben. Obwohl dieses Phenomen bereits oft in Krebszellen beobachtet wurde, ist es in nicht-bösartigen Zellen selten. Funktionell bilden zusätzliche Zentriolen ein **überaktives MTOC**, welches durch erhöhte PCM-Rekrutierung und MT-Nukleation gekennzeichnet ist. Hier haben wir gezeigt, dass Zellen mit mehreren Zentriolen eine höhere Kapazität zur Aktivierung von T-Zellen aufweisen.

Um die zugrunde liegenden Prozesse zu verstehen, haben wir die **räumliche und zeitliche Dynamik** der Zentriolen in DCs bei Kontakt mit Antigen-spezifischen T-Zellen visualisiert. Wir haben beobachtet, dass multiple Zentriolen während der DC-T-Zell Interaktionen **eng gruppiert** auftreten. Darüber hinaus, im Gegensatz zu T-Zellen, war keine MTOC Polarisation in DCs zu beobachten. Stattdessen blieben die DC Zentriolen **zentral in der Zelle** in unmittelbarer Nähe zum Zellkern lokalisiert. Die dreidimensionale (3D) Veranschaulichung von DC-T-Zell-Konjugaten in peripheren Lymphknoten hat

diese Ergebnisse *in* vivo bestätigt. In weiteren Experimenten führte pharmakologische Störung der Zentriolen-Gruppierung in DCs zu verminderter T-Zell Aktivierung.

Die Sekretion löslicher Mediatoren wurde bereits als intrazellulärer Prozess beschrieben, der mit dem MT Zytoskelett in Verbindung steht. Daher wurde eine umfassende Sekretomanalyse von DCs mit bestimmter Zentriolenanzahl durchgeführt. Die Ergebnisse deuteten darauf hin, dass sich das **Sekretionsprofil von DCs** mit zwei und multiplen Zentriolen unterscheidet. Angesichts der Tatsache, dass die Sekretion von DCs einen großen Einfluss auf das Mikromillieu anderer Immun- und Nicht-Immunzellen hat, werfen diese Ergebnisse weitere Fragen bezüglich der Antwort umliegender Zellen auf.

Insgesamt unterstreichen unsere Ergebnisse die entscheidende Rolle der Integrität des Zentrosoms und der korrekten Organisation der MT in DCs für die T-Zell Aktivierung (zusammengefasst in **Figure 1.1**). Die Anhäufung von Zentriolen und deren optimale räumliche Konfiguration und Position innerhalb DCs fördern die effiziente Auslösung adaptiver Immunantworten. Zukünftige Studien, die den Einfluss von Veränderungen des Zentrosoms oder der MT Anordnung aufklären, werden unser Verständnis der Funktionsweise von Immunzellen voranbringen und könnten die Entwicklung neuer therapeutischer Strategien, beispielsweise im Zusammenhang mit der Krebsbehandlung, ermöglichen.

2. Introduction

2.1. The centrosome as microtubule-organizing center

2.1.1. Centrosome structure and duplication cycle

The initial discoveries of the centrosome trace back to Edouard van Beneden and Theodor Boveri in the 1870s and 1880s (Sluder 2014). In over a century of research, a detailed knowledge about the structure, assembly and function of this membrane-less organelle has emerged. Here, in this scope, only major structural and functional components are described. Centrosomes are present in most eukaryotic cells and in interphase one centrosome consists of two centrioles and a surrounding proteinaceous matrix called pericentriolar material (PCM) (**Figure 2.2 A**)(Bornens et al. 1987). Each centriole has a cylindrical structure composed of microtubule (MT) triplets arranged in a nine-fold radial symmetry (Bornens 2012). Notably, the centriole is also the core structure which can initiate the formation of a cilium in cell cycle arrested cells (**Figure 2.2 B**)(Breslow and Holland 2019). In a mature centrosome, one centriole, which is called parent centriole, carries distal and subdistal appendages involved in cilia formation and responsible for anchoring MTs while the second centriole (daughter centriole) lacks these proteins (Paintrand et al. 1992; Piel et al. 2000). The two centrioles are connected via a flexible linker composed of multiple proteins such as centrosomal Nek2-associated protein 1 (C-Nap1), Rootletin and centrosomal protein 68 (CEP68) (Fry et al. 1998; Bahe et al. 2005; Graser et al. 2007; Theile et al. 2023). Despite the fact that the structure of the linker is still not fully understood, impairment of linker function has been shown to induce centriole separation which subsequently can have detrimental effects for cell division (discussed in (Remo et al. 2020)). To administrate diverse functions, the PCM surrounding the centrioles is a structured compartment build of multiple proteins which are subject to constant exchange (Mennella et al. 2012; Lawo et al. 2012; Sonnen et al. 2012). For example, γ-tubulin ring complex (γ-TuRC) forms the platform for MT nucleation (Joshi et al. 1992; Moritz et al. 1995). To this end, γ-TuRC is associated with the adapter neural precursor cell expressed, developmentally down-regulated 1 (NEDD1) and multiple copies of CDK5 regulatory subunit-associated protein 2 (CDK5RAP2) which promote γ-TuRC closure and activation (Gao et al. 2025). Also, another centrosomal protein, called pericentrin (PCNT), which is involved in recruitment of other PCM proteins and new centriole assembly and elongation, is often used in immunofluorescent staining as PCM marker (Ito et al. 2019). Additionally, numerous recruited proteins regulate centriole duplication and thereby cell cycle progression. Examples are the localization of multiple cyclin-dependent kinases (CDKs) to the centrosomes or PCM1 which recruits polo-like kinase 1 (PLK1) for centrosome maturation processes (Arquint et al. 2014; Loncarek et al. 2010).

Importantly, centrosome duplication is strongly coordinated with the cell cycle to ensure exactly two centrosomes (four centrioles) for proper formation of two spindle poles which enable accurate chromosome separation (Nigg and Holland 2018; Fırat-Karalar and Stearns 2014). The centrosome is duplicated in a semi-conservative manner, meaning that at each centriole one new centriole is formed and the daughter cell later contains one older and one younger centriole. The duplication of the centrosome starts during G_1/S transition where the mother and the daughter centriole disengage by separase activity and new procentriole formation begins at the cartwheel (**Figure 2.2 B**)(Tsou and Stearns 2006). This step is controlled by PLK4 which recruits spindle assembly abnormal 6 (SAS-6) (Kim et al. 2013). SAS-6 is a structural component of the cartwheel which forms the template structure for the new centriole (Nakazawa et al. 2007). The centrioles elongate during S phase. In G_2 phase the cell contains four centrioles: two parental centrioles associated with PCM and two younger procentriole still lacking appendages and the ability to recruit PCM (Loncarek et al. 2008). During G_2/M transition PLK1 dependent centrosome maturation is induced resulting in PCM expansion and the linker is fully resolved to separate the two centriole pairs (Faragher and Fry 2003; Lane and Nigg 1996).

An accurate centrosome duplication is important for bipolar spindle assembly. To this end, correct centriole numbers rely on the one hand on coordination with the cell cycle and on the other hand on precise control of only one copy number per pre-existing centriole. Thus, duplication is regulated by several proteins which need to be expressed and localize to the centrioles to initiate reduplication (Breslow and Holland 2019). In addition, disengagement of the centrioles is required for new procentriole formation (Tsou and Stearns 2006). Despite regulatory mechanisms of centrosome duplication are in place ensuring that centriole numbers match cell cycle progression, alterations in centriole numbers occur during organismal development and cell differentiation or specialization which give rise to cells without centrioles or with amplified centrioles (Meyer-Gerards and Bazzi 2025). Mechanisms by which cells acquire amplified centrioles and the subsequent consequences for cellular function and organismal health will be discussed in chapter 2.1.3.

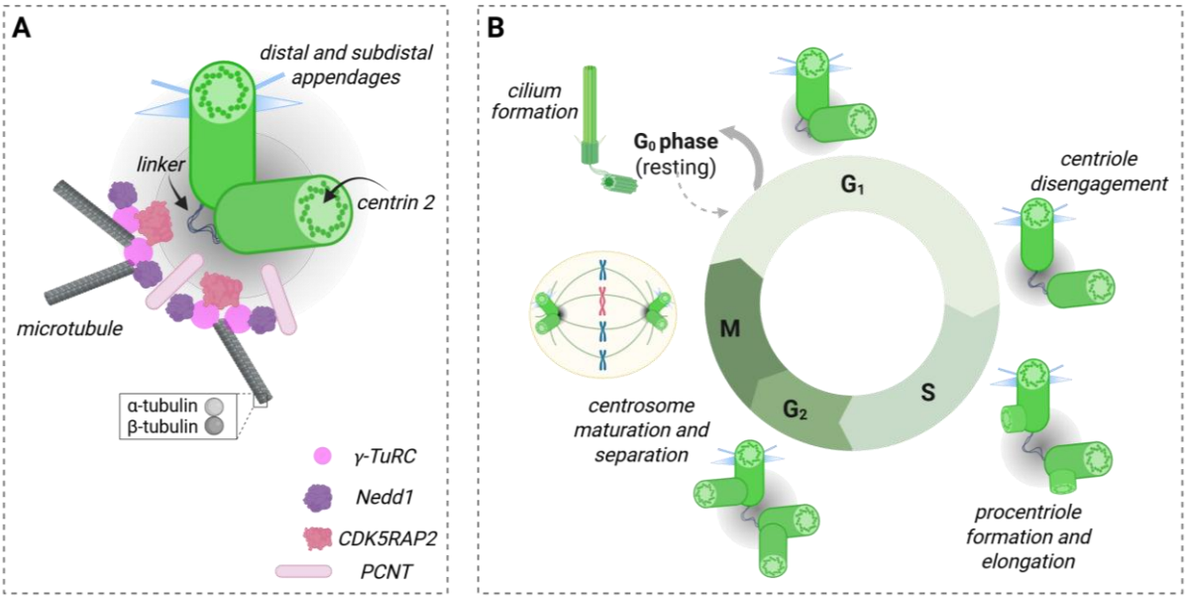

Figure 2.2 Centrosome structure and duplication cycle
(**A**) The centrosome consists of two centrioles: a parent centriole with distal and subdistal appendages and a daughter centriole lacking appendages. The two centrioles are connected by a flexible linker and surrounded by PCM containing the proteins for MT nucleation. Specific proteins and their location at the centrosome or MTs are depicted in the scheme. (**B**) Centrosome duplication starts with centriole disengagement at the G_1/S transition. Next, procentrioles form and elongate during S phase. During G_2/M phase transition the centrosomes mature and separate in order to build two spindle poles during mitosis. In G_0 arrested cells, the centrosome can build the core structure of a cilium. Figure created using Biorender.

2.1.2. Core functions of centrosomes and microtubules

The centrosome serves as main microtubule-organizing center (MTOC) in most animal cells. Its capability to nucleate and anchor MT filaments evokes pivotal functions within the cells. It is worth noting that in some cells like hepatocytes, neurons or muscle cells, MT nucleation can also take place at the Golgi or nuclear envelope (Tassin et al. 1985; Chabin-Brion et al. 2001; Ori-McKenney et al. 2012). MTs are composed of alpha-(α-)/beta-(β-)tubulin dimers which build cylindrical and inherently polar filaments with a diameter of approximately 25 nm (Goodson and Jonasson 2018). While the relatively static minus-end is attached to the site of MT nucleation, MT growth mainly takes place at the plus-end (Mitchison and Kirschner 1984; Moritz et al. 1995). Furthermore, tubulin isotypes and post-translational modifications (PTMs) strongly influence MT shape, stability and interactions with MT-associated proteins (MAPs) which mediate additional functionalities of MTs (Janke and Magiera 2020).

Centrosome and MT array organization are crucial for several cellular processes. Briefly, during mitosis, MTs emanating from the centrosome – or more precisely – from two centrosomes capture the chromosomes at the kinetochore which enables proper segregation of the genetic material into

daughter cells. Centrosome abnormalities have been shown to interfere with stable bipolar spindle assembly leading to chromosomal instability and cancer progression which will be discussed in chapter 2.1.3 (Pihan et al. 2003; Ganem et al. 2009). Moreover, during cellular navigation through the body, cells constantly need to adapt their cell shape and polarity (Kopf and Kiermaier 2021). The pivotal role of MTs for this process is highlighted by MT depolymerization in leukocytes resulting in cell rupture during locomotion in complex environments (Kopf et al. 2020). In addition, cell polarity marked by centrosome reorientation is established during immune synapse (IS) formation (Kupfer and Dennert 1984a). Further, MTs form tracks within the cytoplasm which allows targeted vesicle and organelle transport to specific sites (Yaffe et al. 1996; Lasek and Brady 1985). For example, vesicle secretion is reduced by drug-induced depletion of MTs (Schmoranzer and Simon 2003). To enable directed movement, the motor protein dynein drives ATP-dependent transport from MT plus-end to minus-end while kinesins transport cargos from minus- to plus-end (Barlan and Gelfand 2017). Additionally, the centrosome has been reported to act as important signaling hub contributing to inflammasome assembly in macrophages which is formed in response to pathogen encounter (Magupalli et al. 2020). Collectively, centrosome and MT array organization play important roles for enabling cell division, regulating cell polarity and motility as well as facilitating intracellular transport and cellular signaling (**Figure 2.3**).

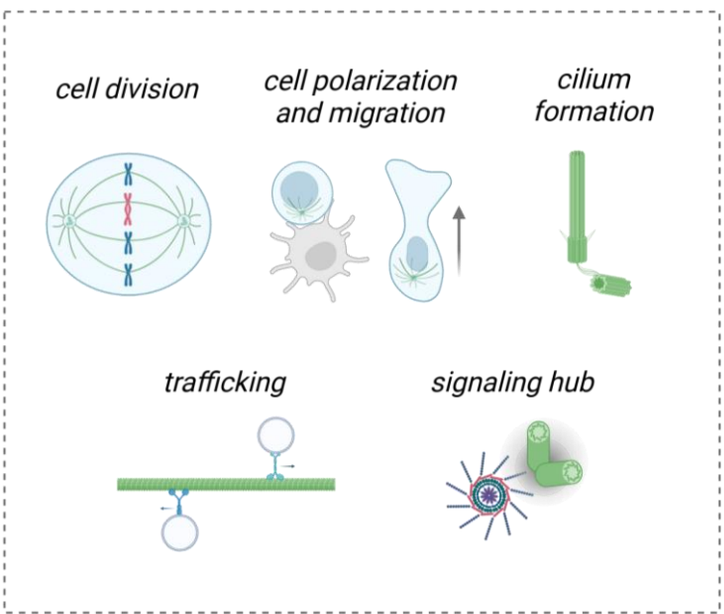

Figure 2.3 Centrosome and MT functions
Centrosomes with their capacity to nucleate and anchor MTs fulfill various functions in the cells: forming spindle poles during mitosis, enabling stable cell polarization and migration, building a cilium, facilitating intracellular transport and cellular signaling. Figure created using BioRender.

2.1.3. Centriole amplification in cancer and non-malignant cells

The centrosome duplication cycle is strongly regulated by requiring the action of multiple kinases at the right time and localization. Thus, classically all interphase cells harbor one centrosome consisting of two centrioles while a cell contains two centrosomes (4 centrioles) before entering mitosis.

However, elevated centriole numbers occur in cancer cells and in highly specialized cell types such as hepatocytes, osteoclasts, megakaryocytes, cardiomyocytes, early B cell progenitors and mature dendritic cells (DCs) (Schapfl et al. 2024; Weier et al. 2022; Philip et al. 2022; Guidotti et al. 2003; Becker et al. 2024; Chan 2011; Zebrowski et al. 2015). We refer to the phenomenon of extra centrioles – more than two centrioles in interphase cells – as multiple centrioles or centriole amplification. The underlying mechanisms of centriole acquisition vary ranging from overduplication and failed mitosis to cell fusion events (Denu et al. 2018; Godinho et al. 2009). As example and important for the present study, elevated centriole numbers in DCs are provoked by antigen encounter (Weier et al. 2022). Upon maturation, DCs arrest in G_1 phase of the cell cycle and acquire more than two centrioles by incomplete mitosis and/or PLK2 upregulation which is a kinase required for centriole duplication (Weier et al. 2022; Cizmecioglu et al. 2008).

Once amplified centrioles are acquired, especially highly proliferating cancer cells need to cope with this alteration during mitosis. Therefore, cells cluster multiple centrioles to form pseudo-bipolar spindles, which helps limit chromosome mis-segregation and cell death (Ring et al. 1982; Quintyne et al. 2005; Kwon et al. 2008). Nevertheless, a high centriole amplification rate is associated with chromosomal instability and increased metastasis (Pihan et al. 2003; LoMastro and Holland 2019; Ganem et al. 2009). Mechanistically, increased metastasis is caused by several processes such as formation of invasive protrusions, disrupted E-cadherin junctions and secretion of pro-invasive molecules (Godinho et al. 2014; Arnandis et al. 2018). Whether centriole amplification is a cause or a consequence of cell transformation and cancer progression is controversially discussed. On the one hand, centriole amplification induced by PLK4 overexpression was shown to be sufficient for tumor development – even in the absence of additional genetic defects (Levine et al. 2017). On the other hand, centriole amplification can trigger apoptosis and thereby limit tumorigenesis (Braun et al. 2024). Overall, targeting amplified centrioles is a promising approach for cancer treatment. For example, de-clustering agents as well as MT-destabilizing agents were shown *in vitro* or *in vivo* to inhibit cell migration and/or induce cancer cell apoptosis (Raab et al. 2012; Pannu et al. 2014; Perez 2009; Altmann et al. 2000). Additionally, cells with amplified centrioles have been studied extensively *in vitro* discovering altered signaling events and intracellular organization. More precisely, at mature amplified centrioles PIDDosome assembly, which is a multiprotein complex with structural similarity to the inflammasome, induces cell cycle arrest and cell death via a Caspase-2 and p53-, p21-dependent pathway (Fava et al. 2017). Moreover, PIDD1-dependent immune cell activation has been observed (Garcia-Carpio et al. 2023). In response to centriole amplification, tubulin acetylation is changed resulting in broad organelle repositioning and enhanced nucleus deformability (Monteiro et al. 2023).

The changed nucleus rigidity, in turn, enables more efficient cellular transmigration through constriction sites.

In contrast to the context of cancer and malignancy, the effects and functions of amplified centrioles in non-cancerous cells are studied to a lesser extent. Extra centrioles recently observed in B cell progenitors are tolerated and do not perturb differentiation, even though they are cleared in more mature B cell stages. This leaves the question unanswered whether a biological function is linked to the presence of extra centrioles (Schapfl et al. 2024). Intriguingly, in DCs carrying multiple centrioles, enhancement of directional migration and T cell priming capacity has been documented (Weier et al. 2022). Further evidence for beneficial effects of extra centrioles comes from experiments in which centrioles were artificially duplicated in B cells and microglia. Extra centrioles promoted T cell stimulation by B cells and enhanced dead cell clearance by microglia (Möller et al. 2022; Yuseff et al. 2011).

In summary, amplified centrioles potentially play a double-edged role depending on whether they are found in harmful cancerous cells or benign cells of the immune system.

2.2. Dendritic cells induce adaptive immune responses

In 1973, Ralph Steinman and Zanvil Cohn described a new cell type in murine spleen which they named according to the morphology: dendritic cells (DCs) (Steinman and Cohn 1973). Only a few years later, the role of DCs in stimulating mixed lymphocyte reactions (MLRs) was discovered (Inaba and Steinman 1987). Until today, the knowledge of DC diversity, distribution, function and also their potential in clinical therapy has expanded enormously (Rowley and Fitch 2012). DCs are known as professional antigen-presenting cells (APCs), which are key for linking innate and adaptive immunity. DCs arise from hematopoietic stem cells which reside in the bone marrow (Cabeza-Cabrerizo et al. 2021). They exit from the bone marrow into the blood stream as precursor cells and enter peripheral tissues where they fully differentiate and patrol to protect the body. Under inflammatory conditions, also monocyte-derived DCs develop and enter the tissues to facilitate the immune response. For sensing danger signals, DCs bear various pattern recognition receptors (PRRs) on their cell surface and intracellularly (**Figure 2.4** A). Upon antigen encounter, a specific maturation program is induced leading to migration towards lymphatic vessels (**Figure 2.4** B). Through the lymphatics, DCs reach the draining lymph nodes (LNs) where they face lymphocytes, which enter the LN through high endothelial venules (HEVs). In the LN, direct DC-T cell interaction induces clonal expansion of antigen-specific T cells (**Figure 2.4** C). In addition to the LNs, T cell activation also takes place in the spleen where the cells mainly encounter blood borne pathogens. Furthermore, DCs influence B cell expansion and antibody production (Dubois

et al. 1997). In the following paragraphs, mechanisms of antigen uptake and presentation as well as the induction of T cell activation by DCs will be explained in more detail.

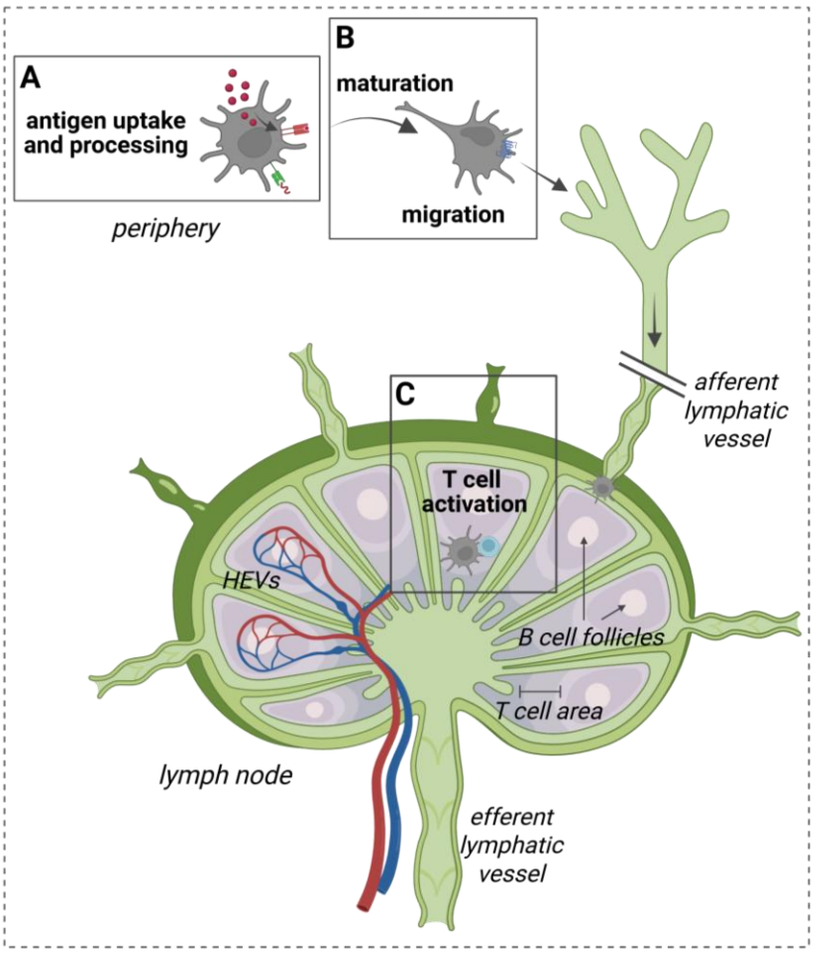

Figure 2.4 Route of DCs to prime T cells in the lymph nodes
DCs patrol for antigens in peripheral tissues (**A**). Upon antigen uptake and processing, they undergo a maturation program which upregulates chemokine receptors and enables migration towards lymphatic vessels (**B**). Through the lymphatics they can reach the LNs where they induce T cell activation (**C**). Figure created using BioRender.

2.2.1. Antigen uptake, processing and presentation by DCs

Immature DCs patrol in peripheral tissues, constantly sampling their surroundings to detect antigens and propagating potentially harmful signals to induce an immune response. Uptake of environmental samples can be achieved by different mechanisms (Liu and Roche 2015). Macropinocytosis is an actin-driven process in which extracellular fluid is taken up via the formation of large membrane ruffles which then fold back onto the cell and fuse with the plasma membrane (Mylvaganam et al. 2021). The process of clathrin-mediated endocytosis as well as phagocytosis are mediated via PRRs on the cell surface (Janeway et al. 1996). PRRs discriminate between self-structures and pathogen-associated molecular patterns (PAMPs) or damage-associated molecular patterns (DAMPs) (Matzinger 2002). Most prominent receptors include C-type-lectin family members as well as Toll-like receptors (TLRs) (Théry and Amigorena 2001; Medzhitov 2001; Sallusto et al. 1995). Upon recognition by one of the receptors, either antigen uptake, various intracellular signaling pathways, or a combination of both is initiated.

After antigen uptake, exogenous antigens first enter the endosomal compartment. To enable antigen recognition by T cells, antigens need to be presented on major histocompatibility complexes (MHC) I or II. As only short peptide fragments can be loaded on MHC molecules (MHCI: 8-10 amino acids; MHCII: 9-22 amino acids) antigen processing is required (Madden 1995; Stern and Wiley 1994). For presentation of exogenous antigens on MHCII, antigen fragmentation is achieved by acidification of early endosomes or phagosomes when maturing into late phago-/endosomes and (phago-)lysosomes (McCoy et al. 1989). The acidic pH activates proteases to degrade the antigens into peptide fragments. Next, antigen containing vesicles fuse with vesicles containing MHCII molecules which enables antigenic peptides to bind MHCII. In addition, cytosolic antigens such as viruses or self-proteins can be presented on MHCII when they are enclosed by membrane during the process of autophagy and thereby enter the vesicular compartment. The resulting complex of a peptide bound to MHCII (pMHC) can be recognized by the T cell receptor (TCR) of cluster of differentiation 4^+ ($CD4^+$) T cells which is necessary for T cell activation. Alternatively, antigens can be presented on MHCI to enable recognition by $CD8^+$ T cells. To this end, classically cytosolic proteins are degraded by the proteasome and delivered via the transporter associated with antigen processing (TAP) to the endoplasmic reticulum (ER) where MHCI is retained until peptide binding (Norbury et al. 1997). This is a ubiquitous process nearly all cells perform. In contrast, MHCII is only expressed on particular antigen presenting cells (APCs) like DCs, B cells, macrophages and thymic epithelial cells (Roche and Furuta 2015). In addition, a process called cross-presentation enables – mostly in DCs – the presentation of internalized antigens on MHCI. Therefore, either antigens remain in the endosomal-lysosomal compartment and are loaded directly after lysosomal degradation on MHCI or alternatively they are translocated from the vesicular system into the cytosol and then follow the path of proteasomal degradation and MHCI loading (Kovacsovics-Bankowski and Rock 1995; Embgenbroich and Burgdorf 2018; Shen et al. 2004; Ackerman et al. 2003; Palmowski et al. 2006). The presentation of exogenous antigens on MHCI by professional APCs is important to drive a $CD8^+$ T cell response against tumor cells or viruses which do not infect APCs.

2.2.2. DC maturation and migration

Apart from processing of antigens, recognition of a stimulus by PRRs induces intracellular signaling cascades leading to DC maturation. For example, the bacterial cell wall component lipopolysaccharide (LPS) activates TLR4 which then in turn activates the transcription factors (TFs) AP-1, NF-κB, IRF-3 and IRF-5 (Akira et al. 2006). Subsequent TF translocation into the nucleus induces changes in gene transcription.

Thus, DC maturation leads to C-C motif chemokine receptor 7 (CCR7) upregulation which enables migration via chemokine gradients towards lymphatic vessels and allows propagation to the LNs

(Förster et al. 1999; Sallusto et al. 1998; Dieu et al. 1998). In the LNs, DCs prime antigen-specific T cells leading to clonal expansion. To this end, maturation evokes elevated levels of the antigen-presentation molecule MHCII and T cell co-stimulatory molecules such as CD80 and CD86 on the cell surface (Cabeza-Cabrerizo et al. 2021; Steinman 1991; Banchereau and Steinman 1998). Furthermore, a variable set of soluble mediators is secreted by DCs. Diverse cytokines direct naïve T cell differentiation into different classes of effector or memory T cells (see chapter 2.2.3). Cytokines like tumor necrosis factor (TNF)-α or interferons activate the endothelium to facilitate immune cell entry or alternatively modulate immune cell activation (Detmar et al. 1990; González-Navajas et al. 2012). Chemokines like C-X-C motif chemokine ligand 1 (CXCL1), Chemokine C-C Motif Ligand 17 (CCL17) and CCL22 recruit other immune cells to the site of infection or attract T cells to interact with DCs in the LNs (Korbecki et al. 2022; Imai et al. 1999; Lieberam and Förster 1999; Imai et al. 1998). Of note, the DC secretory response is highly diverse which highlights the crucial role of DCs for shaping the immune response.

2.2.3. Induction of T cell responses

Immunity against infections and tumors relies on proper T cell responses while dis-balanced immune functions can cause autoimmune diseases. For T cell priming, naïve T cells scan through multiple DCs in secondary lymphoid organs until they recognize the respective antigen with their T cell receptor (TCR). The cell-cell interaction between APC and T cell is called immune synapse formation and the distinct structure of this contact will be discussed in chapter 2.3. Altogether, the synapse provides a well-organized area which allows efficient binding and signaling of receptors and subsequent initiation of T cell clonal expansion. Importantly, T cells recognize antigens on MHC molecules via the highly specific TCR and the co-receptors CD4 or CD8 (Meuer et al. 1982). The TCR of conventional T cells consists of alpha (α)- and beta (β)-chains and a zeta (ζ)-chain homodimer which contains three immunoreceptor tyrosine-based activation motifs (ITAMs) to enable induction of a phosphorylation cascade within the T cell (Klausner et al. 1990; Reth 1989). Additionally, the TCR is coupled to four chains of CD3 *(epsilon gamma, epsilon delta)* with each chain containing one ITAM (Borst et al. 1983). As a second signal, DCs provide co-stimulation necessary for T cell survival and proliferation. Furthermore, DC cytokine secretion drives T cell activation and differentiation into subtypes and thereby determines the direction of the immune response.

Two main conventional T cell classes are determined by either CD4 or CD8 expression on their surface. After activation, $CD4^+$ and $CD8^+$ T cells differentiate into effector or memory cells to mediate direct killing, diverse immune regulation or long-term protection (Sun et al. 2023). $CD8^+$ T cells are also called cytotoxic T cells and are important for fighting against intracellular pathogens as well as malignant cancer cells. After priming in the LN, effector cytotoxic T cells fulfill their function by recognizing

infected cells and secreting cytotoxic granules containing effector molecules such as perforin, granzymes, granulysin (Tschopp and Nabholz 1990; Rouvier et al. 1993; Sun et al. 2023; Suda et al. 1993). Alternatively, killing is achieved by expressing Fas Ligand on their surface which directly induces apoptosis in target cells (Suda et al. 1993). In addition, activated $CD8^+$ T cells secrete TNF-α and interferon (IFN)-γ which induce cell death programs in target cells or activation of surrounding immune cells (Chun et al. 2021; Nathan et al. 1983). $CD4^+$ T cells are also called T helper cells as they directly interact with B cells to stimulate their proliferation and antibody production (Miller and Mitchell 1968). Additionally, after priming within the LNs T helper cells secrete cytokines supporting macrophage activation or $CD8^+$ T cells survival, expansion and memory (Novy et al. 2007). There are different subclasses of T helper cells which allow specialization of the immune response according to the type of infection. The specialization of $CD4^+$ T helper cells is reviewed by (Aguiar and Vieira 2024) and summarized in **Figure 2.5**.

Briefly, Th1 cells are induced by interleukin-12 (IL-12) in response to viruses, intracellular bacteria or tumors and respond by secreting IFN-γ and TNF-α. Th2 cells develop in the presence of IL-4 in response to allergens or helminths and Th2 cells secrete IL-4, IL-5 and IL-13 which induce tissue repair and mucus production. Th9 cells are relatively newly identified cells involved in infectious diseases, cancer, allergy and autoimmune diseases (Veldhoen et al. 2008; Li et al. 2016). Th9 cells are induced in the presence of IL-4 and transforming growth factor (TGF)-β and produce IL-9, IL-10 and IL-21 (You et al. 2017). Th17 cells develop as response to extracellular bacteria and fungi via the cytokines IL-6 and TGF-β and Th17 cells in turn secrete IL-17 and IL-22 and recruit neutrophils. Th22 cells are induced for epithelial barrier protection in response to IL-6 and TNF-α and subsequently secrete IL-22. T follicular helper (T_{fh}) cells are induced by OX40L and ICOSL binding and IL-6 in response to all encounters. T_{fh} cells secrete IL-21 and are necessary for B cell activation including germinal center formation, affinity maturation and class switching. Another important subset are T regulatory (T_{reg}) cells which are induced by TGF-β and retinoic acid and B and T lymphocyte attenuator (BTLA) binding in response to harmless self-antigens, dietary antigen or microbiota. T_{reg} cells secrete IL-10 and TGF-β to reduce inflammation and induce tolerance.

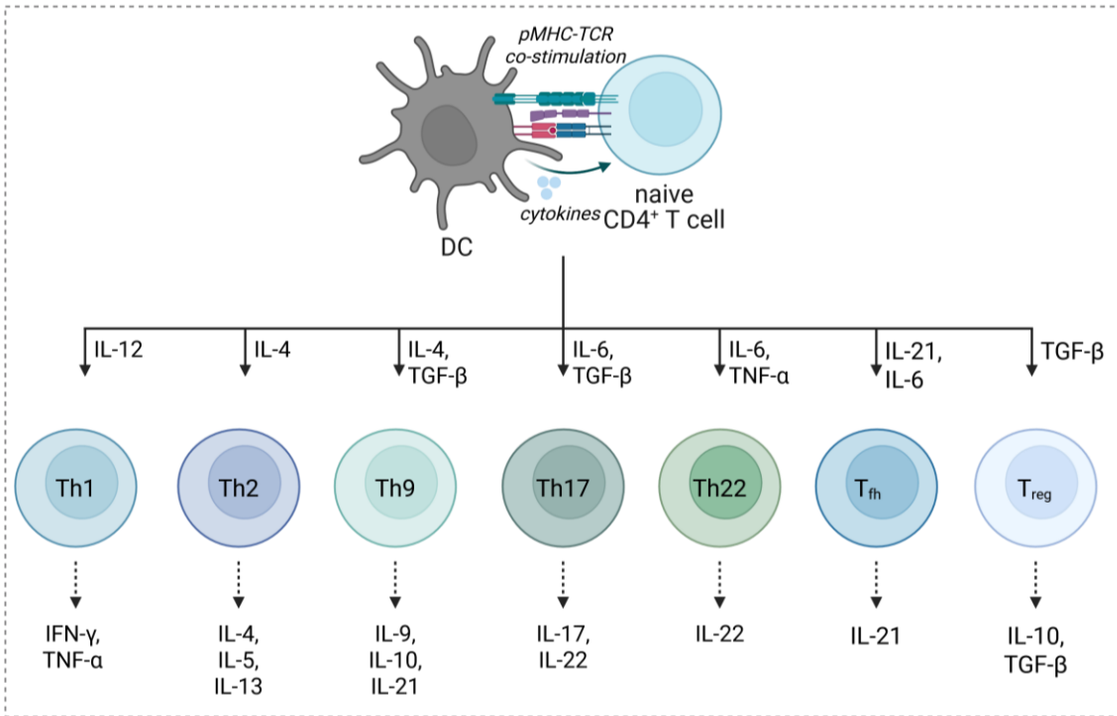

Figure 2.5 CD4⁺ T cell differentiation into different subsets
Three DC-derived signals are required for efficient T cell expansion: pMHC, co-stimulation and secreted cytokines. The specific cytokines directing naïve CD4⁺ T cell into different subtypes are depicted on the arrows above the cell type. Then, these cell types (Th1, Th2, Th9, Th17, Th22, T_{fh}, T_{reg}), in turn, secrete effector cytokines mentioned below the dashed arrow. Figure created using BioRender.

2.3. The immune synapse as specialized cell-cell junction

The term immune synapse (IS) commonly refers to the cell-cell junction formed between APC and T cell. This contact bears similarities with the cytotoxic synapse formed between a cytotoxic T cell or a natural killer (NK) cell and a target cell. Notably, on the T cell or NK cell side, this involves significant cytoskeletal rearrangement. Additionally, some features are shared with synapses of the nervous system such as the organization in microdomains with a central active zone and surrounding adhesion molecules (Dustin and Colman 2002). The IS formed between APC and T cell is a key step for the induction of an adaptive immune response and supplies the three necessary signals for T cell activation described already above (see chapter T cell activation 2.2.3). Imaging cell dynamics in murine LNs as well as *in vitro* co-culture of APCs and T cells revealed consecutive stages of T cell activation by APCs which are marked by distinct T cell migratory behavior and intracellular and membrane organization changes (Ueda et al. 2011; Miller et al. 2004). First after LN entry, T cells make short contacts with multiple DCs before a long-lived and stable interaction follows. Next, T cells get highly migratory and start to proliferate. Through this, the final aim of the interaction is accomplished.

2.3.1. Structure of the APC – T cell synapse

The dynamic cell-cell interaction between APC and T cell integrates different receptor molecules to allow efficient downstream signaling. The classical IS structure can be described as a “bull’s eye” (**Figure 2.6 A** monocentric synapse). In the center – the so called central supramolecular activation cluster (cSMAC) – TCR/CD3 interact with peptide-MHC molecules (Monks et al. 1998). In addition, co-stimulatory receptors such as CD28 are localized on the T cell surface and interact with CD80/86 on the APC surface in the cSMAC (Tseng et al. 2008; Harding et al. 1992; Green et al. 1994). Another well characterized receptor-ligand pair is CD40L (T cell) and CD40 (APC) (Boisvert et al. 2004). The central structure is surrounded by the peripheral SMAC (pSMAC) enriched in the integrin lymphocyte function-associated antigen 1 (LFA-1) (T cell) binding the intercellular adhesion molecule 1 (ICAM-1) on the APC side to stabilize the synapse (Monks et al. 1998; Grakoui et al. 1999). In the distal SMAC (dSMAC) structure, small microclusters of TCR-MHC are formed and then move through the pSMAC into the cSMAC in an actin-dependent manner (Yokosuka et al. 2005). Therefore, actin in the dSMAC area assists to form initial microclusters and protrusions and actin in the pSMAC area, which is linked to integrins, generates forces for centripetal movement of TCR microclusters (Campi et al. 2005; Kaizuka et al. 2007; Leithner et al. 2021). The dSMAC also excludes molecules from the IS center such as CD45 and CD43 on the T cell side which are phosphatases having potential inhibitory functions (Delon et al. 2001; Leupin et al. 2000). On the APC side, actin is excluded from the central region and forms a ring structure which controls contact duration and T cell priming efficiency (Leithner et al. 2021).

Of note, an alternative structure has been described and referred to as ‘multifocal’ or ‘multicentric’ synapse (**Figure 2.6 B** multicentric synapse) (Brossard et al. 2005). Multicentric synapses are marked by small accumulations of TCR bound to MHC and LFA-1-ICAM-1 spread throughout the cell-cell interphase (Thauland et al. 2008). Potential factors or conditions determining which synapse structure is formed include interacting cell types and strength of antigen recognition (Verboogen et al. 2016; Thauland et al. 2008; Thauland and Parker 2010; Tseng et al. 2008).

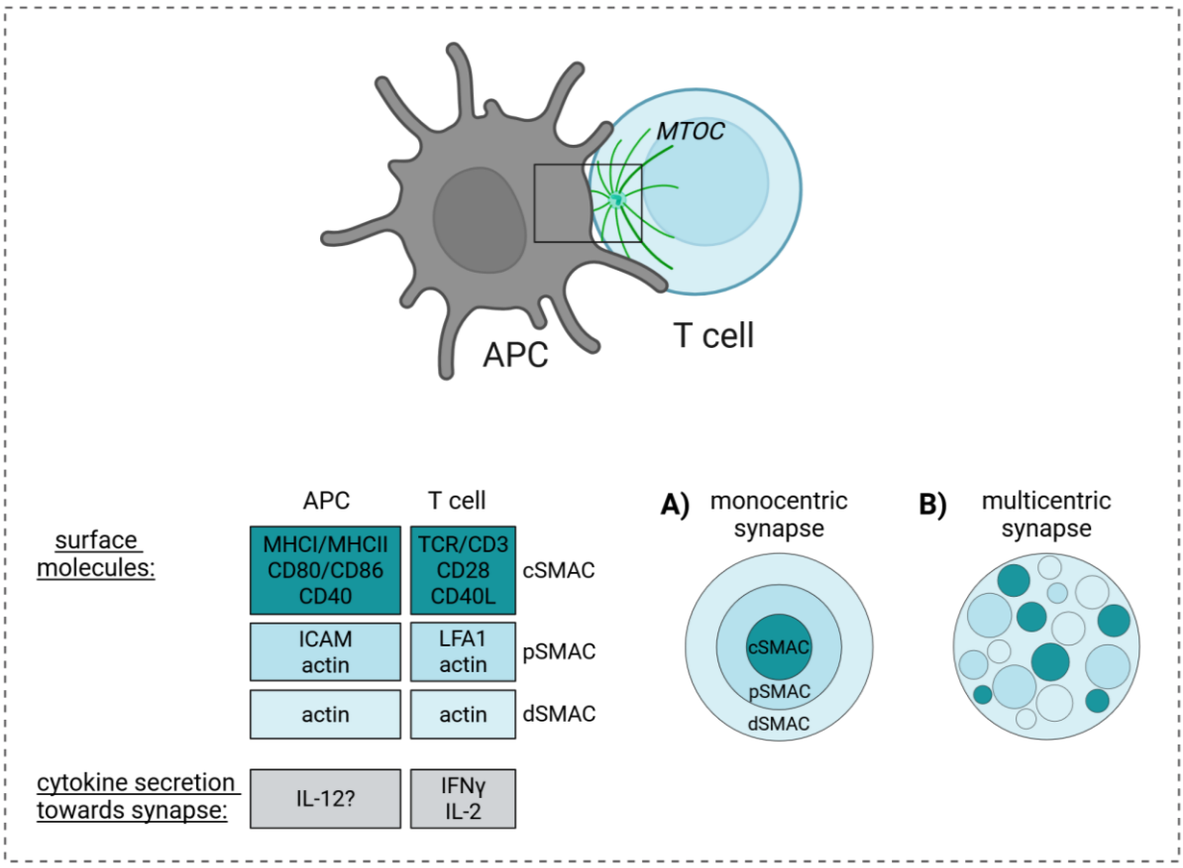

Figure 2.6 Immune synapse structure
APC and T cell form a close cell-cell contact to initiate T cell activation. Variable surface molecules interact on the APC and T cell side either in a monocentric synapse (**A**) with organization of a cSMAC, pSMAC and dSMAC or divided into smaller clusters in a multicentric synapse (**B**). Additionally, some cytokines are secreted in a polarized manner towards the synapse region which allows communication across the interphase. In T cells, MTOC reorientation is also associated with efficient IS formation. Figure created using BioRender.

2.3.2. Communication at the APC – T cell synapse

Communication across the synapse area is established by direct receptor-ligand binding like MHC-TCR and CD80-CD28 or secretory mechanisms such as DC cytokines stimulating T cell differentiation (**Figure 2.6**). T cells in turn secrete exosomes or ectosomes upon antigen-trigger in a polarized unidirectional manner (Mittelbrunn et al. 2011; Choudhuri et al. 2014). Exosomes have been shown to contain micro RNAs which have the capability to alter gene expression in the recipient cell (Mittelbrunn et al. 2011; Okoye et al. 2014). Ectosomes arise from the cSMAC surface area and therefore are enriched in TCR molecules (Choudhuri et al. 2014). Additionally, cytokines like IFN-γ and IL-2 are secreted in a polarized manner which allows high specificity of T cell activation. In contrast, cytokines such as TNF-α and several chemokines can be released non-directionally allowing paracrine communication with surrounding cells (Huse et al. 2006). Further studies are necessary to clarify the role of different routes

and secretion mechanisms to sort cytoplasmic and membrane-associated cargo during IS communication.

Focusing on the DC side, directional secretion of IL-12 to $CD8^+$ T cells during synapse formation has been reported (Pulecio et al. 2010). Intriguingly, a study showing that IL-12 production in DCs is driven by efficient DC-T helper cell interaction did not report IL-12 localization to the synapse (Bertrand et al. 2010). Moreover, recruitment of CD40L to the synapse region on the T cell side is required for the induction of cytokines such as IL-12 in DCs but the CD40-CD40L axis is not required for expression of co-stimulatory molecules in DCs (Tourret et al. 2010; Ferrer et al. 2012). Further, the crosstalk between $CD4^+$ T cells and DCs has anti-apoptotic and survival effects on DCs which are also mediated via CD40 signaling (Riol-Blanco et al. 2009; Miga et al. 2001). Taken together, these results provide only a glimpse into the complex nature of this contact, which is fundamental for the induction of the immune response.

2.4. Function of the microtubule cytoskeleton during immune synapse formation

2.4.1. Centrosome localization and dynamics

General functions of the MT cytoskeleton have been described in chapter 2.1.2. Here, more detailed information on the role of the cytoskeleton for IS formation and functionality will be provided.

In T and NK cells, centrosome repositioning towards the interacting cell has been reported to be particularly important for sustained T cell activation signaling and T cell- or NK cell-mediated killing of target cells (Kupfer and Dennert 1984b; Martín-Cófreces et al. 2008; Kupfer et al. 1985; Geiger et al. 1982). More precisely, T cell centrosome reorientation depends on antigen recognition by the TCR (Kupfer and Singer 1989; Sedwick et al. 1999). Centrosome displacement is achieved by MTs docking at the cell cortex to the pSMAC area where LFA1 clusters are present (Kuhn and Poenie 2002). For the next step, two mechanisms are described: either cortical sliding of dynein to the minus-end of MTs pulls the centrosome towards the cell cortex or dynein attaches the MT plus-ends to the cortex and MT-depolymerization from the plus-ends induces force generation and MTOC repositioning (Yi et al. 2013; Kuhn and Poenie 2002). Centrosome movement is accompanied by relocalization of other organelles such as the Golgi apparatus or secretory vesicles in cytotoxic T cells and T helper cells establishing spatial and temporal cell polarization (Kupfer and Dennert 1984b; Ueda et al. 2011). Importantly, perturbance of T helper cell MTOC polarization impairs synapse structure and efficient signaling between DCs and T cells (Tourret et al. 2010). Also B cells use this conserved mechanism of MTOC polarization to enable polarized lysosome secretion which is important for efficient extraction and processing of immobilized antigens (Yuseff et al. 2011; Pineau et al. 2022). In addition to the

observations from antigen presenting B cells, one study shows DC centrosome reorientation during priming of $CD8^+$ T cells which, in turn, promotes secretion of vesicles containing T cell stimulatory molecules (Pulecio et al. 2010). However, other publications focusing mainly on the T cell cytoskeleton or on the T cell priming capacity of plasmacytoid DCs (pDCs) note the absence of DC MTOC polarization (Mittelbrunn et al. 2009; Bouma et al. 2011). Altogether, centrosome polarization to the cell-cell contact site during IS formation is well described in T cells, B cells and NK cells while there are contrary studies on DC centrosome positioning.

2.4.2. Effects of centriole or microtubule loss

After describing a specific localization of the centrosome during immune cell actions, it is not surprising that loss of centrioles impacts the immune response. Depletion of centrioles during B cell development induces cell cycle arrest and apoptosis (Schapfl et al. 2024). However, if B cells lacking centrioles survive, they are able to proliferate and mount a humoral immune response. Experiments depleting centrioles in cytotoxic T cells showed a reduced cytotoxic capacity which is caused by impaired lytic granule biogenesis and perturbed filamentous actin (F-actin) remodeling at the synapse leading to reduced force exertion (Tamzalit et al. 2020). The authors noted residual PCM and MT organization. Thus, they tested the effect of nocodazole-induced MT depolymerization and observed that MTs are important for delivering granules to the cell surface. Particularly, overall cytotoxic capacity was impaired when MTs were depleted; however, the granules that were secreted still localized to the synapse region. This suggests that while the MT cytoskeleton facilitates cytotoxic granule secretion, it does not control the direction of secretion (Tamzalit et al. 2020). Furthermore, MT depletion in T helper cells disrupted polarized secretion of IFN-γ to the synapse region (Huse et al. 2006). In addition, MT depletion as well as perturbance of MTOC polarization in T cells impaired proper localization of CD40L to the IS, resulting in reduced DC activation and subsequent DC IL-12 secretion (Tourret et al. 2010).

In B cells, MTs are crucial for synapse functionality: on the one hand, MT stabilization is required for efficient lysosome secretion and on the other hand, MTs regulate actin ring formation at the synapse (Sáez et al. 2019; Pineau et al. 2022). Thereby, MTs ensure the formation of a single, focused synapse rather than multiple synapses across the cell body, with maintaining a single polarity axis, which may help to effectively stimulate T cells.

Overall, multiple studies report impaired IS formation and efficiency when B or T cells were lacking centrioles or MTs, while the understanding of centriole or MT alterations in other immune cells is still incomplete.

2.5. Aim of the thesis

Cytoskeletal integrity and dynamics are essential for behavior of immune cells. However, precise roles and molecular mechanisms of centrioles and MTs during immune cell functions are only partially understood. For instance, how the centrosome in DCs contributes to IS formation remains largely unknown. With this research, we aim to understand how centrosome integrity, function and organization in DCs impact T cell priming. Therefore, in this project, we manipulated centrosomal components or MT array organization in DCs and investigated the impact on T helper cell activation. Additionally, we focused on the remarkable phenomenon of extra centrioles occurring in DCs, which was reported by previous members of the working group (Weier et al. 2022). While multiple centrioles have long been observed in cancer cells, they have recently been identified in physiological contexts as well, which suggests more diverse functions of the centrosome but to date these functions are rarely described (Guidotti et al. 2003; Schapfl et al. 2024). For example, DCs with multiple centrioles show enhanced directional locomotion and augmented induction of T cell proliferation, although the detailed mechanisms remain unclear (Weier et al. 2022). Thus, we shed light on the organization of multiple centrioles in DCs during antigen-specific T helper cell interactions in single cells and within lymphoid tissues. Ultimately, to elaborate on the effects of centriole multiplication, we thought to perform comprehensive secretome analysis correlating DC centriole numbers with their secretory profiles. In summary, elucidating the function and organization of centrioles and MTs in DCs during IS formation provides novel insights into the initiation of immune responses and might identify potential targets for therapeutic interventions.

3. Materials

3.1. Mice, cell lines, bacteria

Name	Source
CETN2-GFP mice *(CB6-Tg (CAG-EGFP/CETN2)3-4Jgg/J)*	Jackson Laboratory (Higginbotham et al. 2004)
Nur77^{GFP} mice *(B6N.B6-Tg(Nr4a1-EGFP/cre)820Khog/J)*	Jackson Laboratory (Moran et al. 2011)
Flt3-ligand producing hybridoma cells	Prof. Dr. Michael Sixt, IST Austria
GM-CSF producing hybridoma cells	Prof. Dr. Michael Sixt, IST Austria
HEK293T (human embryonic kidney cells)	Sigma-Aldrich
Hoxb8 CETN2-GFP cell line	Prepared by Kiermaier group
One Shot Stbl3 E. coli	Invitrogen
One Shot OmniMAX 2T 1R E. coli	Invitrogen
OT-II mice *(B6.Cg-Tg(TcraTcrb)425Cbn/J)* *(or inter-crossed with B6.SJL-Ptprca Pepcb/BoyJ)*	Prof. Dr. Sven Burgdorf, LIMES, Bonn University or Charles River (Barnden et al. 1998)
wildtype (WT) mice *genetic background: C57BL/6JRcc*	Genetic Resources Centre, LIMES Institute, Bonn University

3.2. Reagents, dyes, kits

Name	Source/Company
2-Chloroacetamide	Thermo Fisher Scientific
Acetonitrile	Thermo Fisher Scientific
ACK Lysing Buffer	Gibco
Agarose	VWR Avantor
Ampicillin	Carl Roth
Ascorbic acid	Sigma-Aldrich
BAMHi-HF	New England Biolabs
Blasticidin	Carl Roth
Bovine serum albumin (BSA)	Sigma-Aldrich
BSMBI	New England Biolabs
C18 solid phase extraction with Evotips	Evosep Biosystems
Cal520	Abcam
Ce3D tissue clearing solution	BioLegend
CellTrace CFSE Cell Proliferation Kit	Invitrogen
CellTrace Far Red Cell Proliferation Kit	Invitrogen
Centrinone	Tocris
CutSmart 10 x Buffer	New England Biolabs
DAPI	Sigma
Dimethylsulfoxid (DMSO)	Sigma
DMEM (Dulbecco's Modified Eagle Medium) Medium	Gibco
DNA loading dye 6x	Thermo Fisher Scientific
Doxycycline	Sigma
DRAQ7 DNA Dye (used 1:500)	BioLegend

EasySep Mouse Naïve $CD4^+$ T cell Isolation Kit	STEMCELL Technologies
eBioscience Foxp3/Transcription Factor Staining Buffer Set	Thermo Fisher Scientific
EDTA (Ethylenediaminetetraacetic acid) (0.5 M), pH 8.0, RNase-free	Life Technologies
EndoFree Plasmid Maxi Kit	Qiagen
Estradiol	Sigma-Aldrich
Fetal bovine serum (FBS)	Gibco
Flt-3-ligand (supernatant from Flt-3-ligand hybridoma cells)	Self-produced (Kiermaier group)
Fluoromount-G Mounting Medium with DAPI	Thermo Fisher Scientific
Formaldehyde 16 %, methanol free	Thermo Fisher Scientific
Gateway BP Clonase II enzyme-mix	Thermo Fisher Scientific
Gateway LR Clonase II enzyme-mix	Thermo Fisher Scientific
GM-CSF (supernatant from GM-CSF hybridoma cells), 250-300 ng/mL	Self-produced (Kiermaier group)
HBSS 10x	Gibco
IL-2 ELISA Kit	Invitrogen
Kanamycin	Carl Roth
LB (lysogeny broth) agar	Carl Roth
LB medium	Carl Roth
Lenti-X Concentrator	Takara
Lipofectamine 2000 Transfection Reagent	Invitrogen
Lipopolysaccharide (LPS)	Sigma-Aldrich
LysC	Wako Chemicals
MagReSyn® Hydroxyl magnetic microparticles	Resyn Biosciences
Monarch DNA Gel Extraction Kit	New England Biolabs
Monarch Plasmid Miniprep Kit	New England Biolabs
Opti-MEM, Reduced Serum Medium	Gibco
Ovalbumin-peptide 323-339 ($ova_{323-339}$)	InvivoGen
Paraffin wax	Sigma
Penicillin/streptavidin	Gibco
Phenol red-free RPMI (Roswell Park Memorial Institute) 1640 Medium	Gibco
Phosphate buffered saline (PBS) (pH 7.4)	Gibco
PJ-34 hydrochloride hydrate	Sigma-Aldrich
Platinum Hot-Start Green PCR Master Mix (2x)	Thermo Fisher Scientific
Polybrene Infection/Transfection Reagent	Sigma-Aldrich
Pretubulysin	Provided by Uli Kazmaier and Laura Schaedel
Quick-Load 1 kb DNA Ladder	New England Biolabs
Rneasy Mini Kit	Qiagen
RPMI (Roswell Park Memorial Institute) 1640 Medium	Gibco
S.O.C. Medium	Thermo Fisher Scientific
SalI-HF	New England Biolabs
Sodium bicarbonate solution, 7.5 %	Sigma
Sodium deoxycholate	Thermo Fisher Scientific
Sucrose	Carl Roth

SYBR Safe DNA Gel Stain	Thermo Fisher Scientific
TaqMan RNA-to-CT 1-Step Kit	Thermo Fisher Scientific
Tissue-Tek O.C.T. Compound	Sakura
TopVision Agarose	Thermo Fisher Scientific
Trifluoracetic acid	Thermo Fisher Scientific
Tris(2-chlorethyl)phosphate	Thermo Fisher Scientific
Triton X-100	Carl Roth
Trypsin	Sigma
UltraPure agarose	Invitrogen
UltraPure DNase/RNase-Free Distilled Water (=ddH_2O)	Gibco
Vybrant DyeCycle Violet Stain (used 1:1000)	Invitrogen
Zombie Aqua Fixable Viability Kit	BioLegend
β-mercaptoethanol (β-ME)	Gibco

3.3. Media and buffers

Name	Components
FACS buffer	PBS + 2 mM EDATA + 2 % FBS
HEK293T cell medium	DMEM + 10 % FBS + 100 U/mL Penicillin, 100 µg/mL Streptomycin
Hoxb8 medium	RPMI-10 medium + 5 % Flt3-ligand containing supernatant + 1 µM Estradiol
RPMI-10 medium	RPMI 1640 + 10 % FBS + 100 U/mL Penicillin, 100 µg/mL Streptomycin + 50 µM β-ME
RPMI-20 medium	RPMI 1640 + 20 % FBS + 100 U/mL Penicillin, 100 µg/mL Streptomycin + 50 µM β-ME

3.4. Antibodies

Antibodies for flow cytometry

Target	Fluorochrome	Clone	Dilution	Company
mouse CCL5	PE	2E9/CCL5	1:300	BioLegend
mouse CD11c	PE	N418	1:500	BioLegend
mouse CD11c	APC	N418	1:500	Thermo Fisher Scientific
mouse CD16/CD32	unconjugated	93	1:100	eBioscience
mouse CD19	PE	6D5	1:500	BioLegend
mouse CD19	Pacific Blue	6D5	1:500	BioLegend
mouse CD4	APC	RM4-5	1:500	BioLegend
mouse CD62L	PE-Cy7	MEL-14	1:500	BioLegend
mouse CD69	FITC	H1.2F3	1:200	BioLegend
mouse CD69	PE-Dazzle	H1.2F3	1:200	BioLegend
mouse CXCL1	Alexa Fluor 594	1174A	1:300	R&D Instruments
mouse IL-6	PE	MP5-20F3	1:300	BioLegend

mouse MHCII (I-A/I-E)	APC-Cy7	M5/114.15.2	1:800	BioLegend
mouse MHCII (I-A/I-E)	eFluor450	M5/114.15.2	1:800	Invitrogen
mouse MHCII (I-A/I-E)	PE-Dazzle	M5/114.15.2	1:600	BioLegend
mouse OX40 (CD134)	BV711	OX-86	1:300	BioLegend

Primary antibodies for immunofluorescence staining

Target	Host Species	Clone	Dilution	Company
mouse acetylated-tubulin	mouse	6-11B.1	1:500	Sigma-Aldrich
mouse α-tubulin	rat	YL1/2	1:500	Invitrogen
mouse CDK5RAP2	rabbit	polyclonal	1:500 (LNs: 1:100)	Sigma-Aldrich
mouse pericentrin	rabbit	EPR21987	1:200 (LNs: 1:100)	Abcam
mouse TCRß chain-Biotin	hamster	H57-597	1:100	BD Bioscience
mouse γ-tubulin	mouse	GTU-88	1:500	Sigma-Aldrich
mouse γ-tubulin	rabbit	polyclonal	1:500	Abcam

Secondary antibodies/dyes for immunofluorescence staining

Target	Conjugate	Host Species	Dilution	Company
mouse IgG (H+L)	Cy3	donkey	1:400	Jackson Immuno Research
mouse IgG (H+L)	Alexa Fluor 647	donkey	1:400	Jackson Immuno Research
rabbit IgG (H+L)	Cy3	goat	1:400	Jackson Immuno Research
rabbit IgG (H+L)	Alexa Fluor 647	donkey	1:400	Jackson Immuno Research
rat IgG (H+L)	Cy3	donkey	1:400	Jackson Immuno Research
Streptavidin	Cy3	-	1:400	Jackson Immuno Research

3.5. Primer

Name	Sequence	Company
Nedd1_pDonR_FW	5'GGGGACAAGTTTGTACAAAAAAGCAGGCTTAATGCAGGAAAACCTCAGATTTGCC3'	Eurofins
Nedd1-rCM1_pDonR_REV	5'GGGGACCACTTTGTACAAGAAAGCTGGGTATTAGTAGATGTGCTCTGTGGG3'	Eurofins
TaqMan Mm01277042_m1 Tbp (TATA-binding protein) FAM		Thermo Fisher Scientific

TaqMan Mm00446190_m1 IL-6 FAM	Thermo Fisher Scientific
TaqMan Mm01302427_m1 CCL5 FAM	Thermo Fisher Scientific
TaqMan Mm04207460_m1 CXCL1 FAM	Thermo Fisher Scientific

3.6. Plasmids

Name	Resistance [bacteria/mammalian cells]	Source	Catalogue number
pDonR221	Kanamycin / -	Invitrogen	12536017
pBactin-Nedd1-mOrange2-rCM1	Ampicillin / -	Frank Bradtke, Addgene	196861
pInd20-blast	Ampicillin / Blasticidin	Addgene	109334
pInd20-blast-Nedd1-mOrange2-rCM1	Ampicillin / Blasticidin	Self-produced	-
psPAX2	Ampicillin / -	Addgene	12260
pMD2.G	Ampicillin / -	Addgene	12259

3.7. Consumables

Name	Source
Cell culture dishes (10 cm)	Greiner Bio-One
Cell strainer (40 µm and 70 µm)	VWR Avantor
Cover glasses (10 mm)	VWR Avantor
Filter tips (10/200/1000 µL)	Sarstedt
Glass bottom dishes (Ø 35 mm): Ø glass 14/20 mm	MatTek
Hard-Shell 96-well PCR plate	Bio-Rad Laboratories
Microscope slides	Epredia
Needles	Braun
Petri dishes (6 or 10 cm)	VWR Avantor or Sarstedt
Plastic tips (10/200/1000 µL)	Starlab
Tubes (15/50 mL)	Sarstedt
Tubes for flow cytometry (5 mL)	Sarstedt
96-well plate, U-bottom, non-treated	VWR Avantor
Cell culture plates (6/12/24/96 wells)	Greiner Bio-One International
Reaction tubes (0.5/1.5/2 mL)	Starlab
Syringe filters (0.22 or 0.45 µm)	Carl Roth
Syringes (2/10 mL)	Braun
Serological pipettes (5/10/25 mL)	Sarstedt

3.8. Laboratory equipment

Device	Company
BD FACS Aria III	BD Biosciences
BD LSR II	BD Biosciences
Bravo automated liquid handling platform	Agilent
Centrifuges (8510R, 5424R, 5415R)	Eppendorf
ChemiDoc MP Imaging System	Bio-Rad Laboratories
Cryotome	Leica CM3050S
Electrophoresis chamber and power supply	Bio-Rad Laboratories
Evosep One LC system	Evosep Biosystems
Heating plate: Cimarec^{+}	Thermo Scientific
HSC Ceramic Hotplate Stirrer	VELP Scientifica
Incubator (5 % CO_2, 37°C)	Binder or Labotec
Incubator/Shaker Innova 44	New Brunswick Scientific
Laminar flow hood	BDK or Nunc
LSM880 with Airyscan module *Objectives: EC Plan-Neofluar 10x/0.30, Plan-Apochromat 63x/1.4 oil DIC*	Carl Zeiss Microscopy
Neubauer improved counting chamber	Marienfeld
Nikon Eclipse Ts2	Nikon
Objective Heater temp control 37-2 digital	Pecon
Pipettes (2.5-1000 µL)	Eppendorf
Plate reader Infinite M200	Tecan
Radio	Terris
Scales (microscale AG285, JB2002-G)	Mettler Toledo
Spectrophotometer NanoDrop 2000	Thermo Scientific
TempController 2000-2	Pecon
Thermocyclers (C1000 Touch Thermal Cycler, CFX Touch Real-Time PCR detection system)	Bio-Rad Laboratories
Thermomixer	Eppendorf
timsTOF Pro 2 mass spectrometer with Aurora Elite CSI 15 cm length x 75 µM inner diameter C18 UHPLC column	Bruker Ionopticks
Vacuum pump BVC Professional	Vacuubrand
Waterbath	VWR Avantor or Memmert

3.9. Software

Software	Company
Affinity Designer 2	Serif
BioRender	BioRender
CFX Manager Software Version 3.1	Bio-Rad
Citavi 6	Citavi
Compass Data Analysis software	Bruker
FACS Diva Software 6.1.3	BD Bioscience
FlowJo X 10.8.1	FlowJo
Graphpad Prism 10	GraphPad
ImageJ v1.54	ImageJ
ImageLab	Bio-Rad
Imaris 10.2.0	Bitplane
ND-1000 V3.5.2	NanoDrop Technologies
Perseus v1.6.15	MaxQuant

TECAN Plate reader software i-control 1.10	Tecan
ZEN 2.3 SPI	Carl Zeiss Microscopy

4. Methods

4.1. Mice

All mice used in this study were bred on a C57BL/6J background and maintained at the institutional animal facilities in accordance with the German law for animal experimentation. Permission of all experimental procedures involving animals was granted and approved by the local authorities (Landesamt für Verbraucherschutz und Ernährung North Rhine-Westphalia [LAVE NRW under AZ81-02.05.40.19.022 and AZ81-02.04.2021.A319]). CETN2-GFP and $Nur77^{GFP}$ mice were purchased from Jackson (CB6-Tg(CAG-EGFP/CETN2)3-4Jgg/J and B6N.B6-Tg(Nr4a1-EGFP/cre)820Khog/J). OVA-specific OT-II mice were a gift of Sven Burgdorf. Alternatively, OT-II mice were purchased from Charles River and intercrossed with B6.SJL-Ptprca Pepcb/BoyJ (congenic CD45.1 mice, also purchased from Charles River) for one generation to obtain heterozygous OT-II CD45.1/2 mice that were then used as donors for the *in vivo* experiments.

4.2. Adoptive transfer experiments

Mouse experiments were performed in collaboration with Luisa Bach from Dirk Baumjohann's group. For *in vivo* DC-T cell interaction experiments, naïve OT-II T cells were isolated using the EasySep Mouse Naïve $CD4^+$ T Cell Isolation Kit according to the manufacturer's instructions. Naïve $CD4^+$ OT-II T cells were labelled with the CellTrace Far Red Cell Proliferation dye at a concentration of 0.5 µM and $2*10^6$ naïve OT-II cells were injected into the tail vein of wildtype mice. After 24 h, $1*10^6$ mature CETN2-GFP expressing BMDCs, which were loaded with 1 µg/mL OVAp, were injected subcutaneously into the hocks of both hind legs. Popliteal and inguinal LNs were harvested after 48 h and incubated in 1 % paraformaldehyde (PFA) in PBS over night at 4°C. Subsequently, LNs were washed with PBS and dehydrated in a sucrose gradient (10 % - 30 % sucrose in PBS). LNs were embedded in cryomedium (Tissue-Tek O.C.T. Compound) and stored at -80°C until they were cut into 20 µm thick sections.

4.3. Cell isolation, generation and culturing

4.3.1. BMDC generation and culture

Femurs and tibias from legs of 3–5 month-old CETN2-GFP expressing mice were removed and placed in 70 % ethanol for 2 min. Bone marrow was flushed with PBS using a 26 gauge needle. $2*10^6$ cells were seeded per 10 cm petri dish containing 9 mL of RPMI-10 medium and 1 mL of granulocyte-macrophage colony-stimulating factor (GM-CSF). On day 3 and 6 RPMI-10 medium supplemented with 20 % GM-CSF was added to each dish. To induce DC maturation, cells were stimulated overnight (starting day 7 or 8) with 200 ng/mL LPS and used for experiments on day 8 or 9. Alternatively, DCs were frozen in FBS containing 10 % DMSO on day 7 and for experimental use, they were thawed the day before the experiment and stimulated with 200 ng/mL LPS overnight.

4.3.2. BMDC drug treatments

To prevent new pro-centriole formation BMDCs were cultured in the presence of the PLK4 inhibitor Centrinone (250 nM or 500 nM) or control (solvent DMSO) during differentiation and maturation. To induce microtubule depolymerization, cells were treated with 1 µM pretubulysin or control (solvent DMSO) after antigen-loading either for 1 h or for the duration of the experiment. Cells were washed (wash-out) or not (w/o wash-out) with full media before T cell addition. To induce centrosome de-clustering PJ-34 was used. Cells were loaded with OVAp for 2 h and subsequently treated with 50, 100 or 200 µM of PJ-34 or control (solvent H_2O) for 3 h. Cells were washed two times with RPMI-10 medium and incubated with OT-II-specific T cells at the indicated time points.

4.3.3. Hoxb8 CETN2-GFP Nedd1-mOrange2-rCM1 cell line generation and differentiation

To boost MT nucleation in DCs, we were inspired by the recent publication of Vinopal et al. (2023) showing that Nedd1-rCM1 overexpression in neurons induces elevated MT nucleation events. For manipulating DCs, we made use of a hematopoietic progenitor cell line (Homeobox b8: Hoxb8) expressing CETN2-GFP which was already described in (Redecke et al. 2013; Weier et al. 2022). Shortly, this cell line was generated by retroviral introduction of an estrogen-regulated form of the Hoxb8 TF into bone marrow cells of CETN2-GFP expressing mice (virus plasmid: addgene #212932). Hoxb8 CETN2-GFP cells were cultured in the presence of estradiol to retain the progenitor cell stage. Estradiol removal and GM-CSF addition induces the differentiation into the DC lineage.

Generation of pInd20-blast-Nedd1-mOrange2-rCM1 plasmid

We are very thankful that we got a plasmid containing the sequence of Nedd1-mOrange2-rCM1 fusion protein from Frank Bradtke.

Nedd1-mOrange2-rCM1 was cloned into the pInd20-blast vector using the Gateway strategy (see plasmid scheme **Figure 4.7**). All kits were used according to the manufacturer's protocols unless stated otherwise.

First, we performed a PCR, which creates overlaps, with the Platinum Hot-Start Green PCR Master Mix and the primers Nedd1_pDonR_FW and Nedd1_rCM1_pDonR_REV according to **Table 1**. After checking the correct size on an agarose gel, we extracted the DNA from the gel using the Monarch DNA Gel Extraction Kit. Next, performing the BP reaction (recombination between attB and attP sites) with the Gateway BP Clonase II enzyme-mix introduces the PCR product into the pDonR221 vector. The resulting plasmid was transformed into One Shot OmniMAX 2T 1R E. coli and colonies grown on Lysogeny Broth (LB) agar plates with 50 µg/mL kanamycin antibiotics at 37°C. Next day, colonies were selected and bacteria grown in LB medium overnight at 37°C. Then, DNA was extracted using the

Monarch Miniprep Kit. After restriction enzyme digest with BAMHi-HF and SalI-HF using the CutSmart Buffer, the correct plasmid size was checked on an agarose gel. For additional confirmation of the correct sequence, the plasmid was sent for sequencing (Eurofins). Afterwards, ligation-recombination (LR) reaction with the Gateway LR Clonase II enzyme-mix introduces the protein sequence into pInd20-blast vector which contains the gene for blasticidin S deaminase leading eventually to a Blasticidin resistant cell line (**Figure 4.7**). In addition, this plasmid contains components of Tet-on system (**Figure 4.7**). Mechanistically, in the Tet-On system, added doxycycline can bind to the reverse tetracycline-controlled transcriptional activator (rtTA), which is constitutively expressed under the ubiquitin C (UbC) promoter (Gossen et al. 1995). The doxycycline-rtTA complex then binds to the tetracycline response element (TRE), activating transcription of the target gene. The resulting plasmid was transformed into One Shot Stbl3 E. coli and colonies grown on agar plates with 50 µg/mL kanamycin antibiotics. Next day, colonies were selected and bacteria grown in LB medium overnight. Then, DNA was extracted using the Monarch Miniprep Kit. After restriction enzyme digest with BSMBI using the CutSmart Buffer, the correct plasmid size was checked on an agarose gel. The bacterial culture in LB medium was expanded overnight and the EndoFree Plasmid Maxi Kit used to extract the DNA.

Temperature	Incubation time
94°C	2 min
94°C 66°C 72°C	30 sec 30 sec 3 min ➔ 35 cycles
72°C	10 min

Table 1: PCR protocol for creating Gateway overlaps

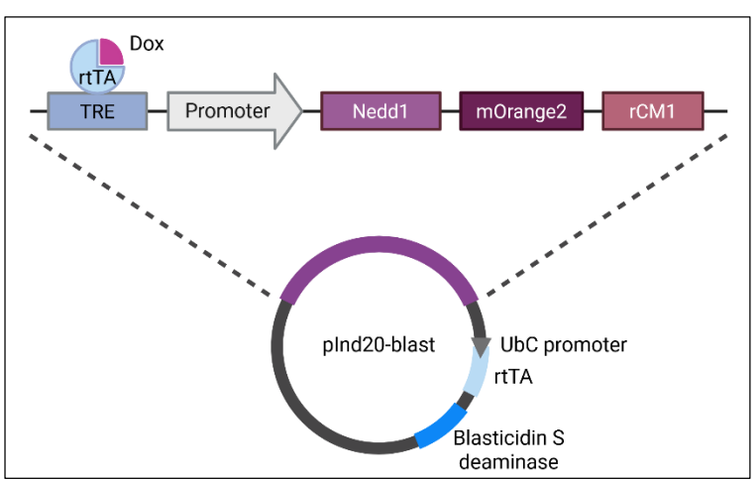

Figure 4.7 Scheme of pInd20-blast vector with Nedd1-mOrange2-rCM1 sequence and Blasticidin resistance gene

Lentivirus production in HEK293T cells

For lentivirus production, $3.8*10^6$ HEK293T cells were plated in 7.5 mL DMEM in a 10 cm culture dish. The next day, medium was changed to Opti-MEM. A plasmid mixture of psPAX2, pMD2.G and the transfer plasmid pInd20-blast-Nedd1-mOrange2-rCM1 was prepared in a ratio of 2:3:4 and a total DNA amount of 12.1 µg in 0.7 mL Opti-MEM. 40 µL Lipofectamin-2000 were mixed with 0.7 mL Opti-MEM. Both suspensions were incubated for 5 min before combining and waiting for additional 10 min. Next, the plasmid-lipofectamine mixture was added gently onto HEK293T cells. After 5 h, medium was changed to 7.5 mL DMEM. The virus was harvested after 48 h and three times concentrated using the Lenti-X Concentrator.

Lentivirus infection of Hoxb8 CETN2-GFP cell line

For infecting the CETN2-GFP expressing Hoxb8 progenitor cells with the lentivirus containing Nedd1-mOrange2-rCM1 DNA sequence, $3*10^5$ Hoxb8 cells were plated in a 12-well plate in 1 mL Hoxb8 medium. 500 µL of virus-containing supernatant and polybrene (final concentration 6 µg/mL) were added. Plates were centrifuged for 1 h at 1 500 x g at 30°C. 1.5 mL fresh Hoxb8 medium was added and the cells cultured at 37°C and 5 % CO_2. After 3 days, selection of transfected cells was started by adding 10 µg/mL Blasticidin to the medium. When control cells without virus infection were dying, cell selection was considered complete and the new Hoxb8 Nedd1-mOrange2-rCM1 cell line frozen, cultured at a progenitor cell level or differentiated into Hoxb8-derived DCs.

Differentiation of Hoxb8 progenitor cells into DCs

For differentiation of Hoxb8 progenitor cells into DCs, estradiol was removed by two times washing with RPMI-10 medium (see composition 3.3 Media and buffers). Next, $3*10^5$ cells were plated on a 10 cm dish with 10 mL RPMI-10 medium containing 10 % GM-CSF. Blasticidin was continuously included in the medium throughout differentiation to maintain selection pressure. On day 3 and day 6 of culture, 10 mL RPMI-10 medium containing 20 % GM-CSF were added to each dish. To induce DC maturation, cells were harvested on day 7 or 8 and stimulated overnight with 200 ng/mL LPS. For inducing Nedd1-mOrange2-rCM1 overexpression, doxycycline (2 µg/mL) was added from day 3 of differentiation until full maturation. Mature Hoxb8-derived DCs were used for MLRs as described in 4.4.3).

4.4. Cell-based assays

4.4.1. Flow cytometry

For flow cytometric analysis, cells were washed with PBS once and incubated 10 min with anti-CD16/CD32 antibody (1:100) in FACS buffer. Staining with fluorescently labelled antibodies diluted in FACS buffer was carried out for 20 min at 4°C. For intracellular cytokine staining, cells were fixed and permeabilized with the Foxp3/Transcription Factor Staining Buffer Set according to the manufacturer's protocol. The used antibodies are listed in chapter 3.4. For live dead staining DRAQ7 (1:500) or the Zombie Aqua Fixable Viability Kit was used. After staining, cells were washed once with FACS buffer and data acquired at the LSRII flow cytometer. Data analysis was performed using FlowJo v10.8.1.

To determine T cell activation via CD69 upregulation and CD62L downregulation, DC co-cultures with splenocytes were analyzed after 20-22 h via flow cytometry. OX40 upregulation on the T cell surface was determined after 2.5 days. T cell proliferation rates were assessed by dilution of CFSE after 2.5 days of co-culture. To this end, prior to incubation with DCs, splenocytes were stained with a final concentration of 0.5 µM CFSE for 7 min at 37°C in PBS and washed with RPMI-10 medium. Nur77-dependent GFP upregulation was also determined via flow cytometry after the indicated timepoints of naïve $CD4^+$ T cell co-culture with DCs.

4.4.2. Sorting of 2N BMDCs

To sort DCs based on their DNA content, mature BMDCs were harvested and stained with Vybrant DyeCycle Violet Stain (1:1000) in RPMI without phenol red for 20 min at 37°C. Cells were sorted at the ARIAIII Sorter according to their ploidy level with focusing on diploid cells (2N) and dismissing polyploid cells. Additionally, for some experiments cells were further separated into two DC 'subpopulations' according to CETN2-GFP signal intensities resulting in CETN2-GFP^{low} and CETN2-GFP^{high} cells. DCs were re-analyzed after the sort to ensure purity of the individual subpopulations. Afterwards, cells were recovered in RPMI-10 medium at 37°C for at least 30 min.

4.4.3. Mixed lymphocyte reactions (MLRs)

For DC-T cell co-culture assays sorted DCs (1-2*10^4 cells/well) were seeded in 96-well U-bottom plates. After recovering time of 30 min, cells were incubated with OVAp antigen ($OVA_{323-339}$: specifically recognized by $CD4^+$ OT-II T cells; 0.01 µg/mL, 0.1 µg/mL, 1 µg/mL) or without OVAp (controls) for 2 h. In the meantime, splenocytes were isolated from OT-II mice or $Nur77^{GFP}$/OT-II mice. Therefore, splenic, inguinal, axillary and brachial LNs were removed and smashed through a 70 µm filter using PBS and a syringe piston. After centrifugation (400 x g 5 min), ACK lysis buffer was added for 5 min at room temperature (RT) before stopping the red blood cell lysis with PBS containing 2 % FBS and 2 mM

EDTA. Cells were filtered through a 40 µm filter, centrifuged and adjusted to the respective cell number to co-culture with DCs or for subsequent naïve $CD4^+$ T cell isolation. Naïve $CD4^+$ T cell isolation was performed according to the manual of the EasySep Mouse Naïve $CD4^+$ T Cell Isolation Kit. After removing the antigen from the DCs, T cells were added in a ratio of 1:2 or 1:5 (DCs:T cells).

4.4.4. Under-agarose interaction assay

To monitor centrioles during live cell imaging, DC-T cell co-cultures were injected under a block of agarose. This prevents cell floating during the imaging period and allows visualization of centrioles within a single z-plane. Therefore, a custom-made chamber was built by gluing a 1 cm plastic ring with paraffin into a glass-bottom dish. 1 % agarose solution was prepared by mixing 0.2 g UltraPure agarose with 5 mL water, 5 mL 2x HBSS and 10 mL phenol red-free RPMI-20 medium. For live cell imaging, ascorbic acid was added to a final concentration of 50 µM. 500 µL of the heated agarose was poured into each chamber. After polymerization, the dishes were filled with water around the agarose and incubated for 45-60 min at 37°C, 5 % CO_2 to equilibrate the agarose. For the experiment, cells were injected with a 10 µL tip under the agarose in a volume of 0.4-0.6 µL. To allow visualization of interaction during time-lapse imaging T cells were stained with the Calcium-sensitive dye Cal520 (Ca^{2+}-Cal520) prior to injection. For efficient staining, T cells were incubated with 3 µM Cal520 in phenol red-free RPMI-20 medium for 30 min at 37°C. To avoid toxic effects, the dye was efficiently removed by washing two times. Live cell imaging was started directly after injection of DCs and T cells. Alternatively, to allow immunofluorescence staining in flattened cells, cells were fixed after 60-90 min incubation with 4 % paraformaldehyde (PFA) solution overnight at 4°C. On the following day, the agarose was carefully removed and the cells were washed with PBS two times before staining. For assessing MT numbers in Nedd1-mOrange2-rCM1 expressing Hoxb8 CETN2-GFP-derived DCs, Shaunak Ghosh kindly helped with under agarose cell injection.

4.5. Biochemical and molecular biology assays

4.5.1. IL-2 ELISA of MLR

For quantification of IL-2 cytokine levels via ELISA, DCs and T cells were co-cultured as described above (MLR). $5*10^4$ DCs and $10*10^4$ T cells were co-cultured in 200 µL culture volume for 20 h. Supernatants were harvested and incubated with the mouse IL-2 ELISA Kit according to the manufacturer's instructions.

4.5.2. mRNA expression levels

For mRNA quantification after PJ-34 treatment, $1*10^6$ BMDCs were harvested in 350 µl Lysis Buffer (RNeasy Lysis Buffer + 1 % ß-Mercaptoethanol), and RNA isolation was carried out using the RNeasy Mini Kit. RNA concentration was determined using Nanodrop 1000 spectrophotometer. Gene expression was assessed using the TaqMan RNA-to-CT 1-Step Kit with a reaction volume of 20 µL containing 250 ng RNA template and 1 µL of Taq Man Gene Expression Assay (duplicates performed). Samples were run on a CFX96 Real-Time System according to the manufacturer's instructions. Data were normalized according to the expression of a housekeeping gene in DCs (TATA-binding protein). Analysis of relative gene expression was carried out using the CFX Manager Software Version 3.1.

4.5.3. Immunofluorescence

Cells were immobilized by incubating 1-2 µL of cell suspension on cover slips for 5 min at 37°C before adding 4 % PFA for 20 min. For MT staining, cells were fixed after injection under agarose as described above. Fixed cells were washed twice with PBS for 10 min. To allow intracellular antibody staining cells were permeabilized adding 0.2 % Triton X-100 in PBS for 30 min at room temperature. After washing 3 × 10 min with PBS samples were incubated in blocking solution (5 % BSA in PBS) for 1 h to prevent unspecific binding of the antibodies. Next, samples were incubated with primary antibodies diluted in blocking solution over night at 4°C. Staining for PCNT was carried out for 1 h at room temperature. Afterwards, cover slips were washed 3 x 10 min with PBS and stained with secondary antibodies diluted in blocking solution in the dark for 1 h at room temperature. After three times washing 10 min with PBS cover slips were mounted with DAPI-containing mounting medium and sealed with nail polish prior to imaging. The utilized primary and secondary antibodies are listed in chapter 3.4.

Staining of cryosections

Staining of cryosections was carried out at room temperature. Sections were permeabilized with 0.3 % Triton X-100 in PBS for 10 min and then blocked with 1 % BSA in 0.3 % Triton X-100 in PBS for 30 min. All primary and secondary antibodies were used in a dilution of 1:200 in 1 % BSA in 0.3 % Triton X-100 in PBS. Sections were incubated with primary antibodies overnight. After washing 3 x 10 min with PBS, secondary antibodies were added for 2 h. DAPI staining (1:1000 in PBS, Stock 1 mg/mL) was carried out for 30 min. After 3 × 10 min washing in PBS, sections were incubated in Ce3D tissue clearing solution for at least 2 h and then mounted with mounting medium.

4.6. Microscopy and image analysis

Confocal microscopy was performed on a motorized stage at room temperature with an inverted microscope equipped with an Airyscan module; an EC Plan-Neofluar 10×/0.30 objective; a Plan-Apochromat 63×/1.4 oil DIC objective; 488, 561, and 633 laser lines; and a photomultiplier tube (all Zeiss). For fixed samples 0.2 µm sections were acquired leading to z-stacks of mostly 4-8 µm height (cells) or 16-20 µm height (tissue samples). To analyze MT filaments, images were acquired using the Airy module and posttreated by deconvolution. The same confocal imaging set up was used for live cell imaging. During live cell acquisition, dishes were placed in a 37°C chamber and cells imaged at a 10 to 20 second interval for 30-60 min. The auto-focus option was used to keep the centrioles in focus. For all experiments, imaging software ZEN Black 2.3 SP1 was deployed.

Image analysis

Image processing and data analysis was performed using ImageJ. Centriole numbers were determined manually from multi-z-stack images by counting individual CETN2-GFP$^+$ foci co-localizing with a PCM marker (γ-tubulin, CDK5RAP2, PCNT) or acetylated-tubulin. Quantitative intensity measurements were carried out on maximum z-projections measuring RAW integrated density or integrated density of selected region of interests (ROIs). ROIs around the centrioles were selected by keeping the same size (~ 8 µm², see also **Figure 5.10 a**). Overlapping cells were excluded from the analysis. For determining intracellular MT numbers, MT filaments were counted manually at a defined round-shaped area (25 µm²) around the centrioles or acentriolar MTOCs (see also **Figure 5.10 c**). All z-planes were used to precisely detect individual MT filaments. Tracing of MTs was carried out with the NeuronJ plugin using maximum z-projections. MTOCs were defined by the following criteria: *i)* a clear PCM foci (γ-tubulin, CDK5RAP2 or PCNT) is visible, which *ii)* nucleates MT filaments from the respective region.

For measurements of distances between or from centrioles, maximum z-projections of fixed samples were used to determine centriole coordinates in two dimensions leading to x and y values. However, whole confocal stacks were used to determine the position of the T cell's centrosome and identify cell-cell contacts. In time lapse videos, centrioles were tracked by using the Manual Tracking plugin. Obtained coordinates were used to calculate the centriole center point (CP) coordinates using the following formulas: $x_{CP} = \frac{\sum x_n}{n}$ *and* $y_{CP} = \frac{\sum y_n}{n}$ with n: number of single centriole.

In maximum z-projections of fixed samples as well as in time lapse videos, cell outlines were marked with the 'freehand selection' tool. Subsequent measurement of this ROI revealed area and centroid. Distances between two points were calculated using the formula: distance $d = (x_2\text{-}x_1)^2+(y_2\text{-}y_1)^2$.

3D reconstruction of DC-T cell contacts in LNs

DCs, their nuclei and centrioles, and T cells were 3D reconstructed from z-stacks of LN sections by Philip Weidner and Stefan Uderhardt. Therefore, 3D TIF files were processed and analyzed using Imaris 10.2.0 (Bitplane) for quantitative analysis. T cells and DCs and their respective nuclei were segmented based on DAPI staining or cytoplasmic fluorescence signals from either the CellTrace Far Red Cell Proliferation dye (T cells) or from CETN2-GFP expression (DCs). The built-in watershed algorithm in Imaris was used for cell boundary delineation, and centriole detection utilized the 'spots' function with automated size filtering, followed by 3D distance calculations between paired structures using Imaris' measurement function. All volumetric reconstructions were generated through Imaris' integrated rendering engine.

4.7. Mass spectrometry measurement and data analysis

BMDCs were sorted into diploid cells and further into two DC 'subpopulations' according to CETN2-GFP signal intensities. The resulting CETN2-GFP^{low} and CETN2-GFP^{high} cells were immobilized and the centriole numbers quantified according to CETN2-GFP^{+}/γ-tubulin^{+} foci. In addition to cell immobilization, sorted DCs were recovered for 30 min at 37°C and 5 % CO_2 at a cell concentration of $0.8*10^6$ cells/mL. Cells were washed two times with FBS-free medium and then cultured for 20 h in FBS-free medium before supernatant was harvested and frozen until mass spectrometry (MS) sample preparation. Following MS sample preparation, measurement and analysis was thankfully carried out by Stefan Ebner (group of Felix Meissner).

A detailed outline of the protein aggregation capture (PAC) method is provided in (Batth et al. 2019). Therefore, 20 µL DC supernatants were denatured in 1 % sodium deoxycholate (SDC) in 50 mM Tris pH 8.5. Proteins were reduced with 10 mM Tris(2-chlorethyl)phosphate and alkylated with 2-Chloroacetamide in the dark for 10 min at 90°C while shaking. Supernatant proteins were cooled to 4°C on ice. Sample preparation was performed using the Bravo automated liquid handling platform (Agilent). Per sample, 1 µl MagReSyn® Hydroxyl magnetic microparticles (20 mg/mL suspension) were equilibrated in 70 % acetonitrile (ACN) and washed twice with 70 % ACN. Beads were collected at the bottom of a 96-well plate, ACN was removed and samples were added to the beads. ACN was added to achieve a total concentration of 70 % before incubation for 10 min to achieve on-bead protein precipitation. Protein-loaded beads were placed on a magnetic rack to clear and the supernatant was discarded. Beads were washed with 100 % ACN, then 70 % ethanol and finally resuspended in 50 mM Tris pH 8.5, containing 5 ng Trypsin and LysC per sample, to digest for 5 h at 37°C on a Thermomixer (800 rpm). Digestion was quenched with 1 % trifluoracetic acid (TFA). The digested peptides were

collected and pooled with a second washout of the magnetic beads with 1 % TFA. Peptides were cleaned up using C18 solid phase extraction with Evotips, following the manufacturer's instructions. Samples were measured with the Evosep One LC system coupled to a timsTOF Pro 2 mass spectrometer (Bruker) using an Aurora Elite CSI 15 cm length x 75 µM inner diameter C18 UHPLC column. Peptides were separated using the Whisper 40 SDP method over a 31 min non-linear gradient of 0-80 % buffer B (0.1 % formic acid in acetonitrile), with a constant flow rate of 100 nL/min and the column oven temperature set to 50°C. The mass spectrometer was operated in data-independent acquisition (DIA) mode, combined with parallel accumulation-serial fragmentation (DIA-PASEF) with optimized scan windows, excluding singly charged ions and covering a survey scan range of 300 to 1200 m/z (mass to charge ratio) with variable windows using Python package for DIA with an automated isolation design (py_diAID) according to (Skowronek et al. 2022). MS data was acquired using the Compass Data Analysis software (Bruker). MS/MS spectra were searched against the mouse UniProt FASTA database (Swissprot, updated 2022.12.28) and a common contaminant database with the proteomics platform Spectronaut (Ver. 18, Biognosys). The digestion modes Trypsin/P and LysC/P were used, with a minimum peptide length of 7 aa and a maximum of two missed cleavages. Cysteine carbamidomethylation was set as a fixed, methionine oxidation and N-terminal acetylation as variable modifications. A false discovery rate (FDR) of 1 % was used on peptide and protein level. Peptide identification was performed with an allowed initial precursor mass deviation of up to 4.5 ppm and an allowed fragment mass deviation of 20 ppm.

Quality control and statistical analysis of MS/MS data was performed using Perseus (Ver. 1.6.15, (Tyanova et al. 2016)). Protein groups were filtered for potential contaminants, decoys and modifications. Intensities were Log2 transformed. Missing values were imputed from a normal distribution with an imputation window of 0.3 and a downshift form the normal distribution of 1.8. Euclidean distance clustering was performed to visualize significantly changing hits identified by one-way ANOVA (analysis of variance) across all samples. Two-sided t-tests were performed and visualized in a volcano plot (FDR cutoff = 0.05; S_0 = 0.1). As quality control, the metrics number of protein groups, protein occurrence in samples and molecular weight bias were checked.

4.8. Statistical analysis

Data analysis was carried out with GraphPad Prism 10. Samples were tested for Gaussian distribution using D'Agostino-Pearson omnibus normality test to fulfill the criteria for performing Student's *t*-tests. Welch's correction was applied when two samples had unequal variances. When data distribution was not normal, Mann-Whitney test was carried out. For small data sets, Gaussian distribution was

assumed but could not be formally tested. For analysis of Nur77^{GFP} expression, CETN2-GFP^{low} and CETN2-GFP^{high} samples derived from one DC differentiation batch were paired. For multiple comparisons where data distribution was normal, one-way ANOVA was used followed by Dunnett's multiple comparisons as post-hoc test. When data distribution was not normal, Kruskal-Wallis test with Dunn's multiple comparisons was used. All graphs display mean values $\pm$ s.d. (95 % Confidence Interval) unless otherwise specified in the figure legends. Investigators were not blinded during experiments and outcome assessment, except for counting MT numbers in Nedd1-mOrange2-rCM1 expressing Hoxb8 CETN2-GFP-derived DCs. Individual experiments were validated separately and only pooled if showing the same trend. The level of significance is denoted in the figure legends.

5. Results

5.1. Centrosome and MT integrity in DCs are required for T cell priming

To investigate the role of the centrosome in APCs for T cell priming, we used antigen-presenting DCs derived from bone marrow of CETN2-GFP expressing mice. Cells were differentiated using GM-CSF and subsequently stimulated with LPS overnight to induce cell maturation. Mature BMDCs are a heterogenous population of diploid (2N) and tetraploid (4N) cells, arising from incomplete mitosis (Weier et al. 2022). To exclude effects due to polyploidy, BMDCs were separated based on DNA content into 2N and 4N cells (**Figure 5.8 a**). Unless otherwise stated, all subsequent experiments were performed exclusively on the 2N cell fraction.

To initiate adaptive immune responses, DCs form antigen-specific contacts with T cells. In our experimental system, BMDCs were incubated with or without the model antigen ovalbumin-peptide (OVAp) and then co-cultured with (naïve) $CD4^+$, OVA-specific T cells, which express a transgenic TCR recognizing the OVAp (OT-II T cells). Under these conditions, BMDCs established contacts with either one or multiple T cells, even in the absence of antigen, consistent with previous reports (**Figure 5.8 b**) (Mittelbrunn et al. 2009; Benvenuti et al. 2004). T cells were efficiently activated, which was measured by the upregulation of CD69 and downregulation of CD62L on the T cell surface (**Figure 5.8 c** and **d**). T cell proliferation was evaluated by proliferation-mediated dilution of the fluorescent dye carboxyfluorescein succinimidyl ester (CFSE) (**Figure 5.8 e** and **f**) (Quah et al. 2007).

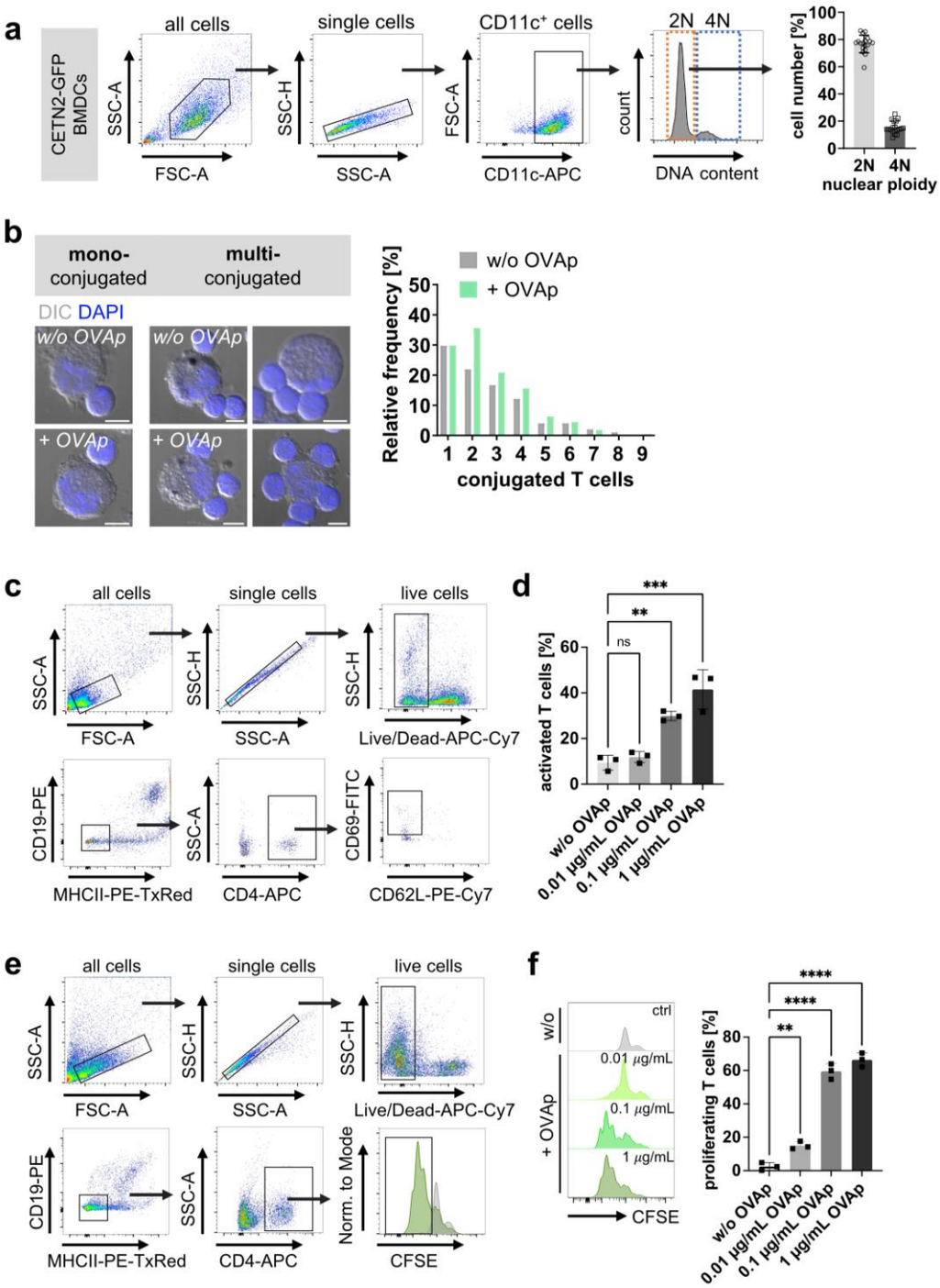

Figure 5.8 Sorted diploid BMDCs induce antigen-specific T cell activation and proliferation
(**a**) DNA staining of mature CETN2-GFP expressing BMDCs to determine nuclear ploidy. Gating strategy for identification of 2N and 4N DCs and histogram of DNA content distribution of CD11c$^+$ cells. Graph displays mean values ± s.d. of 18 independent experiments. (**b**) Left: Merged channels of differential interference contrast (DIC, grey) and DAPI (blue) of DC-T cell conjugates after 2 h co-culture without (upper panels) or with (lower panels) previous OVAp loading. Scale bars, 5 µm. Right: Quantification of frequency distribution of bound T cells per DC. Graph displays normalized values ± s.d. *N* = 397 (w/o OVAp) /225 (+ OVAp). (**c**) Gating strategy for analyzing CD69$^+$/CD62L$^-$ activated CD4$^+$ T cells in the absence of antigen (w/o OVAp) or in the presence of different OVAp concentrations. (**d**) Quantification of T cell activation. Graph shows mean values ± s.d. of three technical replicates of one out of four independent experiments. ***, P* < 0.0021; ****, P* < 0.001 (one-way ANOVA with Dunnett's multiple comparisons). (**e**) Gating strategy for quantifying T cell proliferation via CFSE dilution in the

absence of antigen (w/o OVAp) or in the presence of OVAp. (**f**) Quantification of T cell proliferation. Histograms show CFSE signal of $CD4^+$ T cells for different OVAp concentrations. Graph shows mean values ± s.d. of three technical replicates of one out of four independent experiments. ***, P* < 0.0021; *****, P* < 0.0001 (one-way ANOVA with Dunnett's multiple comparisons). (**a, d, f**) *N* = 10.000 cells per condition.

To investigate the function of centrioles, BMDCs were treated with the PLK4 inhibitor Centrinone during differentiation and maturation to inhibit the formation of new daughter centrioles (**Figure 5.9 a**) (Wong et al. 2015). BMDC differentiation was not affected by Centrinone treatment, which is shown by upregulation of DC-specific surface markers CD11c and MHCII (**Figure 5.9 b** and **c**). The frequency of diploid cells was mildly reduced indicating the interplay of centriole numbers and cell cycle progression (**Figure 5.9 c** right). Focusing on diploid cells, quantification of centriole numbers showed complete depletion of CETN2-GFP^+ foci in more than 40 % (250 nM Centrinone) or 60 % (500 nM Centrinone) of all mature cells (**Figure 5.9 d**). As Centrinone treatment only prevents new procentriole formation but does not deplete existing centrioles, 2N BMDCs displayed a mixed population of cells with no, one, two, three or four, or more than four centrioles.

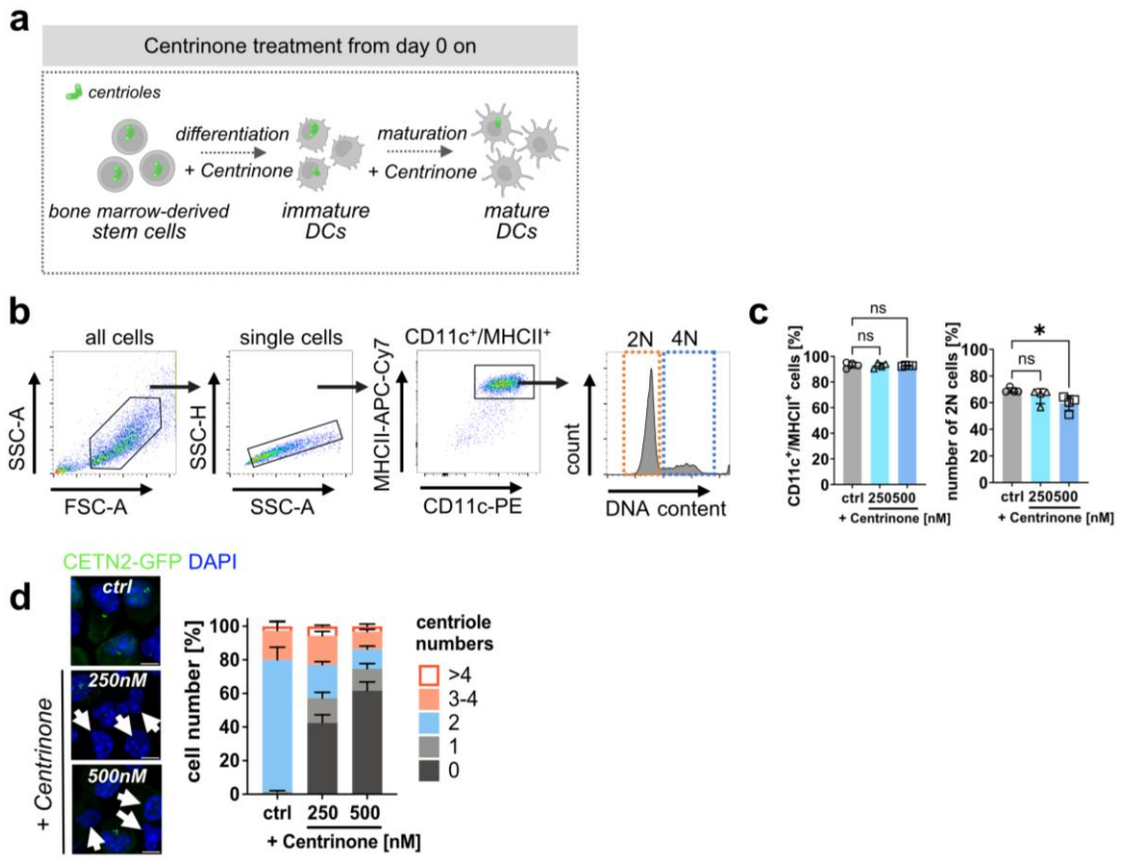

Figure 5.9 Centrinone treatment of BMDCs during differentiation results in cells lacking centrioles
(**a**) Schematic representation of experimental set-up of Centrinone-treatment created with BioRender. (**b**) Gating strategy to assess DC differentiation in Centrinone-treated and control cells. Mature DCs were identified as $MHCII^+/CD11c^+$ cells and further analyzed for DNA content. (**c**) Quantification of $MHCII^+/CD11c^+$ (left graph) and 2N (right graph) cells in Centrinone-treated and control cells. Graphs show mean values ± s.d. of 4

independent experiments with cells derived from 4 different mice. *N* = 10.000 cells analyzed per condition. (**d**) Confocal images of 2N Centrinone-treated and control cells. Maximum z-projections of merged channels of CETN2-GFP (green) and DAPI (blue) are shown. White arrowheads indicate cells without centrioles. Scale bars, 5 µm. Graph shows quantification of centriole numbers after Centrinone treatment. Mean values ± s.d. of three independent experiments with *N* = 224/259/176 (ctrl), 207/263/135 (250 nM Centrinone), 247/210/146 (500 nM Centrinone) cells are displayed.

To elucidate the effects of centriole depletion on PCM recruitment and MTOC function, immunofluorescence staining of the PCM protein γ-tubulin was performed. This showed a reduction in γ-tubulin signal in Centrinone-treated BMDCs compared to control cells (**Figure 5.10 a**). However, we observed residual PCM staining in cells lacking centrioles, which prompted us to examine MT organization in cells lacking centrioles. Visualization of MT filaments was achieved by staining with an α-tubulin antibody followed by high-resolution microscopy. This enabled us to quantify MTs within a defined area surrounding PCM and/or CETN2-GFP$^+$ foci (**Figure 5.10 b** and **c**). The overall number of MTs and MTOCs did not significantly differ in cells treated with Centrinone compared to control cells, collectively indicating that BMDCs lacking centrioles still form functional MTOCs by organizing PCM and nucleating MTs (**Figure 5.10 d**). Ultimately, co-culture of antigen-loaded BMDCs with OT-II T cells revealed a significantly diminished capacity of Centrinone-treated cells to induce CD4$^+$ T cell proliferation compared to control cells (**Figure 5.10 e**). In summary, these results demonstrate that the presence of centrioles and the integrity of PCM in DCs are required for efficient T cell priming.

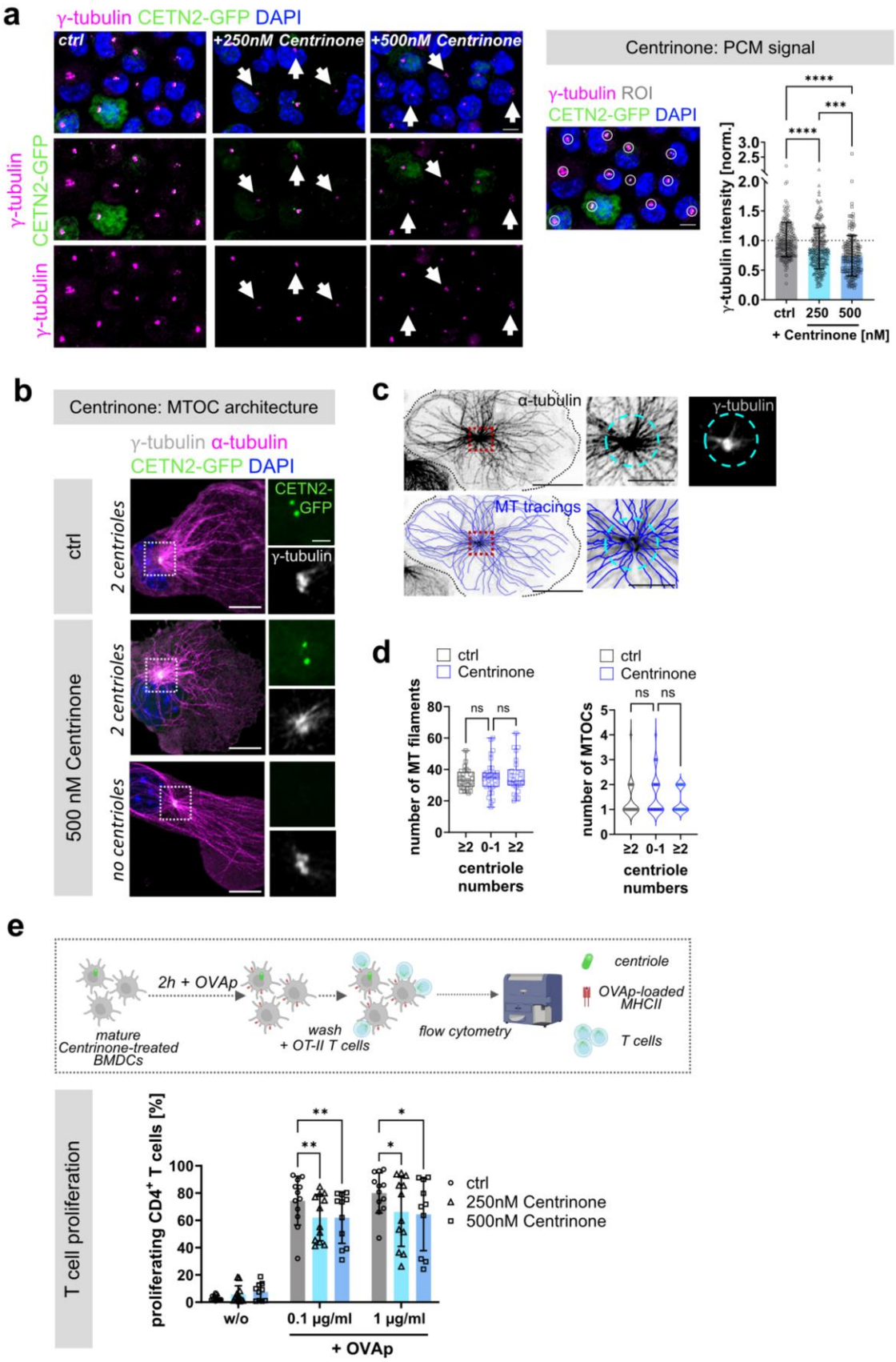
a
γ-tubulin CETN2-GFP DAPI
ctrl
+250nM Centrinone
+500nM Centrinone
γ-tubulin
CETN2-GFP
γ-tubulin
Centrinone: PCM signal
γ-tubulin ROI
CETN2-GFP DAPI
γ-tubulin intensity [norm.]
ctrl
250
500
+ Centrinone [nM]
b
Centrinone: MTOC architecture
γ-tubulin α-tubulin
CETN2-GFP DAPI
ctrl
500 nM Centrinone
2 centrioles
2 centrioles
no centrioles
CETN2-GFP
γ-tubulin
c
α-tubulin
γ-tubulin
MT tracings
d
ctrl
Centrinone
number of MT filaments
number of MTOCs
ns
centriole numbers
e
2h + OVAp
mature Centrinone-treated BMDCs
wash + OT-II T cells
flow cytometry
centriole
OVAp-loaded MHCII
T cells
T cell proliferation
proliferating CD4+ T cells [%]
w/o
0.1 µg/ml
1 µg/ml
+ OVAp
ctrl
250nM Centrinone
500nM Centrinone

Figure 5.10 Centrioles in DCs are required for efficient T cell priming
(**a**) Left: Immunostaining of mature CETN2-GFP BMDCs against γ-tubulin after 250 and 500 nM Centrinone treatment or control. Maximum z-projections of merged and individual channels of CETN2-GFP (green), γ-tubulin (magenta) and DAPI (blue) are shown. Scale bar, 5 µm. White arrowheads indicate cells without centrioles but with prominent γ-tubulin foci. Middle: Example of ROIs drawn around defined areas of γ-tubulin$^+$ foci for quantification of γ-tubulin signal intensity in mature CETN2-GFP expressing BMDCs after Centrinone treatment. Scale bar, 5 µm. Right: Graph shows normalized values relative to cells with two centrioles ± s.d. Each data point represents one cell derived from one representative experiment out of three independent experiments. *N* = 184 (ctrl) /211 (250 nM Centrinone) /186 (500 nM Centrinone) cells. Dotted line drawn at 1.0. *****, P* < 0.0001 (one-way ANOVA with Dunnett's multiple comparisons). (**b**) Immunostaining of MTs in Centrinone-treated and control cells. Maximum z-projections of mature CETN2-GFP (green) BMDCs stained against γ-tubulin (white) and α-tubulin (magenta). Nuclei were counterstained with DAPI (blue). Scale bars, 10 µm. Magnifications of the indicated regions show individual channels of CETN2-GFP (green) and γ-tubulin (white). Scale bars, 2 µm. (**c**) Illustration of MTOC and MT number analysis in DCs stained with α-tubulin (grey-inverted) and γ-tubulin (white). MTOCs were defined as MT nucleation sites with visible γ-tubulin$^+$ foci. MT filaments were counted within the indicated ROI (cyan circle, area: 25 µm²). Tracings of MTs (blue) are shown below. Maximum z-projections are displayed. For MT counting, whole confocal stacks were used. Scale bars, 10 µm. In magnified insets, 5 µm. (**d**) Quantification of MT filaments (left) and MTOCs (right) in mature CETN2-GFP expressing BMDCs after Centrinone treatment. Left graph shows median, interquartile range and minimum to maximum values of at least three independent experiments. *N* = 28 (ctrl) / 32 (Centrinone: 0-1 centrioles)/ 26 (Centrinone: ≥2 centrioles). ns, non-significant (one-way ANOVA with Dunnett's multiple comparisons). Right graph shows median and distribution of data points of at least three independent experiments. *N* = 30 (ctrl) /40 (Centrinone: 0-1 centrioles) /36 (Centrinone: ≥2 centrioles). ns, non-significant (Kruskal-Wallis test with Dunn's multiple comparisons). In both graphs each data point represents one cell. (**e**) Scheme of experimental set-up to quantify T cell proliferation after co-culture with Centrinone-treated BMDCs. Graph displays mean values ± s.d. Each data point represents one independent experiment with at least *N* = 10.000 cells analyzed per condition. Cells were derived from three different mice. **, P* < 0.0332; ***, P* < 0.0021 (two-way ANOVA with Dunnett's multiple comparisons). Schematic picture created with BioRender.

To further assess the role of MT filaments in APCs for T cell activation, we depolymerized MTs specifically in DCs by treating cells with the MT destabilizing agent pretubulysin (Ullrich et al. 2009; Braig et al. 2014). We observed that permanent treatment over 24 h led to complete depolymerization of MTs, while 24 h after drug wash-out, regrowth of individual MT filaments was visible (**Figure 5.11 a**). Of note, quantification of MT filaments in pretubulysin wash-out and control samples revealed a significantly reduced number of MTs in pretubulysin-treated cells compared to controls (**Figure 5.11 b** left). Under both conditions, MTs were predominantly emanating from a single MTOC (**Figure 5.11 b** right). Moreover, pretubulysin wash-out samples showed significantly reduced MT length and straightness, indicating that pretubulysin's effects are, to some extent, irreversible (**Figure 5.11 c**). This makes pretubulysin treatment well suited for studying the role of MTs specifically in DCs, while leaving the T cell's MT cytoskeleton of co-cultured T cells unaffected, which was also confirmed by MT and MTOC analysis of T cells co-cultured with treated DCs (**Figure 5.11 d** and **e**).

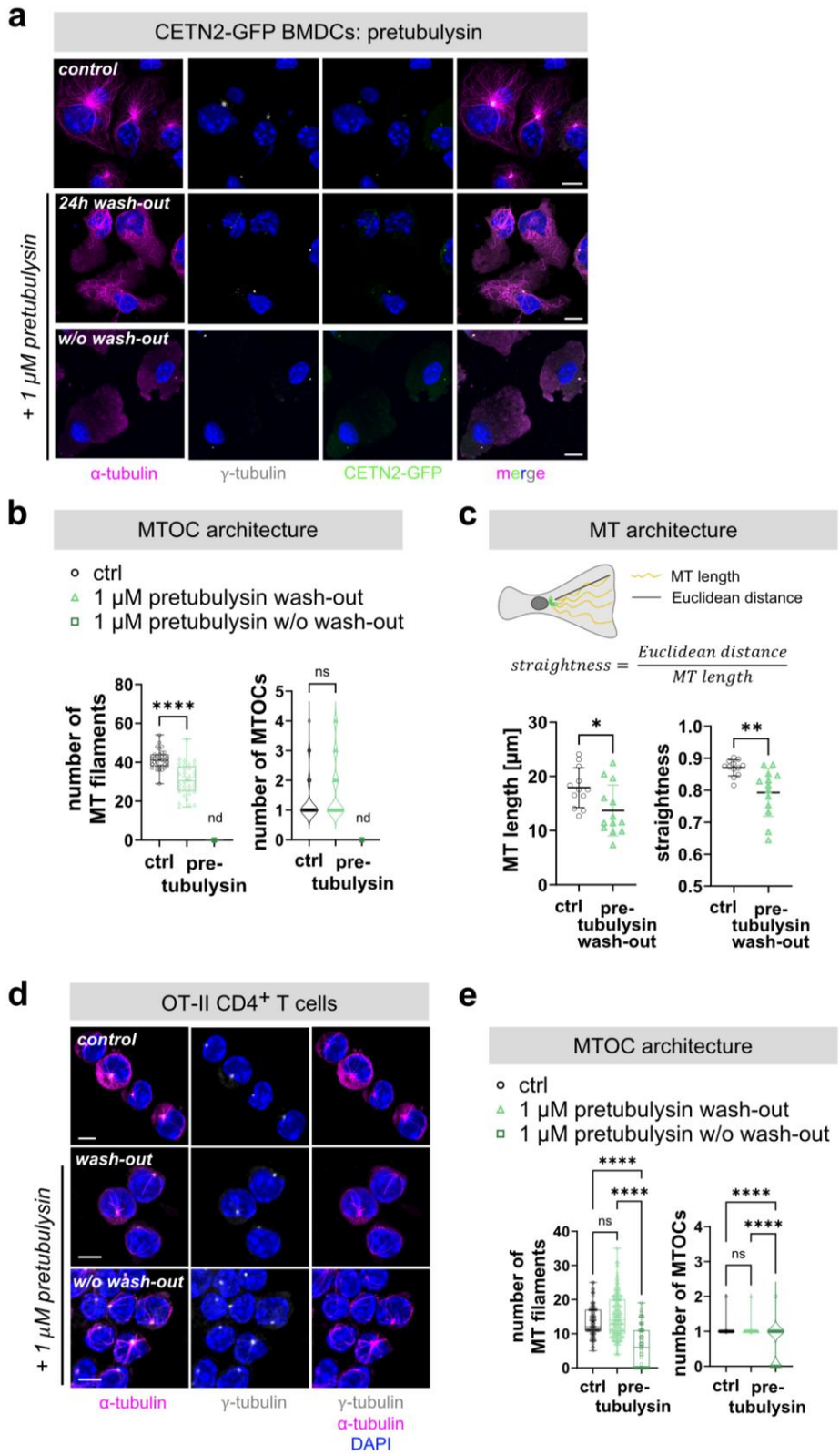

Figure 5.11 Pretubulysin treatment impairs MT structure

(**a**) Immunostaining of CETN2-GFP expressing BMDCs after pretubulysin treatment. Maximum z-projections of merged and individual channels of CETN2-GFP (green), α-tubulin (magenta), γ-tubulin (white) and DAPI (blue) are shown. Scale bars, 10 µm. (**b**) Quantification of MT filaments (left) and MTOCs (right) in BMDCs treated with pretubulysin. Left graph shows median, interquartile range and minimum to maximum values of three independent experiments. *N* = 33 (ctrl) /34 (24 h pretubulysin wash-out). Right graph shows median and

distribution of data points of three independent experiments. *N* = 39 (ctrl) /43 (24 h pretubulysin wash-out). In both graphs each data point represents one cell. ****, *P* < 0.0001, ns, non-significant. (Mann-Whitney test). nd, not determined. (**c**) Quantification of MT length and straightness in CETN2-GFP expressing BMDCs after 24 h of pretubulysin or DMSO (ctrl) wash-out. Both graphs show mean values ± s.d of three independent experiments. Each data point represents one cell. *N* = 13 (ctrl) /12 (pretubulysin wash-out). *, *P* < 0.0332, **, *P* < 0.0021 (Mann-Whitney test). (**d**) Immunostaining of T cells co-cultured for 24 h with BMDCs previously treated with pretubulysin according to scheme **Figure 5.12 a**. Maximum z-projections of merged and individual channels of α-tubulin (magenta), γ-tubulin (white) and DAPI (blue) are shown. Scale bars, 10 µm. (**e**) Quantification of MT filaments (left) and MTOCs (right) in T cells. Left graph shows median, interquartile range and minimum to maximum values of four independent experiments. Each data point represents one cell. *N* = 93 (ctrl) /183 (pretubulysin wash-out) /60 (pretubulysin w/o wash-out). Right graph shows median and distribution of data points of four independent experiments. *N* = 103 (ctrl) /184 (pretubulysin wash-out) /61 (pretubulysin w/o wash-out). ****, *P* < 0.0001. ns, non-significant. (Kruskal-Wallis test with Dunn's multiple comparisons).

To evaluate the T cell activation capacity of DCs after perturbing the MT cytoskeleton, we loaded mature BMDCs with OVAp and subsequently treated the cells with pretubulysin for 1 h (see scheme **Figure 5.12 a**). Next, treated and control cells were either washed or directly co-cultured with OT-II T cells. After 24 h of co-culture, IL-2 levels were measured in the supernatant. IL-2 is a cytokine predominantly produced by activated T cells (Smith 1988). We observed that IL-2 levels were markedly reduced in the presence of pretubulysin or after drug wash-out compared to controls (**Figure 5.12 b**). Notably, when DCs were loaded with 0.1 µg/mL OVAp, IL-2 levels were below the ELISA detection limit. As additional T cell activation measurement, we analyzed the upregulation of the cell surface marker OX40 via flow cytometry (**Figure 5.12 c** and **d**) (Gramaglia et al. 1998). Similar to IL-2 secretion, the frequency of activated T cells (defined by OX40 expression) was reduced in pretubulysin-treated or wash-out samples. Next, the impact of MT depolymerization on T cell expansion was assessed by CFSE dilution over 2.5 days. Consistent with previous results, frequencies of proliferating T cells were significantly decreased when priming with pretubulysin treated DCs (pretubulysin wash-out condition) (**Figure 5.12 e**). Interestingly, the presence of pretubulysin during DC-T cell co-culture, completely abolished T cell proliferation, likely due to impaired mitotic spindle formation when perturbing MTs in T cells. In summary, our results suggest that reduced and perturbed MT filaments within APCs impair T cell activation and proliferation.

Together, these findings highlight that both – centrosome and MT integrity in DCs – are crucial for efficient $CD4^+$ T cell priming and perturbance of these intracellular structures might impact the immune response.

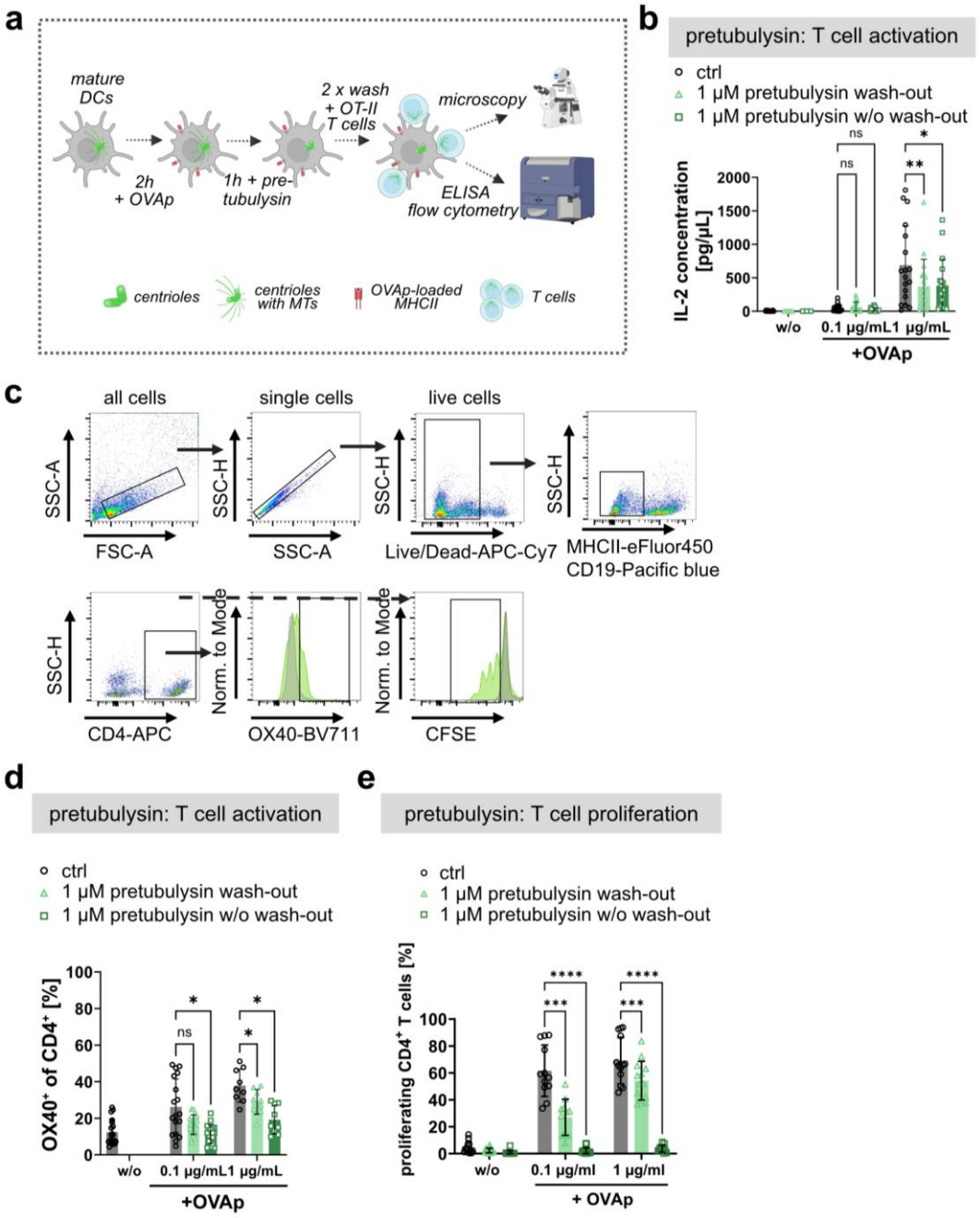

Figure 5.12 An intact MT array is important for optimal T cell priming

(**a**) Schematic representation of experimental workflow of OT-II transgenic T cell activation in the presence of pretubulysin-treated OVAp-loaded BMDCs. Picture created with BioRender. (**b**) Quantification of OT-II T cell activation after co-culture with pretubulysin-treated BMDCs in the absence (wash-out) or presence (w/o wash-out) of pretubulysin during the co-culture. OT-II T cell activation was assessed by measuring IL-2 concentration in the supernatant. Graph displays mean values ± s.d. Each data point represents one independent experiment with cell derived from six different mice. (**c**) Gating strategy to assess OX40 expression and proliferation of $CD4^+$ T cells after co-culture with pretubulysin-treated BMDCs. Grey filled lines in histograms represent condition w/o OVAp; green filled line with 0.1 µg/mL OVAp. (**d**) Quantification of OX40 upregulation on the T cell surface. Graph displays mean values ± s.d. Each data point represents one independent experiment. At least *N* = 10.000 cells analyzed per condition. Cells were derived from six different mice. **, P* < 0.0332; ***, P* < 0.0021 (two-way ANOVA with Tukey's multiple comparison). ns, non-significant. (**e**) Quantification of OT-II T cell proliferation measured by CFSE dilution after co-culture with pretubulysin-treated, OVAp-loaded BMDCs. T cell proliferation was assessed in the absence (wash-out) or presence (no wash-out) of pretubulysin. Graph displays mean values ± s.d. Each data point represents one independent experiment with at least *N* = 10.000 cells analyzed per

condition. Cells were derived from at least three different mice. **, P* < 0.0332; ****, P* < 0.0002; *****, P* < 0.0001 (two-way ANOVA with Dunnett's multiple comparison). ns, non-significant. Experiments assessing T cell proliferation after pretubulysin treatment were performed by Jan Böthling (student supervised by Isabel Stötzel).

5.2. Enhanced MTOC activity in DCs with multiple centrioles during IS formation

As shown above, centrosomal components in DCs are essential for T cell priming. Despite centriole duplication being strongly regulated in proliferating cells, DCs acquire multiple centrioles (>2) upon antigen encounter and maturation. Thus, we aimed to analyze the effect of extra centrioles on MTOC function in DCs. The exact number of centrioles within the diploid BMDC population was determined by CETN2-GFP$^+$/PCNT$^+$ foci showing approximately 80 % of cells with two centrioles and around 20 % of cells with more than two centrioles (**Figure 5.13 a**). Antibody staining and quantification of the PCM proteins PCNT, γ-tubulin or CDK5RAP2 revealed elevated PCM signal intensities in cells with multiple centrioles measured at a defined region surrounding the centrioles (**Figure 5.13 b, c** and **d**). This indicates enhanced recruitment of PCM proteins by extra centrioles. To further address whether this could also be observed during DC-T cell interactions, we loaded BMDCs with OVAp and co-cultured them for 2 h with OT-II T cells. Following fixation and antibody staining against γ-tubulin, similar results were reported: BMDCs with multiple centrioles exhibited enhanced PCM recruitment in comparison to cells with two centrioles during IS formation (**Figure 5.13 e** and **f**). Next, we hypothesized that enhanced PCM protein abundance could enhance MT nucleation. Thus, MT filament analysis in DCs conjugated with T cells showed that cells with multiple centrioles displayed enhanced MT numbers compared to cells with only a single pair of centrioles (**Figure 5.13 e** and **g**) (carried out by Ann-Kathrin Weier). Further, we observed that DCs with multiple centrioles similar to DCs with two centrioles contained mainly a single MTOC per cell (**Figure 5.13 g**). Overall, we concluded that extra centrioles in DCs form one over-active MTOC, which possesses more PCM and an enlarged number of emanating MTs.

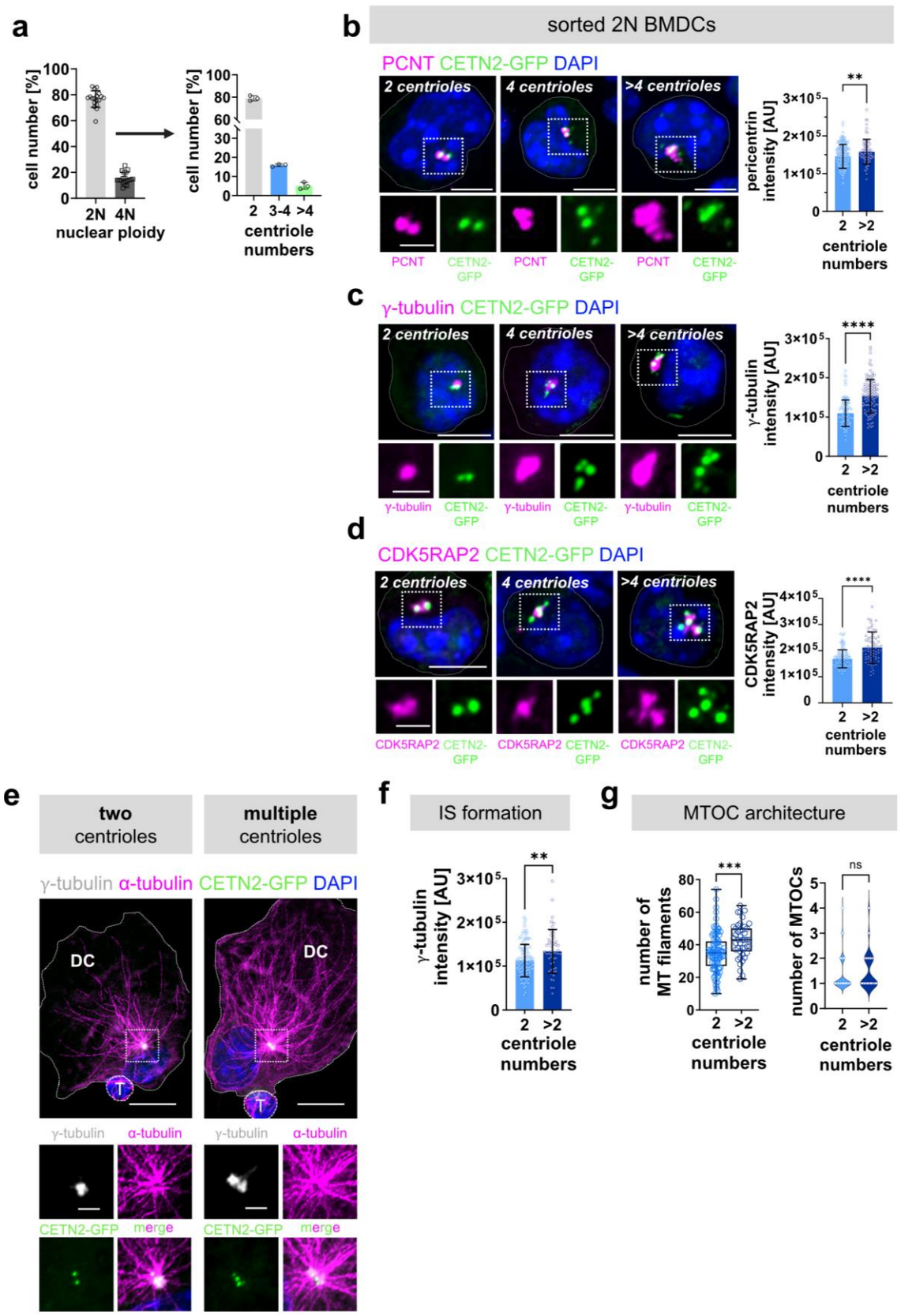

Figure 5.13 Multiple centrioles form a single over-active MTOC
(**a**) Left: Quantification of 2N and 4N cells according to DNA content (see also **Figure 5.8 a**). Right: Quantification of centriole numbers in sorted mature 2N CETN2-GFP BMDCs according to CETN2-GFP$^+$/PCNT$^+$ foci. Graph shows mean values ± s.d. of three independent experiments. *N* = 269/258/242 cells analyzed. (**b, c, d**) Immunostaining

of PCNT, γ-tubulin or CDK5RAP2 in sorted 2N mature CETN2-GFP BMDCs. Merged channels of PCNT/γ-tubulin/CDK5RAP2 (magenta), CETN2-GFP (green) and DAPI (blue) are shown. Scale bars, 5 µm. Insets show magnifications of indicated regions. Individual channels of CETN2-GFP (green) and PCNT/γ-tubulin/CDK5RAP2 (magenta) are shown. Scale bars, 2 µm. Right: Quantification of PCNT/γ-tubulin/CDK5RAP2 signal intensity at the centrioles in DCs. Graphs show mean values ± s.d. of one representative experiment out of at least three independent experiments. Each data point represents one cell. PCNT: *N* = 226 (2 centrioles) /71 (>2 centrioles). γ-tubulin: *N* = 106 (2 centrioles) /117 (>2 centrioles). CDK5RAP2: *N* = 98 (2 centrioles) /74 (>2 centrioles). ***, P* < 0.0021; *****, P* < 0.0001 (Mann-Whitney test). (**e**) Immunostaining of MT filaments in sorted 2N mature CETN2-GFP expressing BMDCs loaded with OVAp and forming conjugates with T cells. White dotted box indicates magnified region below. Merged and individual channels of CETN2-GFP (green), γ-tubulin (white), α-tubulin (magenta) and DAPI (blue) are shown. Scale bars, 10 µm (upper panels) and 2 µm (insets bottom). (**f**) Quantification of γ-tubulin signal intensities at the centrioles in DCs forming conjugates with T cells. Graph shows mean value ± s.d. of one out of three independent experiments. Each data point represents one cell. *N* = 108 (2 centrioles) /49 (>2 centrioles). ***, P* < 0.0021 (Mann-Whitney test). (**g**) Quantification of MT filaments (left) and MTOCs (right) in sorted 2N CETN2-GFP BMDCs loaded with OVAp and forming contacts with T cells. Left: Graph displays median, interquartile range and minimum to maximum values. Each data point represents one cell derived from 3 independent experiments. *N* = 93 (2 centrioles)/43 (>2 centrioles). ****, P* < 0.0002 (two-tailed, unpaired Student's t-test). Data generated by Ann-Kathrin Weier. Right: Graph shows median and distribution of data points of three independent experiments. *N* = 105 (2 centrioles) /25 (>2 centrioles). ns, non-significant. (Mann-Whitney test). (**b**-**e**) All images represent maximum z-projections.

5.3. DCs with multiple centrioles display an enhanced T cell activation capacity

As our previous analysis emphasizes the great importance of centrosomal structures for T cell priming, the phenomenon of extra centrioles forming a single MTOC with enhanced functionality raises the question whether such alterations influence the cell's capacity to induce T cell activation. To this end, we made use of a genetic reporter mouse line expressing GFP under the control of the promoter of Nur77, which is an early T cell activation marker (Liu et al. 1994; Moran et al. 2011). Nur77 gene expression is specifically upregulated by antigen-dependent TCR stimulation. We crossed Nur77^{GFP} mice with OT-II transgenic mice to assess T cell priming by DCs in an OVAp- and MHCII-specific context. Flow cytometry analysis detected GFP upregulation in T cells in an antigen-dependent manner starting after 2 h of DC-T cell co-culture and increasing after 4 h, 6 h and 20 h of incubation (**Figure 5.14 a** and **b**).

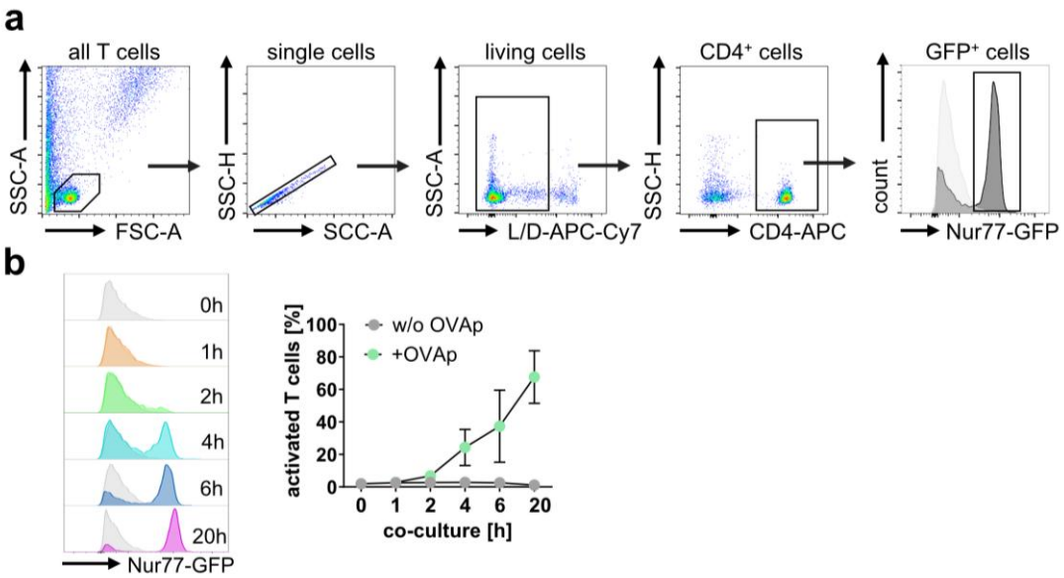

Figure 5.14 Assessing CD4⁺ T cell activation with Nur77^{GFP}/OT-II transgenic mice
(**a**) Gating strategy for analyzing Nur77^{GFP} expression in CD4⁺ T cells. T cells without DC co-culture served as control and are included as light grey filled line. (**b**) Histogram (left) and quantification (right) of Nur77^{GFP} expression after different time points of DC-T cell co-culture in the presence (+ OVAp) or absence (w/o OVAp) of OVAp. Graph represents mean values ± s.d. of 4 independent experiments. *N* = 10.000 cells analyzed per condition.

To analyze Nur77^{GFP} upregulation in dependence of DC centriole numbers, BMDCs were separated into two 'subpopulations' according to their centriolar content. To this end, we further developed a unique FACS-based method that enabled us to sort cells by the GFP-tagged centriolar marker CETN2. Cells were separated according to CETN2-GFP signal intensities which led to two DC 'subpopulations' (CETN2-GFP^{low} and CETN2-GFP^{high} cells) (**Figure 5.15 a** and **b**). To proof a correlation between CETN2-GFP intensity and centrioles, cells showing the highest or lowest CETN2-GFP signals were selected more or less stringent (10 % or 20 % highest or lowest GFP intensity). Following counting of centrioles via immunofluorescence microscopy revealed a greater enrichment of cells with multiple centrioles when only the 10 % highest expressing cells were selected in comparison to 20 % (**Figure 5.15 c** and **d**). Thus, we concluded that centriole numbers correlate with CETN2-GFP signal intensity and enrichment of cells with multiple centrioles varies in dependence of how stringent cells are selected.

In further experiments, keeping the selection of cells between 10 to 20 %, the CETN2-GFP^{high} 'subpopulation' was shown to contain a significantly higher proportion of cells with multiple centrioles than CETN2-GFP^{low} 'subpopulation' (**Figure 5.15 e** left). In this particular assay, DCs with multiple centrioles were enriched by a factor of 2.0 (**Figure 5.15 e** right). To assess T cell activation, sorted BMDCs were loaded with OVAp and incubated with Nur77^{GFP}/OT-II T cells for either 6 h or 20 h. At both timepoints, the frequencies of Nur77^{GFP} positive (activated) T cells were significantly elevated

when T cell priming was accomplished with CETN2-GFP^{high} BMDCs compared to CETN2-GFP^{low}, which indicates that cells with multiple centrioles activate a larger number of T cells within the same time period compared to cells with two centrioles (**Figure 5.15 f**).

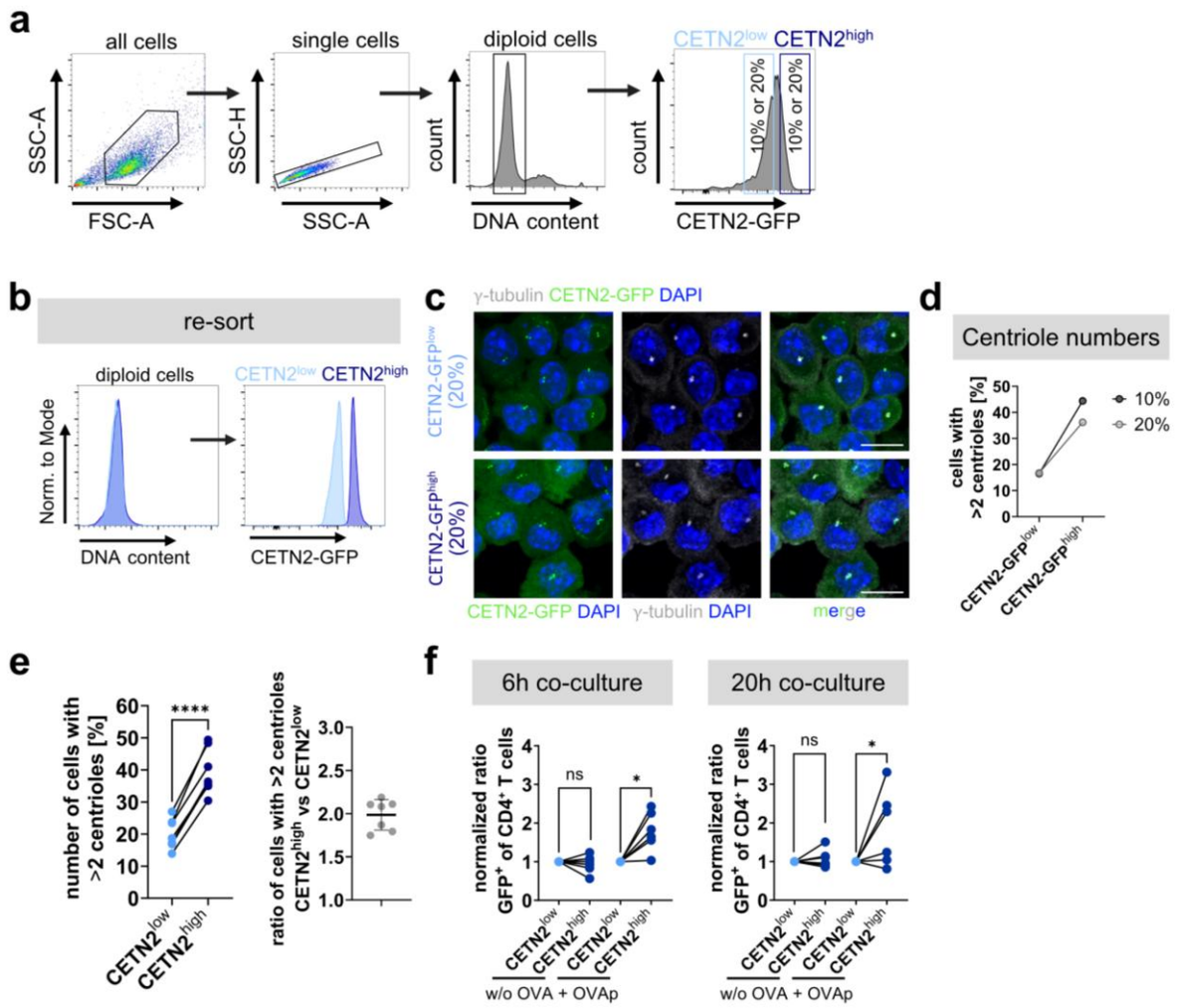

Figure 5.15 Sorting of CETN2-GFP BMDCs into two DC 'subpopulations' with distinct centriole numbers shows different T cell activation capacities

(**a**) Gating strategy for sorting of mature diploid BMDCs according to CETN2-GFP signal intensity. (**b**) Re-sort analysis of CETN2-GFP^{low} (light blue) and CETN2-GFP^{high} (dark blue) expressing cells for DNA content (left) and CETN2-GFP signal intensities (right). (**c**) Immunostaining of CETN2-GFP expressing BMDCs after sorting according to CETN2-GFP signal. Images represent maximum z-projections of merged and individual channels of CETN2-GFP (green), γ-tubulin (grey) and DAPI (blue). Scale bars, 10 µm. (**d**) Centriole numbers in sorted DC 'subpopulations' were quantified according to CETN2-GFP^{+}/γ-tubulin^{+} foci. Graph shows frequency of cells with multiple centrioles in CETN2-GFP^{low} and CETN2-GFP^{high} cells with pairing between stringency of selection (10 % or 20 %). Data derived from one experiment. (**e**) Left: Quantification of percentage of cells with >2 centrioles in CETN2-GFP^{low} (light blue) and CETN2-GFP^{high} (dark blue) expressing cells. Centriole numbers were determined by confocal microscopy according to CETN2-GFP^{+}/γ-tubulin^{+} foci. Each data point represents one independent experiment (n = 7). CETN2-GFP^{low} N = 219/253/238/263/223/226/213; CETN2-GFP^{high}: N = 220/253/176/254/207/234/236. ****, P < 0.0001 (two-tailed, paired Student's t-test). Right: Ratio of cells with multiple centrioles between CETN2-GFP^{high} and CETN2-GFP^{low} cells. (**f**) Activated (GFP^{+}) CD4^{+} T cells [%] after 6 h and 20 h of co-culture with OVAp-pulsed 2N BMDC 'subpopulations'. Each data point represents one independent experiment with pairing between sorted 2N CETN2-GFP^{low} (light blue) and CETN2-GFP^{high} (dark blue) expressing cells. Data was normalized to CETN2-GFP^{low} condition. *, P < 0.0332 (two-tailed, paired Student's t-test).

A key advantage of using Nur77^{GFP} expressing OT-II T cells is the ability to monitor T cell activation at a single cell level while simultaneously assessing centriole numbers in the conjugated CETN2-GFP expressing BMDC. Therefore, DC-T cell mixtures were immobilized after distinct time points of co-culture and stained with antibodies against γ-tubulin or CDK5RAP2 (**Figure 5.16 a** and **b**). With this approach we were able to quantify T cell Nur77^{GFP} intensity, DC centriole numbers and T cell MTOC position simultaneously. Importantly, T cell MTOC reorientation to the IS region, which is a sign of efficient IS formation, was observed at all timepoints analyzed in an antigen-dependent manner (**Figure 5.16 a**). Similar to our flow cytometric analysis, Nur77^{GFP} levels in T cells were increasing over time when they were co-cultured with OVAp-loaded DCs in comparison to cells without antigen (**Figure 5.16 b**). Interestingly, Nur77^{GFP} expression was elevated in T cells that showed a reoriented centrosome compared to cells without a relocalized MTOC demonstrating that Nur77-dependent GFP expression correlates with centrosome reorientation in T cells (**Figure 5.16 c**).

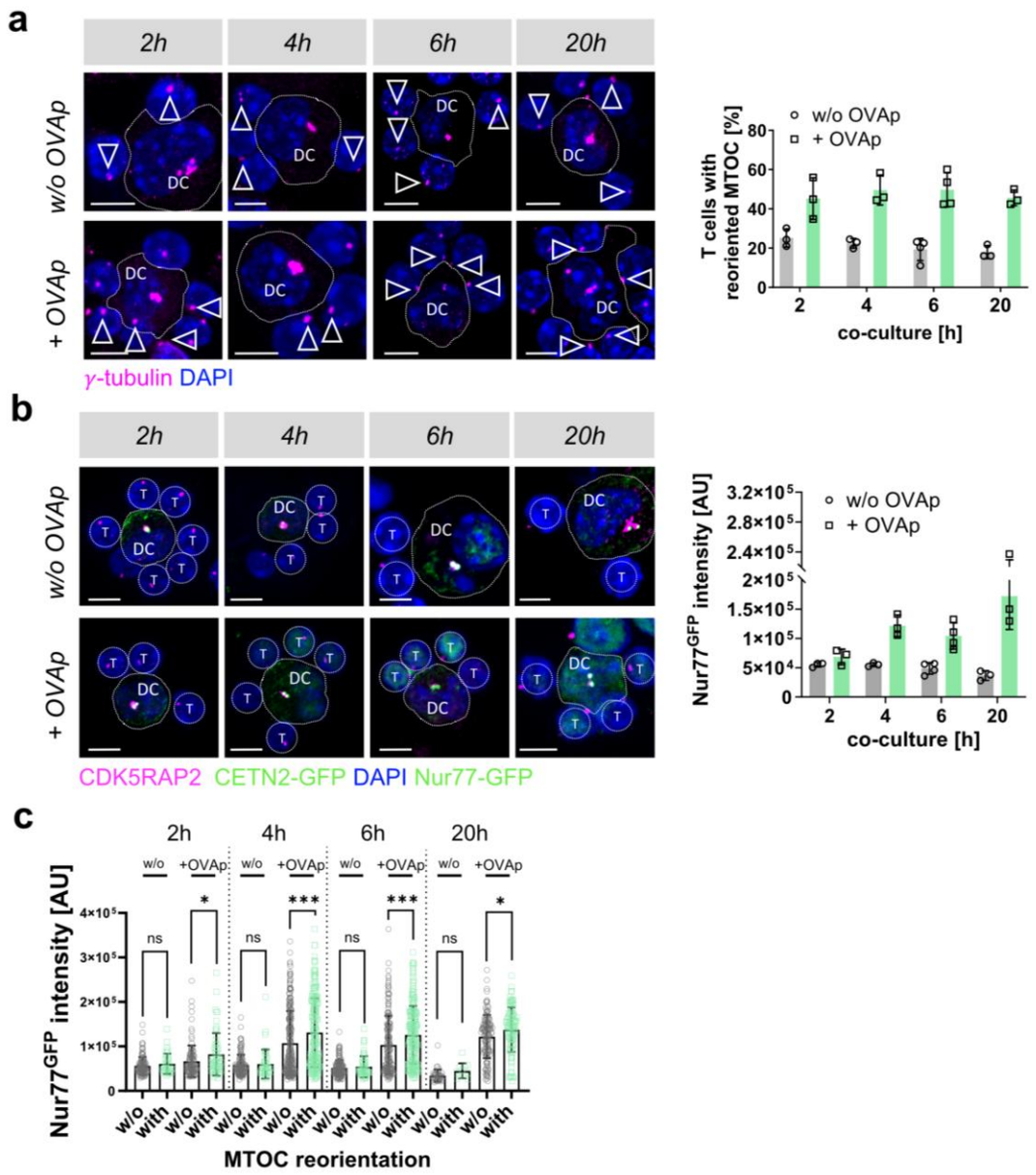

Figure 5.16 T cell activation measurements via microcopy using Nur77^{GFP} upregulation

(**a**) Left: Immunostaining of γ-tubulin (magenta) in DC-T cell conjugates. Merged channels of γ-tubulin (magenta) and DAPI (blue) are shown. DC outline is indicated with dotted line. White arrowheads point to the T cell's centrosome. Scale bars, 5 µm. Right: Quantification of MTOC polarization towards the IS in T cells after different timepoints of co-culture. Graph displays mean values ± s.d. Each data point represents one independent experiment with $N > 100$ cells analyzed per condition. (**b**) Visualization and quantification of Nur77^{GFP} expression in DC-T cell conjugates after different timepoints of co-culture. Left: Immunostaining of CDK5RAP2 (magenta) in CETN2-GFP (green) BMDCs after co-culture with Nur77^{GFP}/OT-II CD4^{+} T cells. Nuclei were counterstained with DAPI (blue). Dotted lines indicate DC outline; round circles the areas of GFP measurements. Scale bars, 5 µm. Right: Quantification of GFP signal intensity in T cells in the presence and absence of antigen. Graph displays mean values ± s.d. Each data point represents one independent experiment with $N > 100$ cells analyzed per experiment. (**c**) Quantification of GFP signal intensities in T cells from microscopic images in the presence and absence of antigen and in dependence of T cell MTOC reorientation towards the IS. Graph shows one representative experiment out of at least three independent experiments. N = 333(2 h)/625(4 h)/584(6 h)/301(20 h). *, $P < 0.0332$; ***, $P < 0.0021$ (one-way ANOVA with Kruskal-Wallis multiple comparisons). (**a, b**) All images represent maximum z-projections.

Ultimately, we determined T cell activation in dependence of DC centriole numbers (**Figure 5.17 a**). Therefore, we defined a threshold for activated T cells based on the GFP intensity in T cells co-cultured with DCs without OVAp (**Figure 5.17 b**). We found that at all timepoints of co-culture analyzed, the frequency of activated T cells was significantly increased when they were activated by DCs that contain multiple centrioles (**Figure 5.17 c, d**).

Similar to our flow cytometric analysis, we were able to show at a single cell resolution that cells with multiple centrioles induce augmented T cell activation in comparison to cells with two centrioles, which confirms optimized T cell responses in the presence of extra centrioles in APCs.

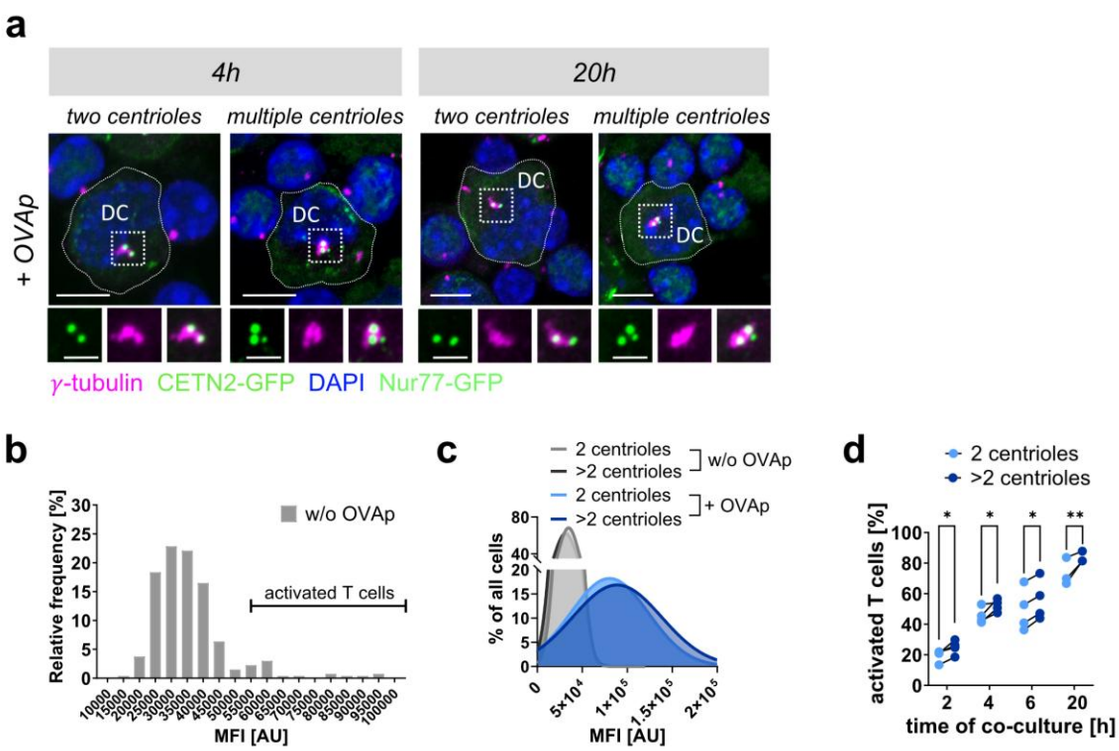

Figure 5.17 DCs containing multiple centrioles induce enhanced T cell activation
(**a**) Analysis of T cell activation in dependence of centriole numbers. Immunostaining of γ-tubulin in DC-T cell conjugates. Merged and individual channels of CETN2-GFP (green), Nur77^{GFP} (green), γ-tubulin (magenta) and DAPI (blue) are shown. Indicated regions are magnified and shown below. Scale bars, 5 µm (top). Scale bars, 2 µm (magnified region). All images represent maximum z-projections. (**b**) Frequency distribution of signal intensities of Nur77^{GFP} expression levels in the absence of OVAp. Threshold for T cell activation was set and is indicated in the graph. (**c**) Gaussian line fitted to frequency distribution of Nur77^{GFP} signal intensities in the absence or presence of OVAp and in dependence of DC centriole numbers. (**d**) Quantification of T cell activation according to Nur77^{GFP} signal intensities in dependence of DC centriole numbers for different time points of DC-T cell co-culture. Each data point represents one independent experiment with pairing between cells with two (light blue) and multiple (dark blue) centrioles from one experiment. *N* > 100 cells analyzed per condition. **, P* < 0.0332; ***, P* < 0.0021 (two-tailed, paired Student's t-test).

5.4. Multiple centrioles cluster and localize in close proximity to the cell center in DCs during IS formation

To elucidate the underlying mechanisms of enhanced T cell activation by DCs with multiple centrioles, we hypothesized that multiple centrioles might de-cluster and subsequently reorient towards different T cell contact sites (**Figure 5.18 a**). This, in turn, might facilitate faster docking of MTs and delivery of stimulatory molecules to the IS, consistent with previous observations that MTOC reorientation enables targeted delivery of vesicles in DCs priming $CD8^+$ T cells (Pulecio et al. 2010).

To test this hypothesis, we analyzed the spatial organization of DC centrioles during antigen-specific T cell contacts. In cells with two centrioles intracentrosomal distances and in cells with multiple centrioles average distances between centrioles were determined in DC-T cell conjugates immobilized after 1 h, 2 h or 4 h of co-culture (see schemes in **Figure 5.18 b** and **c** left). These early timepoints were chosen according to centrosome repositioning occurring in T cells within this timeframe (see also **Figure 5.16 a**) (Ueda et al. 2011). In addition, we extended the analysis also to 6 h and 20 h after cell mixing to include later events during IS formation. Further, we distinguished between DCs priming one T cell (mono-conjugated synapse) or multiple T cells (multi-conjugated synapse) as indicated above the graphs. The results showed that intracentrosomal distances and average distances did not prominently differ between OVAp loaded and unloaded cells or between DCs forming mono- and multi-conjugated synapses, suggesting that DC centrioles maintain a clustered configuration during interactions with antigen-specific T cells (**Figure 5.18 b-e**).

Next, for assessing centriole positioning within DCs during T cell priming, we quantified the ratio of the distance between DC centrioles and T cell and between DC center point (CP) and T cell (**Figure 5.19 a**). Similar to the analysis of centriole clustering, we compared OVAp-loaded and unloaded DCs and mono- and multi-conjugated synapses at different timepoints (1 h, 2 h, 4 h, 6 h, 20 h). In contrast to MTOC polarization previously reported in multiple cell types, DC centrioles were located in close proximity to the geometric cell center during $CD4^+$ T cell priming (**Figure 5.19 b-e**). Additionally, centrioles were positioned near the nucleus at all timepoints analyzed indicating T cell activation without DC MTOC polarization (**Figure 5.20 a** and **b**).

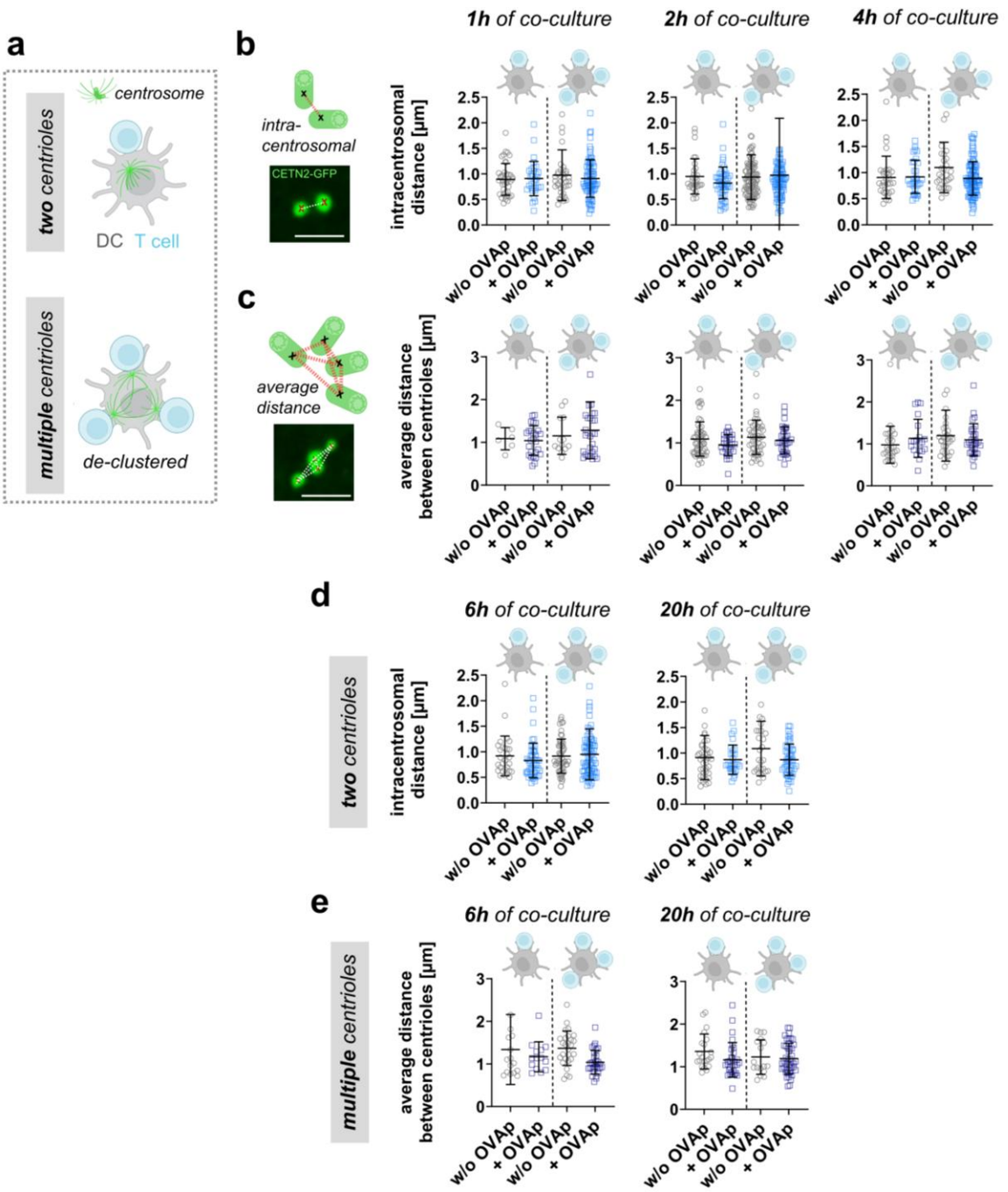

Figure 5.18 DC centriole clustering during antigen-specific T cell contact
(**a**) Sketch illustrating hypothesis about centriole de-clustering and centriole polarization in DCs toward the IS in the presence of two (top) and multiple centrioles (bottom). (**b-e**) Sketches and pictures indicate centriole configuration (CETN2-GFP) during DC-T cell contacts. Scale bars, 2 µm. Graphs show quantification of intracentrosomal distances (**b, d**) and average distances (**c, e**) in DCs with two or multiple centrioles at different time points of co-culture and bound to one or several T cells (separated by dashed line and indicated on top). Graphs display mean values ± s.d. Each data point represents one cell derived from ≥3 independent experiments. (**a-c**) Pictures created with BioRender. Experiments immobilizing DC-T cell conjugates after 1 h, 2 h and 4 h of co-culture were partially performed by Ann-Kathrin Weier.

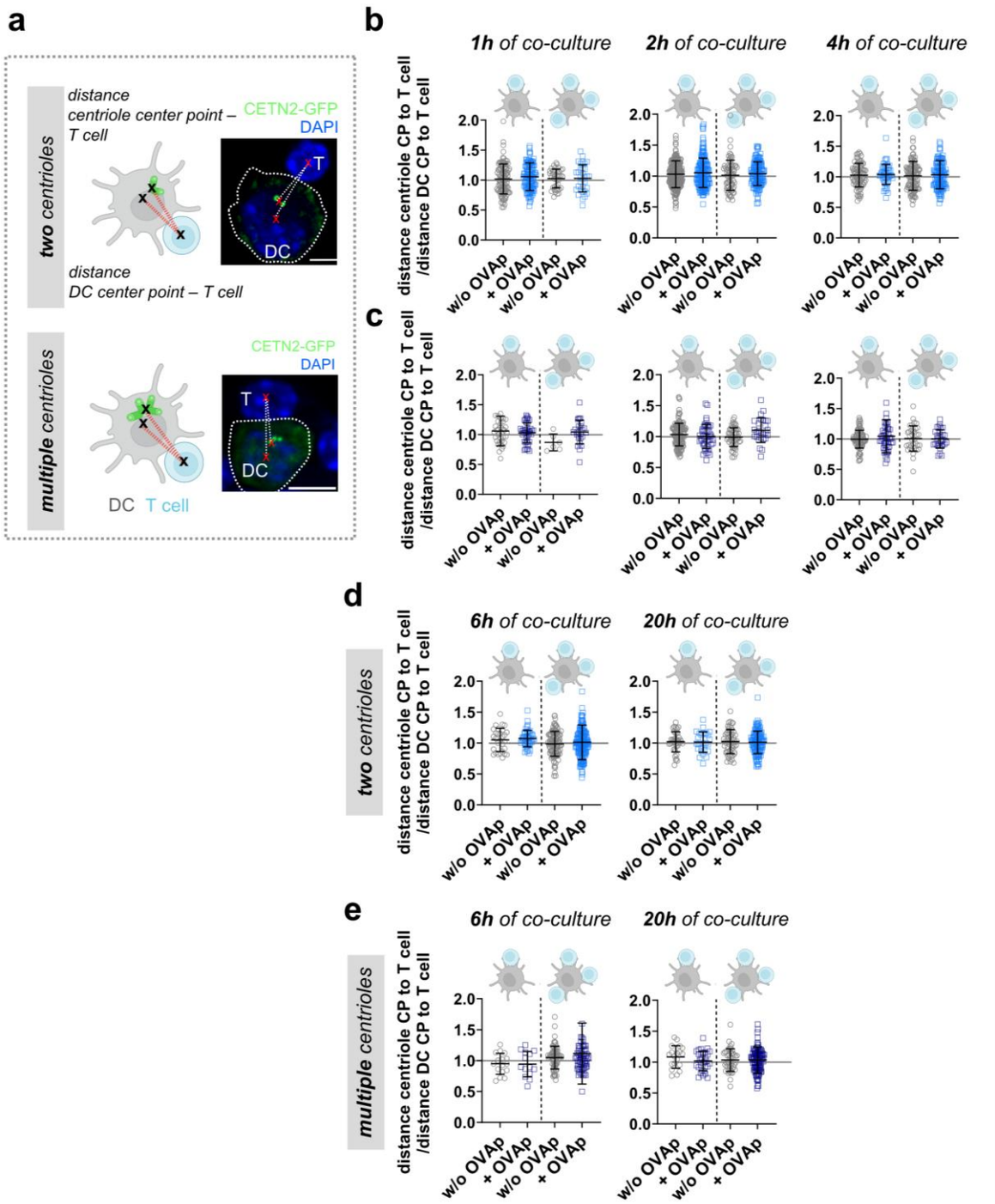

Figure 5.19 Central centriole localization in DCs during antigen-specific T cell contact
(**a**) Sketches and confocal images indicating distances between centriole center point (CP) and T cell CP, and DC CP and T cell CP in cells with two (upper panel) and multiple (lower panel) centrioles. CETN2-GFP (green). Nuclei were counterstained with DAPI (blue). Scale bars, 5 µm. Schemes created with BioRender. (**b**-**e**) Quantification of ratio between distance from centriole CP to T cell CP and distance DC CP to T cell in cells with two (**b, d**) and multiple (**c, e**) centrioles. Graphs show mean values ± s.d. for DCs attached to one T cell (left) and multiple T cells (right) separated by dashed line and indicated on top. Each data point represents one cell derived from ≥3 independent experiments. Experiments immobilizing DC-T cell conjugates after 1 h, 2 h and 4 h of co-culture were partially performed by Ann-Kathrin Weier.

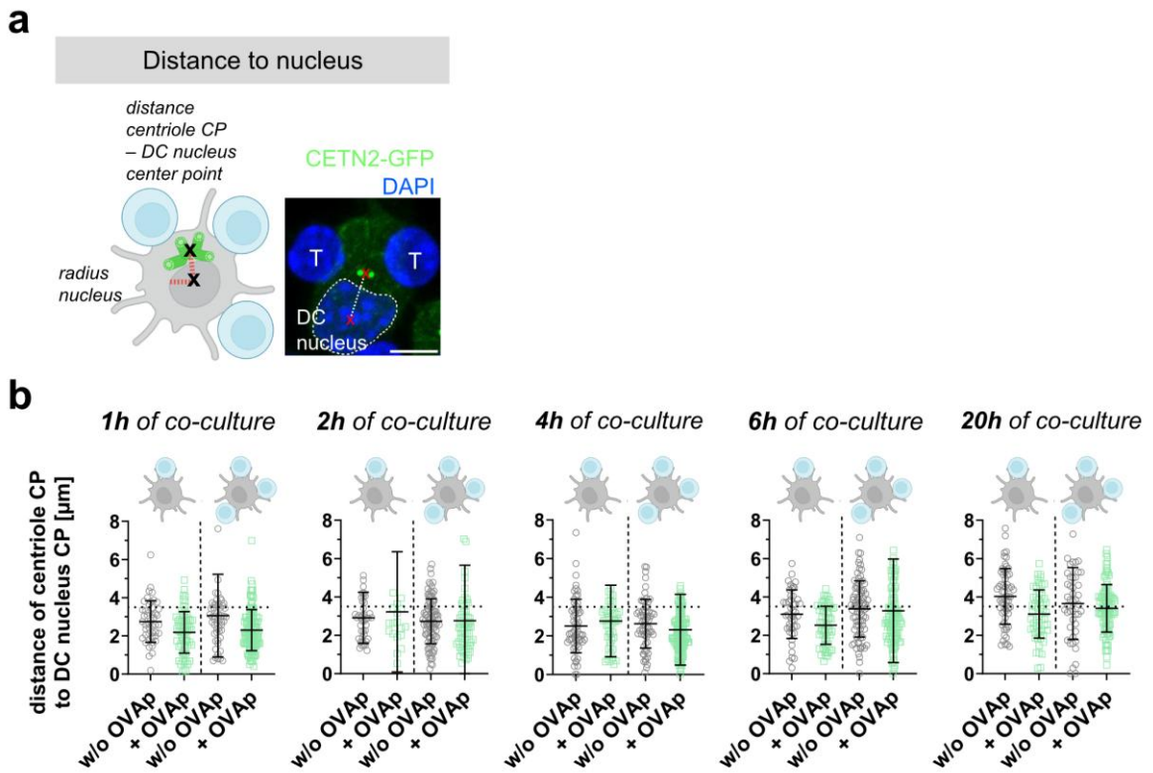

Figure 5.20 Localization of DC centrioles in close proximity to the nucleus during antigen-specific T cell contact (**a**) Sketch indicating distance of centriole CP to center of nucleus and radius of the nucleus (red lines). Scale bar, 5 µm. Sketch created with BioRender. (**b**) Quantification of centriole positioning relative to the nucleus displayed by distance of centriole CP to CP of the DC nucleus. Graphs represent mean values ± s.d. Each data point depicts one cell derived from at least three independent experiments. Dotted lines indicate radius of the nucleus. Experiments immobilizing DC-T cell conjugates after 1 h, 2 h and 4 h of co-culture were partially performed by Ann-Kathrin Weier.

We complemented this analysis with live cell imaging of DC-T cell contacts, which enabled to resolve the temporal dynamics of centrioles during an early period of DC-T cell interactions (first 30-60 minutes after mixing). Efficient interactions between CETN2-GFP expressing BMDCs and OT-II T cells were identified by calcium influx in T cells visualized through a calcium-sensitive dye (Cal520). During interactions with one or multiple T cells, intracentrosomal distances or average distances between centrioles were stable over time, indicating a permanent cohesion of two or multiple centrioles in DCs during antigen-unspecific or -specific T cell contacts (**Figure 5.21 a** and **b**). The distance of the centriole CP to the T cell, which was normalized to the distance of the DC CP to the T cell, did not increase during the time-lapse imaging period in cells with two or multiple centrioles (**Figure 5.21 c**). Further, the localization of the centrioles was independent of the number of T cells associated with the DC. Similar to our findings from immobilized samples, we observed no centriole displacement from the nucleus under any of the conditions analyzed (**Figure 5.21 d**).

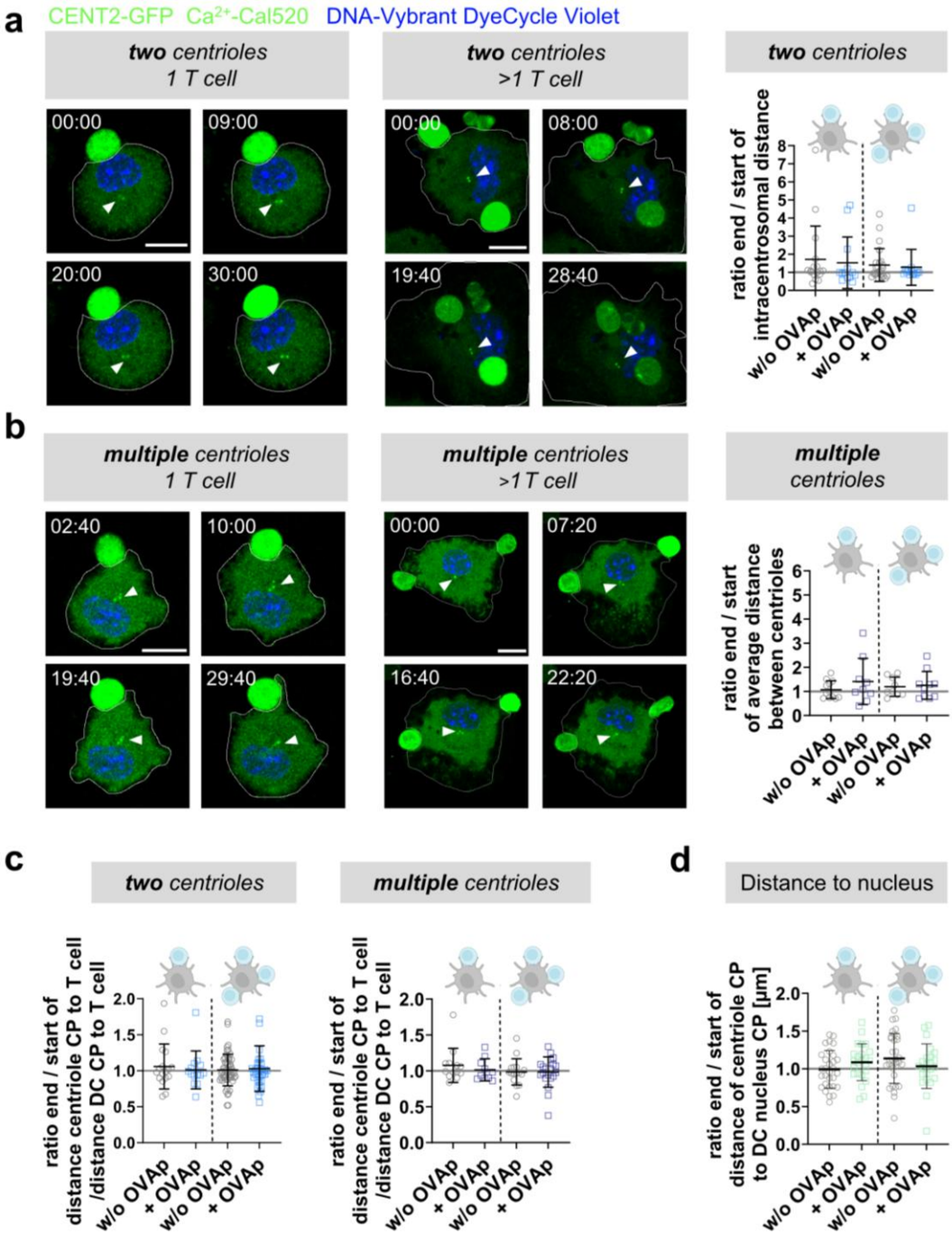

Figure 5.21 Centriole dynamics in DCs during IS formation

(**a, b**) Time-lapse live-cell confocal microscopy of antigen-specific DC-T cell contacts. Left: Merged images of CETN2-GFP (green), Ca^{2+}-Cal520 (green) and DNA stain (Vybrant DyeCycle Violet stain, blue) are shown. Frames were collected every 20 seconds. Only selected frames are shown in montage with precise time points indicated in min:sec. White arrow heads point to position of centrioles. Scale bars, 10 µm. (**a**) Right: Quantification of ratio of end vs. start intracentrosomal distance in cells with only two centrioles and dividing mono-conjugated (left half) and multi-conjugated synapses (right half). Graph shows mean values ± s.d. Each data point represents one cell recorded for at least 30-60 min from at least 5 independent experiments. *N* = 17/13/24/13 (left to right). (**b**) Right: Quantification of ratio of end vs. start average distance between centrioles in cells with multiple centrioles and dividing mono-conjugated (left half) and multi-conjugated synapses (right half). Graph shows mean values ± s.d. Each data point represents one cell recorded for 30-60 min from minimum 5 independent experiments. *N* = 12/9/9/10 (left to right). (**c**) Quantification of ratio of end vs. start of distance centriole CP to T cell CP normalized to the movement of the DC. Left (light blue) graph shows DCs with two centrioles. Right (dark blue)

graph shows cells with >2 centrioles. Graphs show mean values ± s.d. Each data point represents one cell recorded for 30-60 min from at least 5 independent experiments. Left: *N* = 17/14/57/34 (left to right). Right: *N* = 13/10/16/20 (left to right). (**d**) Quantification of ratio of distances between centriole CP and the center of the DC nucleus at the end vs. the beginning of recording. Graphs represent mean values ± s.d. Each data point depicts one cell derived from 5 independent experiments. *N* = 30/24/33/23 (left to right).

Our results on centriole organization were derived from analyses conducted in two dimensions (2D). Especially in live cell imaging experiments, cells were cultured under flat 2D conditions instead of a 3D setup. As cellular behavior might differ between these conditions, analysis within LNs, where T cell priming occurs *in vivo*, resembles the physiologically relevant environment more closely (Baker and Chen 2012). Therefore, we carried out adoptive transfer experiments, in which labelled naïve $CD4^+$ OT-II T cells were injected into wildtype recipient mice and after 24 h OVAp-loaded CETN2-GFP expressing BMDCs were injected into the hock (scheme **Figure 5.22 a**). Popliteal and inguinal LNs were isolated after 48 h. Fixation and staining of cryosections showed BMDC-OT-II T cell contacts within T cell areas (**Figure 5.22 b**). 3D rendering of DCs, their nuclei and centrioles, and T cells from high resolution z-stack images are shown in Figure **Figure 5.22 c**. We were able to identify DCs with two or multiple centrioles forming mono- and multi-conjugated synapses *in vivo*. Measurement of centrosomal clustering revealed intracentrosomal distances of 0.9 ± 0.2 µm (1 T cell) or 0.8 ± 0.2 µm (>1 T cell) and average distances between centrioles of 1.1 ± 0.2 µm (1 T cell) or 1.2 ± 0.3 µm (>1 T cell) indicating a clustered centriole configuration in DCs during conjugation with antigen-specific T cells *in vivo* (**Figure 5.22 d**). Similar to our 2D analysis, two and multiple centrioles localized close to the cell center and did not reorient towards interacting T cells independent of the number of conjugated T cells (**Figure 5.22 e**).

Thus, we concluded that centriole de-clustering and repositioning in DCs is dispensable for T cell activation. Instead, multiple centrioles tightly cluster and remain close to the cell center when mono- or multi-conjugated contacts are formed *in vitro* and *in vivo*.

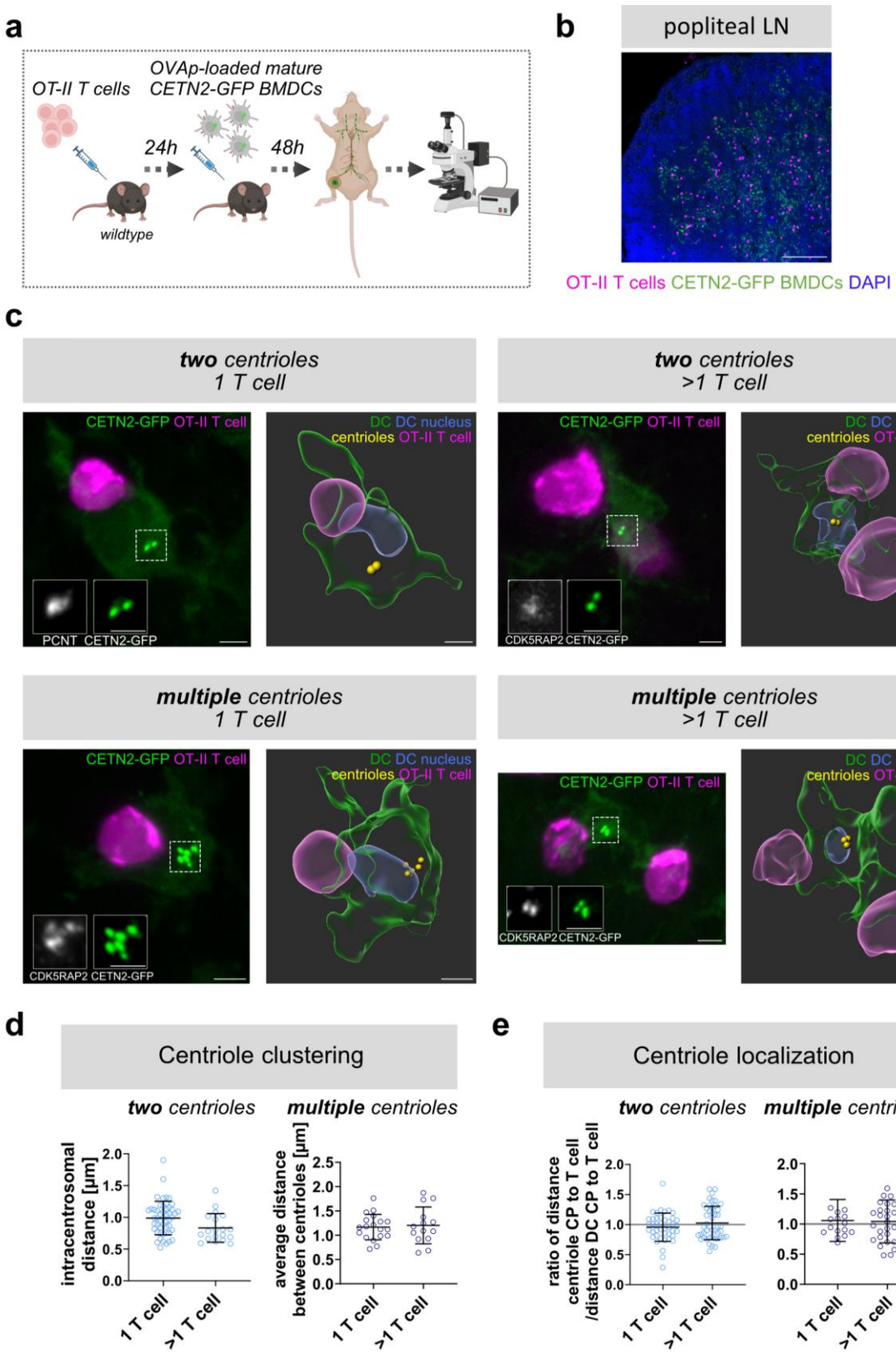

Figure 5.22 Centriole clustering and central localization in DCs within murine lymph nodes
(**a**) Scheme of OT-II T cell and CETN2-GFP expressing BMDC injection. (**b**) Maximum z-projection of popliteal LN containing OT-II T cells (magenta) and CETN2-GFP BMDCs (green) counterstained with DAPI (blue). Scale bar, 200 µm. (**c**) Left (in each panel): Maximum z-projection of merged channels of CETN2-GFP (green) and pre-stained OT-II T cells (magenta). Scale bars, 3 µm. Insets show individual channels of PCNT or CDK5RAP2

(magenta) and CETN2-GFP (green). Scale bars, 2 µm. Right (in each panel): 3D rendering of DC (green), DC nucleus (blue), DC centrioles (yellow) and OT-II T cell (magenta). For better visibility of DC-T cell contacts, 3D rendered images were rotated. Scale bars, 3 µm. (**d**) Quantification of intracentrosomal distances in cells with two centrioles (left) and average distances between centrioles in cells with multiple centrioles (right) during contact with one or multiple T cells. Graphs show mean values ± s.d. Each data point represents one cell derived from at least 4 independent experiments. *N* = 50/19 (two centrioles) and 19/14 (multiple centrioles). (**e**) Quantification of distance centriole CP to T cell CP normalized to distance DC CP to T cell CP in cells with two centrioles (left) and multiple centrioles (right) during contact with one or multiple T cells. Graphs show mean values ± s.d. Each data point represents one cell derived from at least 4 independent experiments. *N* = 42/46 (two centrioles) and 16/30 (multiple centrioles). T cell and DC injections were performed by Luisa Bach and 3D rendering of z-stack images was conducted by Philip Weidner and Stefan Uderhardt.

5.5. Centriole de-clustering impairs T cell activation

We observed a tight clustering of DC centrioles during interactions with antigen-specific T cells. Next, we sought to address whether this configuration is crucial for the induction of T cell priming. Therefore, DCs were treated with the de-clustering agent and poly-ADP-ribose polymerase (PARP) inhibitor PJ-34 (Castiel et al. 2011; Wahlberg et al. 2012). PJ-34 represents a promising target for cancer treatment as it disturbs proliferation of cancer cells (Castiel et al. 2011). In the present study, DCs were incubated for 3 h with PJ-34 to test the effect on centriole organization and to rule out possible effects on transcriptional regulation which might impact T cell activation. Cell surface expression of MHCII was not altered after PJ-34 treatment suggesting regular antigen presentation (**Figure 5.23 a** and **b**). In addition, mRNA expression levels and intracellular protein levels of DC-specific cytokines such as Ccl5, Cxcl1 and Il-6 were analyzed as they are involved in attracting and activating immune cells (Zeng et al. 2022; Korbecki et al. 2022; Dienz and Rincon 2009). With both analyses no significant differences in cytokine production of PJ-34 treated cells compared to controls were detected (**Figure 5.23 a, c** and **d**). Thus, our results indicate that PJ-34 treatment does not impair antigen presentation or cytokine production in DCs.

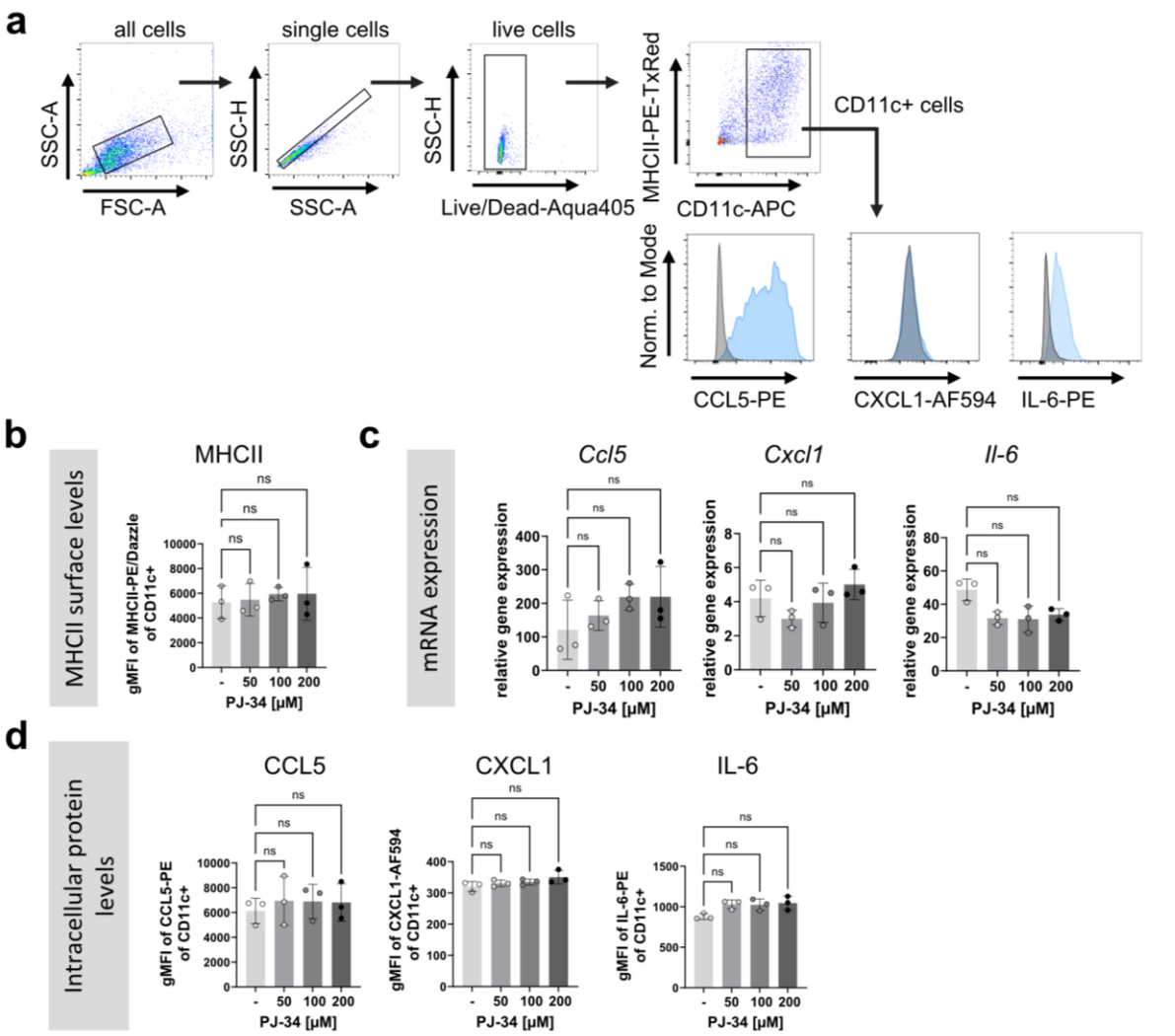

Figure 5.23 PJ-34 treatment does not affect MHCII expression or cytokine production
(**a**) Gating strategy for analyzing MHCII surface levels and intracellular cytokine levels of BMDCs treated with PJ-34. Grey filled lines represent unstained samples. (**b**) Graph shows geometric mean fluorescence intensity (gMFI) of MHCII in CD11c$^+$ DCs. Each data point represents one independent experiment measured in duplicates with *N* = 10.000 cells analyzed per condition. (**c**) Graphs show relative gene expression of Ccl5, Cxcl1 and Il-6 normalized to the house keeping gene TATA-binding protein. Each data point represents one independent experiment measured in duplicates. (**d**) Graphs show gMFI of CCL5, CXCL1 and IL-6 in CD11c$^+$ DCs. Each data point represents one independent experiment measured in duplicates with *N* = 10.000 cells analyzed per condition. (**b-d**) ns, non-significant. (Kruskal-Wallis test with Dunn's multiple comparisons).

To test the effect of PJ-34 on DC centriole organization during antigen-specific T cell contact, we first incubated mature BMDCs with OVAp before treating with PJ-34, washing twice and co-culturing with T cells (**Figure 5.24 a**). DC-T cell conjugates were immobilized to determine intracentrosomal and intercentrosomal distances as described in the scheme (**Figure 5.24 b** and **c**). While intracentrosomal distances were not significantly affected by PJ-34 treatment, cells with multiple centrioles showed a significantly enlarged intercentrosomal distance after PJ-34 treatment, which confirmed efficient de-clustering of centrioles using PJ-34. Next, we analyzed whether de-clustered centrioles nucleate MTs

and form functional MTOCs. Interestingly, we observed a significantly increased number of MTOCs in PJ-34 treated cells, indicating that centriole de-clustering leads to an altered MT array organization (**Figure 5.24 d** and **e**). Despite this change, the total number of MT filaments was unaltered upon PJ-34 treatment. Subsequent flow cytometric analysis of DC-T cell co-cultures revealed that DCs with de-clustered centrioles exhibited a diminished capacity to stimulate T cell proliferation (**Figure 5.24 f**). From these findings, we concluded that the de-clustering of multiple centrioles and the resulting formation of multiple MTOCs impair efficient T cell priming. Overall, these results highlight the essential role of proper centriole and MTOC organization in DCs for efficient T cell activation.

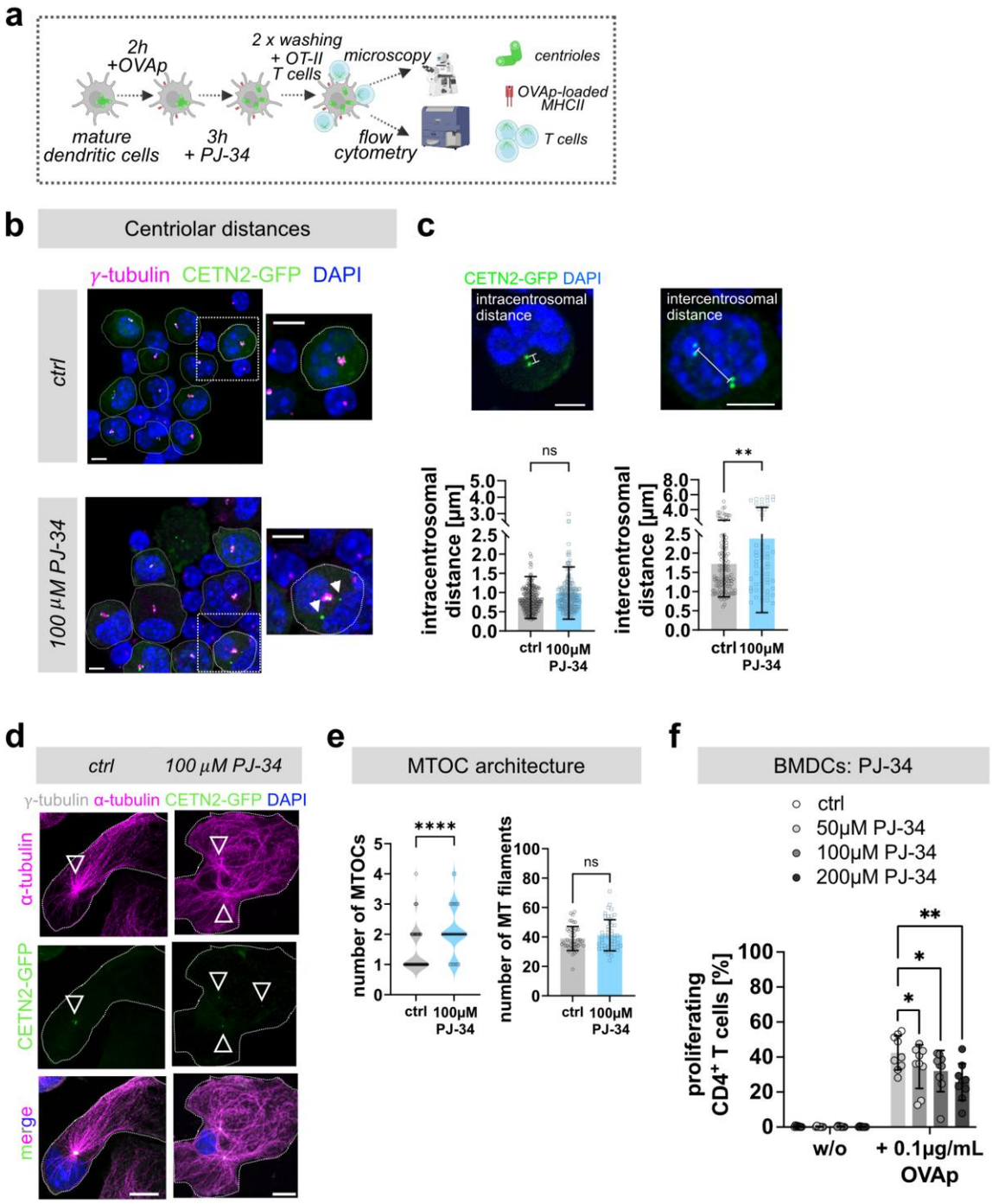

Figure 5.24 PJ-34 treatment induces centriole de-clustering in DCs and impairs their T cell activation capacity
(**a**) Schematic experimental layout of PJ-34 treatment and T cell activation assay. (**b**) 2N CETN2-GFP (green) expressing DCs treated with or without PJ-34 and after 2 h of co-culture with OT-II T cells were stained against γ-tubulin (magenta). Nuclei were counterstained with DAPI (blue). Scale bars, 5 µm. Insets show magnification of indicated regions. Scale bars, 2 µm. White arrowheads point to de-clustered centrioles. (**c**) Quantification of intracentrosomal (left) and intercentrosomal (right) distances in cells treated with PJ-34 according to scheme above the graphs. Graphs display mean values ± s.d. Each data point represents one cell derived from three independent experiments. Upper graph: *N* = 226 (ctrl) /195 (PJ-34) Lower graph: *N* = 120 (ctrl) /56 (PJ-34). ***, P* < 0.0021. ns, non-significant. (two-tailed, unpaired Student's t-test). (**d**) Immunostaining of PJ-34-treated and control cells. Merged and individual channels of CETN2-GFP (green), α-tubulin (magenta), γ-tubulin (white) and DAPI (blue) are shown. Scale bars, 10 µm. (**e**) Quantification of MTOCs (left) and MT filaments (right) in 2N PJ-34 treated and control cells. Left: Graph shows median and distribution of data points of at least three independent experiments. *N* = 54 (ctrl) /51 (PJ-34). *****, P* < 0.0001 (Mann-Whitney test) Right: Graph displays

mean values ± s.d. Each data point represents one cell derived from three independent experiments. *N* = 45 (ctrl) /48 (PJ-34). ns, non-significant. (two-tailed, unpaired Student's t-test). (**f**) OT-II T cell proliferation with or without PJ-34 treatment of OVAp-loaded mature BMDCs was measured via CFSE dilution (gating as described before). BMDCs were sorted for 2N and enriched for cells with >2 centrioles (CETN2-GFP^{high}). Graph displays mean values ± s.d. Each data point represents one independent experiment with at least *N* = 10.000 cells analyzed per condition. Cells were derived from three different mice. **, P* < 0,0332; ***, P* < 0.0021 (two-way ANOVA with Dunnett's multiple comparison). ns, non-significant. (**b-d**) All images represent maximum z-projections.

5.6. Overexpression of the centrosomal protein Nedd1 enhances MT nucleation

Our findings showed that DC centriole numbers and MT organization regulate cellular functionality: We observed in DCs with extra centrioles the formation of an over-active MTOC, which is marked by an elevated number of MT filaments. In addition, we detected increased T cell activation capacity by DCs with extra centrioles and decreased T cell priming by DCs with reduced MT numbers and perturbed MT structure. Building on these findings, we elaborated on the role of MTs in DCs by using genetic perturbation experiments which selectively modify MTs in DCs without affecting MTs in T cells. As MT filaments are notoriously difficult to dampen precisely, we sought of gain-of-function experiments, which allow increased centrosomal MT nucleation while leaving the number of centrioles unaffected. To this end, overexpression of the fusion protein Nedd1-mOrange2-rCM1 was induced in CETN2-GFP expressing Homeobox B8 (Hoxb8) progenitor cells (see Materials and Methods section **Figure 4.7**). In this construct, the PCM protein Nedd1 is fused to a fluorescent reporter (mOrange2) as well as a centrosomin motif originating from rat CDK5RAP2 protein sequence (rCM1). Nedd1-mOrange2-rCM1 localizes to the centrosome and recruits and activates γ-tubulin ring complexes (Haren et al. 2006; Lüders et al. 2006; Xu et al. 2024). Previously, Nedd1-mOrange2-rCM1 was expressed in neurons leading to increased MT nucleation capacity (Vinopal et al. 2023).

In our experimental set-up (**Figure 5.25 a**), we introduced the Nedd1-mOrange2-rCM1 construct under the control of a doxycycline-dependent promotor in CETN2-GFP expressing Hoxb8 cells. Nedd1-mOrange2-rCM1 expression was induced by adding doxycycline from day 3 until the end of differentiation and the expression of the fusion protein was verified by flow cytometry showing a significant increase in Nedd1-mOrange2-rCM1 expression when doxycycline was added to the cells (**Figure 5.25 b** and **c**). Nedd1-mOrange2-rCM1 expression did not impact cell differentiation (**Figure 5.25 b** and **d**). Interestingly, we were able to observe increased MHCII surface levels in doxycycline-treated cells compared to control (**Figure 5.25 d**) which might indicate enhanced maturation and antigen presentation capacity.

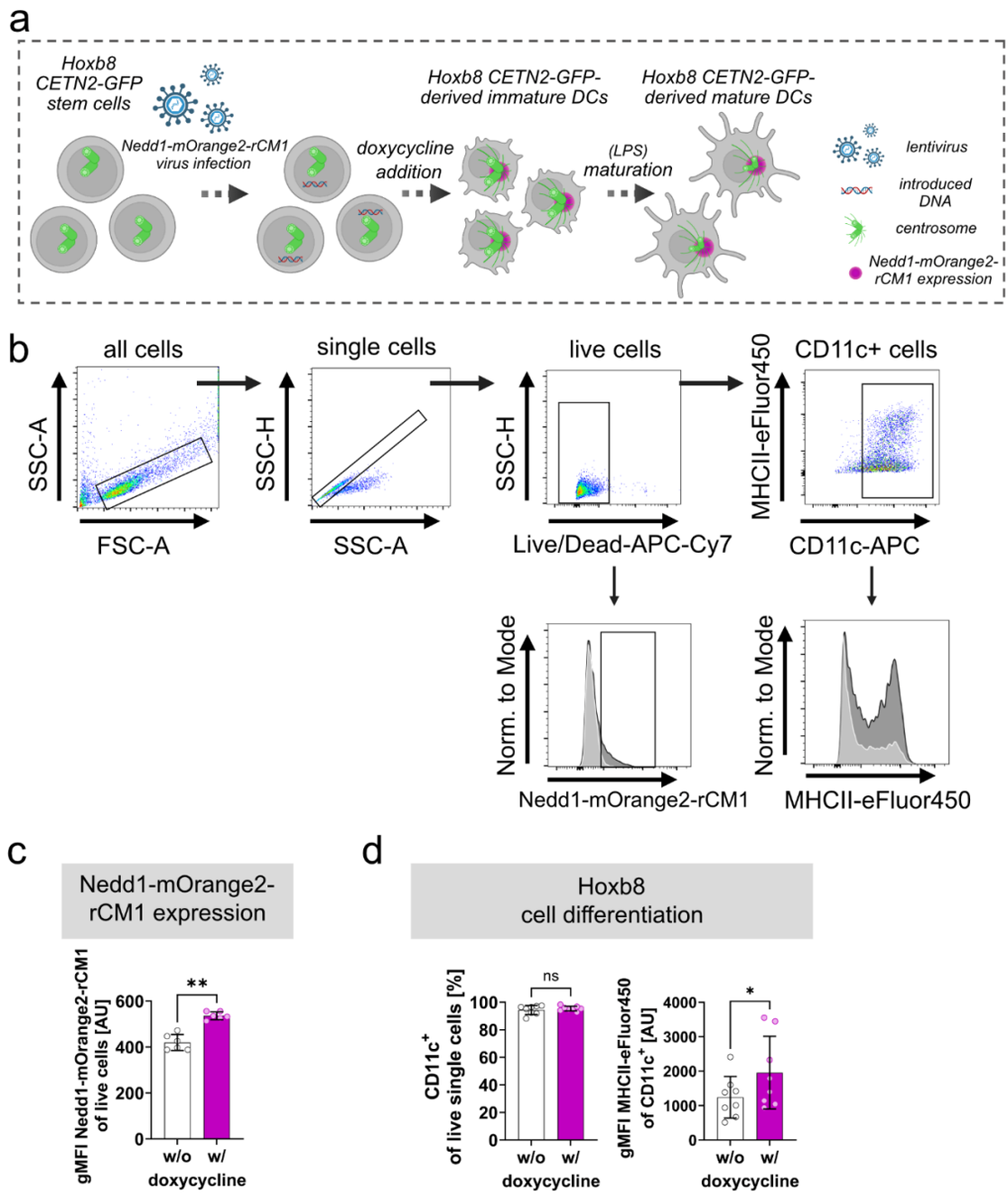

Figure 5.25 Induction of Nedd1-mOrange2-rCM1 expression in CETN2-GFP expressing Hoxb8-derived DCs
(**a**) Scheme illustrating Nedd1-mOrange2-rCM1 expression Hoxb8 CETN2-GFP-derived DCs. (**b**) Gating strategy to analyze DC differentiation and Nedd1-mOrange2-rCM1 expression levels. In histograms light grey presents cells cultured without doxycycline and dark grey with doxycycline. (**c**) Quantification of geometric mean fluorescence intensity (gMFI) of Nedd1-mOrange2-rCM1 in Hoxb8 CETN2-GFP-derived DCs. Graph shows mean ± s.d. of n = 6 experiments with each N = 10 000 events recorded. **, $P < 0.0021$ (Mann-Whitney test) (**d**) Quantification of CD11c$^+$ cells (left) and the gMFI of the DC activation marker MHCII (right). Graphs show mean ± s.d. of n = 8 experiments with each N = 10 000 events recorded. ns, non-significant; *, $P < 0.0332$ (two-tailed, paired Student's t-test).

Next, we studied how Nedd1-mOrange2-rCM1 affects centrosome and MT organization. Centriole numbers were determined in immobilized Hoxb8-derived DCs by CETN2-GFP$^+$ foci co-localizing with γ-tubulin. Importantly, centriole numbers were not altered by Nedd1-mOrange2-rCM1 overexpression (**Figure 5.26 a** and **b**). Next, measurement of centriolar distances revealed that the intracentrosomal distance (distance between two centrioles) is unaffected by Nedd1-mOrange2-rCM1 overexpression, while in DCs with multiple centrioles the average distance between centrioles was enlarged after overexpression of the fusion protein indicating centriole de-clustering upon overexpression (**Figure 5.26 c**).

MT filament numbers were analyzed by staining confined cells with an α-tubulin specific antibody. As expected, due to previous reports using the expression of the Nedd1 fusion protein, MT numbers were increased in Hoxb8 CETN2-GFP-derived DCs by Nedd1-mOrange2-rCM1 overexpression (**Figure 5.26 d** and **e**). Intriguingly, cells with Nedd1-mOrange2-rCM1 expression contained increased numbers of MTOCs per cell (**Figure 5.26 f**). Thus, we concluded from the microscopic analysis that Nedd1-mOrange2-rCM1 overexpression induced enhanced MT numbers, de-clustering of multiple centrioles and a restructured MT array into multiple nucleation sites.

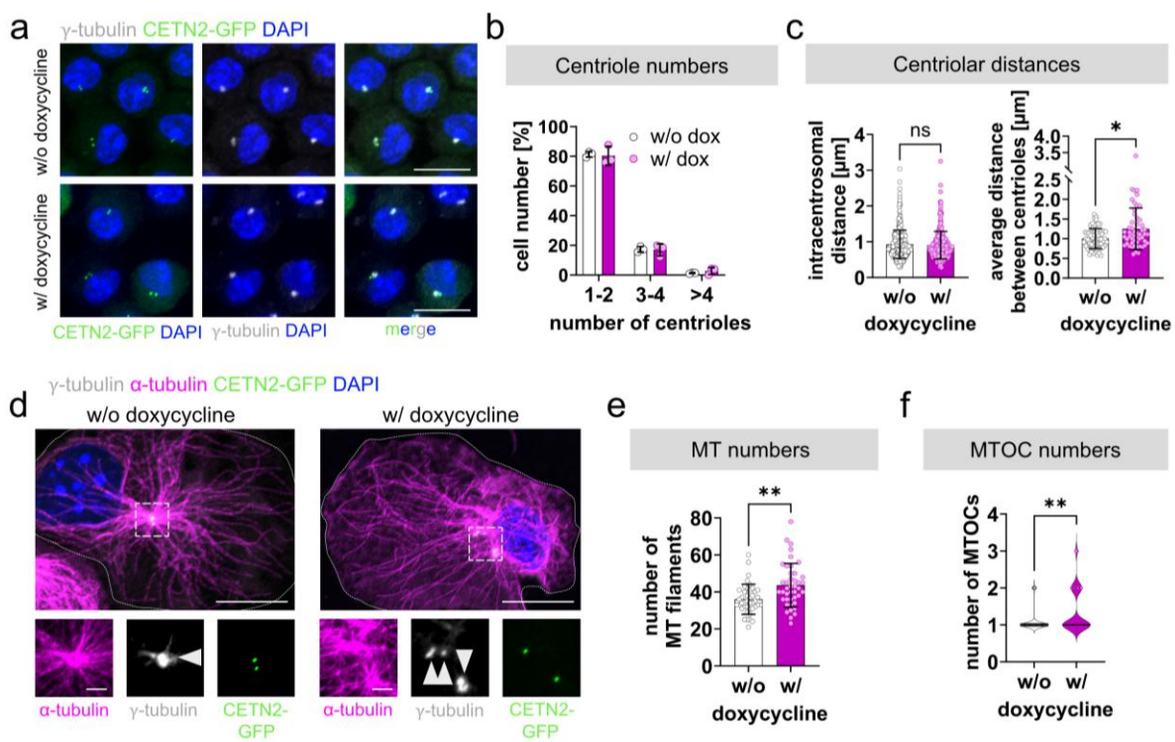

Figure 5.26 Nedd1-mOrange2-rCM1 expression does not alter DC centriole numbers but MT and MTOC numbers

(**a**) Immunostaining of CETN2-GFP expressing Hoxb8-derived DCs after inducing Nedd1-mOrange2-rCM1 expression. Images represent maximum z-projections of merged and individual channels of CETN2-GFP (green), γ-tubulin (grey) and DAPI (blue). Scale bars, 10 µm (**b**) Quantification of centriole numbers in CETN2-GFP expressing Hoxb8-derived DCs with or without Nedd1-mOrange2-rCM1 expression. Graph shows mean ± s.d. of n = 3 experiments with each N > 180 cells analyzed. (**c**) Graphs show quantifications of intracentrosomal

distances (left) and average distances (right) in DCs with two or multiple centrioles. Each data point represents one cell. Graph shows mean ± s.d. of *n* = 3 experiments with in total *N* = 349 (w/o)/291 (w/) (left) or *N* = 71 (w/o)/53 (w/) (right) cells analyzed. (**d**) Staining of MT filaments in CETN2-GFP expressing Hoxb8-derived DCs after inducing Nedd1-mOrange2-rCM1 expression. Maximum z-projections of merged channels and individual channels of magnified regions are shown. α-tubulin (magenta); γ-tubulin (grey); CETN2-GFP (green); DAPI (blue). Scale bars merged image, 10 µm. Scale bars insets, 2 µm. White arrowheads point to MTOCs. (**e**) Quantification of MT filaments in dependence of Nedd1-mOrange2-rCM1 expression induction. Each data point represents one cell. Graph shows mean ± s.d. of *n* = 3 experiments with in total *N* = 40 (w/o)/42 (w/) cells analyzed. (**f**) Quantification of MTOC numbers in dependence of Nedd1-mOrange2-rCM1 expression induction. Graph shows median and distribution of data points of *n* = 3 experiments with in total *N* = 43 (w/o)/49 (w/) cells analyzed. (**c**, **e** and **f**) ns, non-significant; **, P* < 0.0332; ***, P* < 0.0021 (Mann-Whitney test).

To investigate the impact of enhanced MT nucleation in DCs on T cell activation, we performed a MLR. In this experiment, Nedd1-mOrange2-rCM1 expressing DCs were incubated with OVAp and subsequently co-cultured with OT-II T cells (**Figure 5.27 a**). Flow cytometry analysis of $CD4^+$ OT-II T cells showed T cell activation by the upregulation of CD69 and downregulation of CD62L (**Figure 5.27 b**). However, T cell activation capacity was not changed for all OVAp concentrations tested when the Nedd1 fusion protein was expressed in Hoxb8-derived DCs (**Figure 5.27 c**). In summary, these findings suggest that increased MT numbers in DCs, which were accompanied by the formation of de-clustered centrioles and multiple MTOCs per cell, are not associated with a detectable enhancement in T cell activation.

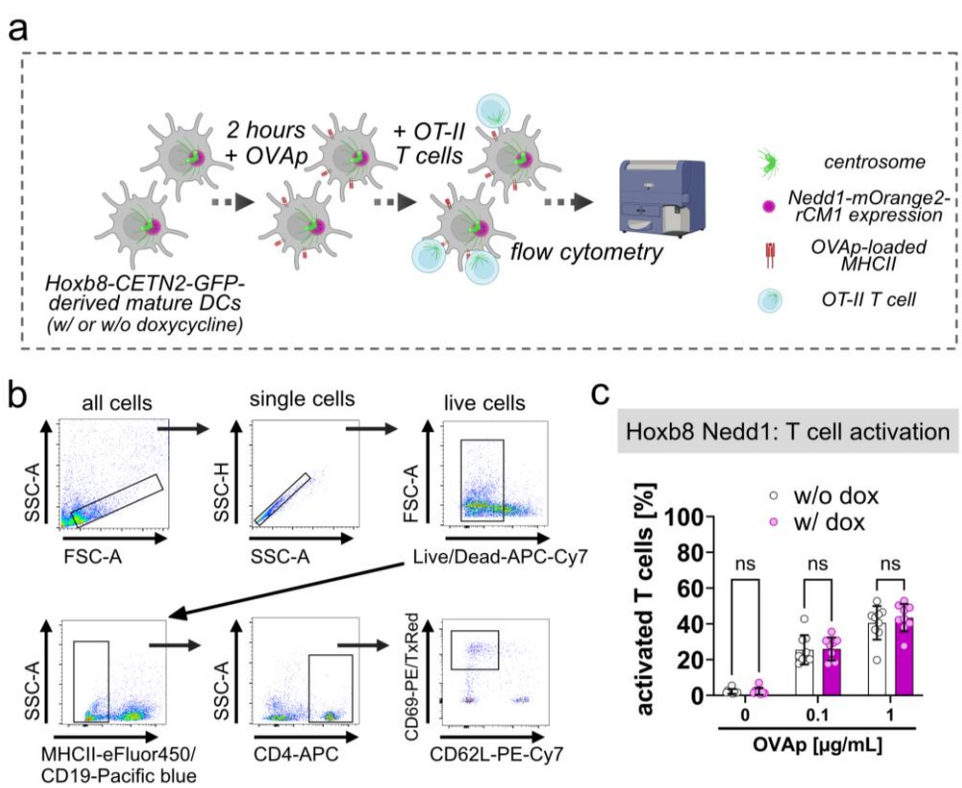

Figure 5.27 T cell activation by DCs expressing Nedd1-mOrange2-rCM1 is unaltered
(**a**) Scheme illustrating experimental set-up of T cell activation by Hoxb8 CETN2-GFP-derived DCs expressing Nedd1-mOrange2-rCM1. (**b**) Gating strategy for analyzing $CD69^+/CD62L^-$ cells of $CD4^+$ T cells. (**c**) Quantification

of activated T cells ($CD69^+/CD62L^-$ cells of $CD4^+$ T cells) after 24 h of co-culture with Hoxb8 CETN2-GFP-derived DCs with or without Nedd1-mOrange2-rCM1 expression induction. Graph shows mean ± s.d. of *n* = 9 experiments which were measured in triplicates with each *N* = 10 000 cells recorded. ns, non-significant (two-way ANOVA with Tukey's multiple comparison).

5.7. Secretion profiles of DCs with distinct centriole numbers show different cell signatures

Previous findings revealed that MT perturbation in DCs results in reduced T cell priming efficiency and on the opposite side DCs with increased centriole and MT numbers display enhanced T cell activation capacity. Next, we sought to further understand the underlying processes of centriole-mediated enhancement of T cell activation. As MT filaments organize routes for trafficking, it is of particular interest whether protein secretion by DCs is altered dependent on DC centriole numbers.

A key approach to investigate such functional differences is sorting cells according to their centriolar content using CETN2-GFP expression as described above (**Figure 5.15 a-d**). This led to a significant enrichment of cells with multiple centrioles in CETN2-GFP^{high} cells compared to CETN2-GFP^{low} (**Figure 5.28 a** left). Here, on average CETN2-GFP^{high} cells contained 2.2-times more cells with multiple centrioles (**Figure 5.28 a** right). For secretome analysis, sorted DC 'subpopulations' were cultured in serum-free medium for 20 h and supernatants subsequently processed for mass spectrometry analysis (carried out in collaboration with the group of Felix Meissner, University Hospital Bonn). From nearly 5000 protein groups identified in all samples, the volcano plot shows changes in the protein abundance comparing supernatants of CETN2-GFP^{high} and CETN2-GFP^{low} cells with around 350 proteins significantly changed between the conditions (**Figure 5.28 b**). Among the proteins increasingly detected in supernatant of CETN2-GFP^{high} cells were CCL17 and CCL22 (gene names *Ccl17* and *Ccl22*), which are two chemokines involved in T cell attraction (Lieberam and Förster 1999; Imai et al. 1998). Additionally, IL-12β (gene name *Il12b*) was significantly enriched in supernatant of CETN2-GFP^{high} cells. This subunit (also called IL-12p40) is a component of the cytokines IL-12 and IL-23, which are T cell stimulatory molecules (Trinchieri 2003; Seder et al. 1993; Hsieh et al. 1993; Oppmann et al. 2000). This data suggests that previously reported enhanced T cell stimulation by DCs with multiple centrioles might be mediated via facilitated T cell attraction and cytokine supply. In comparison, in supernatant of CETN2-GFP^{low} cells increased levels of the alarmins S100a8 and S100a9, which mainly form a heterodimeric complex, were detected (Hunter and Chazin 1998). S100a8 and S100a9 belong to DAMPs and are mostly found in inflamed tissues as they are secreted by activated monocytes, neutrophils, DCs and early differentiation stages of macrophages as well as activated vascular cells (keratinocytes and epithelial cells) (Rammes et al. 1997; Frosch et al. 2000; Hessian et al. 1993; Zwadlo

et al. 1988; Averill et al. 2011). Functionally, S100a8 and S100a9 are described as immunoregulatory mediators mainly having pro-inflammatory effects (Pruenster et al. 2016).

Interestingly, a closer look on the secretion of cytokines revealed enriched secretion of IL-1 superfamily members IL-1β (gene name *Il1b*) and IL-36γ (gene name *Il36g*) by CETN2-GFP^{low} cells in comparison to CETN2-GFP^{high} (**Figure 5.28 c**). IL-1β is cleaved and secreted after inflammasome formation which might hint towards activation of this pathways in CETN2-GFP^{low} cells (Martinon et al. 2002). The cytokine IL-36γ (gene name *Il36g*) functionally has pro-inflammatory effects on surrounding cells like activating endothelium and inducing Th1 polarization of naïve CD4^{+} cells (Bridgewood et al. 2017; Vigne et al. 2012). Due to its role in autoimmune and inflammatory diseases, targeting IL-36 pathway might be interesting for new therapeutic approaches (Queen et al. 2019).

Altogether, our secretome analysis revealed that DCs with multiple centrioles exhibit differential secretion of specific proteins. In addition, cells with two centrioles also displayed a distinct secretory phenotype. These findings give evidence that centriole numbers in DCs influence their secretory profile, which could shape the cellular surrounding and tissue microenvironment.

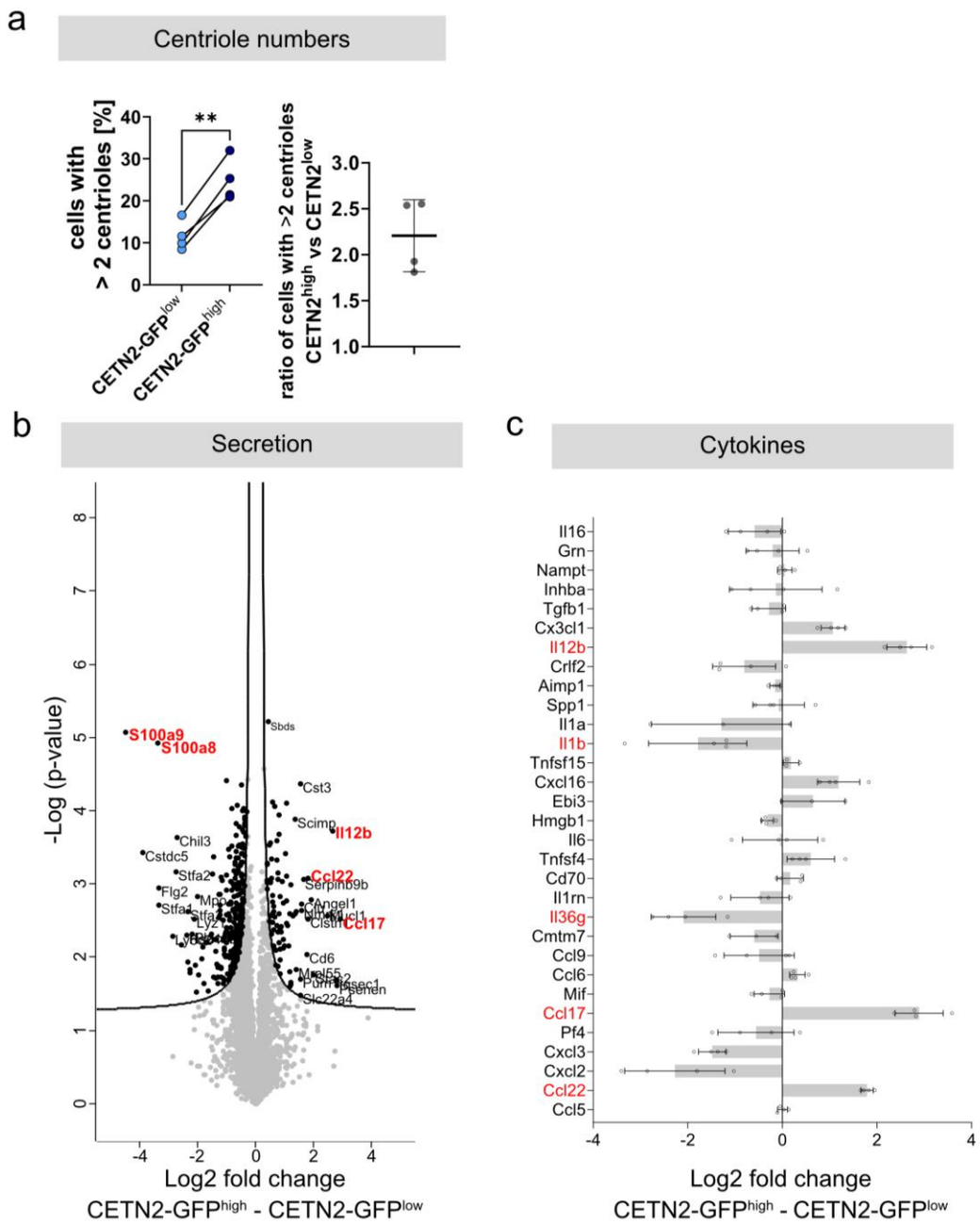

Figure 5.28 Secretion profile of DCs with different centriole numbers

(**a**) Centriole numbers of sorted DC 'subpopulations' were determined by confocal microcopy according to CETN2-GFP^{+}/γ-tubulin^{+} foci. Left: Frequency of cells with multiple centrioles in the BMDC 'subpopulations' CETN2-GFP^{low} (light blue) and CETN2-GFP^{high} (dark blue) with pairing between 'subpopulations' derived from one mouse. Right: Ratio of cells with multiple centrioles comparing CETN2-GFP^{high} and CETN2-GFP^{low} cells. Graph shows mean ± s.d. Each data point represents one independent experiment. $n = 4$. ***, $P < 0.0021$ (two-tailed, paired Student's t-test). (**b**) Supernatants of CETN2-GFP^{low} and CETN2-GFP^{high} cells were analyzed via mass spectrometry. Black dots in volcano-plot show significantly different proteins comparing CETN2-GFP^{high} vs. CETN2-GFP^{low} passing the cut-off of false discovery rate (0.05) and fudge factor $S_0 = 0.1$. (**c**) Fold change of cytokines comparing supernatants of CETN2-GFP^{high} vs. CETN2-GFP^{low} cells. Values below 0 depict enriched secretion by CETN2-GFP^{low} cells and values above 0 enriched by CETN2-GFP^{high} cells. Graph shows mean ± s.d. Each datapoint represents one independent experiment. $n \geq 3$. (**b** and **c**) Measurements and data analysis were performed by Stefan Ebner. Red font is used to highlight particular proteins.

6. Discussion

This study aimed to gain a comprehensive understanding of centrosome biology in DCs, in particular during the induction of an immune response. We showed that DCs containing multiple centrioles, which form over-active MTOCs, foster T cell priming. To shed light on the underlying mechanisms driving improved T cell activation by DCs with multiple centrioles, we analyzed the spatio-temporal dynamics of centrioles. Thereby, we concluded that a centrally localized centriole cluster is the optimal MTOC organization during IS formation. Altogether, various aspects concerning the regulation of these processes remain open for discussion, encouraging further investigations. The following section will highlight some aspects of the present work in greater detail and provide ideas for future studies.

6.1. Understanding the contribution of centriole numbers for DC biology

6.1.1. Centriole loss affects immune cell functionality

In line with our findings that centrosome integrity in DCs is important for efficient T cell activation, proper centrosome functionality is also vital in other cell types of the immune system (**Figure 5.10**). For example, B cell progenitors undergo apoptosis if they are lacking centrioles during development (Schapfl et al. 2024). However, if apoptosis is bypassed by co-depletion of the ubiquitin specific peptidase 28 (Usp28), which is involved in a p53-dependent cell cycle arrest pathway, mature B cells lacking centrioles can still mount a humoral immune response (Fong et al. 2016; Lambrus et al. 2016; Meitinger et al. 2016; Schapfl et al. 2024). It has been reported before that normal cells show p53-dependent cell cycle arrest after centriole loss, while cancer cells proliferate unimpededly (Wong et al. 2015). In comparison, in DCs we did not measure specific apoptosis markers but cell differentiation and maturation were unimpaired in the presence of the PLK4 inhibitor Centrinone (**Figure 5.9 b** and **c**). Thus, we assume that DC cell cycle progression is not majorly perturbed in cells lacking centrioles. Centriole depletion in cytotoxic T cells has been shown to reduce their killing capacity (Tamzalit et al. 2020). Cells lacking centrioles displayed impaired lytic granule biogenesis and defects in synaptic F-actin remodeling leading to reduced force exertion, which normally facilitates cytotoxicity (Tamzalit et al. 2020; Basu et al. 2016). Actin also plays an important role on the DC side of the IS for efficient T cell priming (Leithner et al. 2021). Further studies, analyzing the relation of centrioles and synaptic actin might identify mechanisms how perturbance of centrosome integrity diminishes T cell priming. In summary, while centrioles might be dispensable for cell cycle progression or effector functions in certain cell types, centrosome integrity also determines cell signaling events and essential cell functions during the immune response.

6.1.2. Lessons learned from the primary cilium

It is worth noting, that most cells form a primary cilium grown from the mother centriole when they exit into cell cycle arrest (G_0), while immune cells do not form cilia. It has been shown that lymphocytes have the capacity to form cilia but suppress ciliogenesis via retaining the ciliation inhibitory protein CP110 at the centrosome (Prosser and Morrison 2015). The absence of a cilium might be related to variable and dynamic localization of the centrosome within immune cells which is required for efficient IS formation and T cell activation (Tourret et al. 2010; Martín-Cófreces et al. 2008). In line with this, multiple studies have highlighted similarities between cilium structure and IS formation on the T cell side (Douanne et al. 2021). Examples are the docking mechanism of the centrosome or basal body through distal appendages and the actin rearrangements participating in IS or cilium formation (Stinchcombe et al. 2015; Tanos et al. 2013; Kim et al. 2010). In addition, both structures create specialized signaling hubs which rely on spatial and temporal organization of proteins for signal transduction. Therefore, for instance, the intraflagellar transport 20 (IFT20) protein co-localizes with the Golgi at the base of the cilium and sorts proteins destined for the ciliary membrane (Follit et al. 2006). In parallel, in T helper cells the IFT20 protein is associated with the centrosome and Golgi and is involved in the recruitment of linker for activation of T cells (LAT), a key adaptor molecule for transducing TCR signaling and mediating T cell activation (Vivar et al. 2016; Finetti et al. 2009). In contrast to this observation in T cells, we propose that the centrosome in DCs behaves differently during IS formation and does not reorient to the IS region which will be discussed in chapter 6.2.1. In conclusion, this paragraph highlights that immune cells such as lymphocytes utilize ciliary proteins at the IS and the absence of a cilium likely reflects functional specialization, allowing immune cells to dynamically position their centrosome and mediate efficient IS formation.

6.1.3. Centriole number control in DCs, MCCs and cancer cells

Interestingly, in addition to cells which form one primary cilium, epithelial cells form multiple motile cilia to generate fluid flow for example in the respiratory tract for mucus clearance or in the oviduct for egg migration (Fawcett and Porter 1954; Dirksen and Satir 1972). Multi-ciliogenesis involves a massive amplification of centrioles via two pathways: the parental centriole-dependent pathway, which is characterized by the parental centriole templating the assembly of several procentrioles; additionally, centrioles are formed via deuterosome-dependent biogenesis (Shahid and Singh 2018). During this process centrioles form at, so called, ‘deuterosomes’ which are acentriolar structures and consist of spherical dense masses of fibers organized into inner and outer areas (reviewed by (Shahid and Singh 2018), original: (Anderson and Brenner 1971)). Several proteins such as PLK4, Cep152 and SAS6 have been identified to localize to the deuterosome (Klos Dehring et al. 2013; Zhao et al. 2013).

Remarkably, these proteins also participate in canonical centriole-mediated centriole biogenesis and the regulation of centriole numbers (Kleylein-Sohn et al. 2007; Dzhindzhev et al. 2010; Peel et al. 2007). In line with this, overexpression of Cep152 in multi-ciliated cells (MCCs) resulted in increased MCC size, enhanced deuterosome formation and an elevated number of centrioles generated (Klos Dehring et al. 2013). In contrast, overexpression of PLK4 or SAS6 in MCCs did not affect centriole numbers (Klos Dehring et al. 2013). Notably, centriole amplification in MCCs occurs during terminal differentiation via an alternative cell cycle without DNA replication and classical mitosis (Choksi et al. 2024). These results raise the hypothesize that mature DCs, which are also terminally differentiated and acquire multiple centrioles during maturation, might share mechanisms of centriole amplification with MCCs. To explore potential mechanistic parallels, it would be valuable to determine whether Cep152 is enriched in the PCM of DCs containing multiple centrioles or during their overduplication process. Regarding the regulation of centriole biogenesis, it is known that PLK4 inhibition does not prevent the presence of multiple centrioles in mature DCs, while PLK2-deficient cells display a reduced rate of centriole amplification (Weier et al. 2022). However, the role of PLK2 in centriole amplification within MCCs remains unresolved, and further investigations are necessary to clarify whether a unique cell cycle state or other aspects of cell identity ultimately govern centriole amplification in both MCCs and DCs.

As described above, increases in centriole numbers occur in differentiated cells under physiological conditions but also in cancerous cells. In cancer cells, multiple mechanisms provoke centriole overduplication, for example overexpression of PLK4 or PCNT or centriole disengagement driven by PLK1 (Dwivedi et al. 2023; Habedanck et al. 2005; Dustin and Cooper 2000; Pihan et al. 2001). In DCs, elevated centriole numbers are acquired PLK2-dependent and via mitosis failures (Weier et al. 2022). These previous reports encouraged us to artificially induce overduplication of centrioles by PLK2 or PLK4 overexpression. Unfortunately, Hoxb8 cells were unable to survive in the presence of these genetic modifications (data not shown). This result may be due to a tight regulation of centriole numbers with DNA duplication, which prevented cell proliferation after centriole overduplication. However, genetic manipulation and protein overexpression in DCs was successful in the case of doxycycline-dependent Nedd1-mOrange2-rCM1 expression. Based on this, one could propose to overexpress other PCM proteins such as PCNT to assess whether similar centriole multiplication mechanisms – as in cancer cells – operate in DCs.

6.1.4. Functional consequences of multiple centrioles

6.1.4.1. Immune cells versus cancer cells

High centriole amplification rates in cancer cells have detrimental consequences for human health, for example via promoting an invasive cell-phenotype (reviewed by LoMastro and Holland 2019). Therefore, targeting amplified centrioles is a possible strategy for cancer therapy. For example, the PLK4 inhibitor Centrinone B, a close analogue of Centrinone used in this study, has been shown in preclinical experiments to reduce melanoma cell proliferation and induce apoptosis (Wong et al. 2015; Denu et al. 2018). More recently, the PLK4-inhibiting drug RP-1664 was developed, exhibiting improved potency, selectivity and pharmacokinetic properties. RP-1664 is currently being evaluated in a Phase 1 clinical trial for the treatment of advanced solid tumors (NCT06232408) (Vallée et al. 2025). Whether this agent will prove therapeutically effective remains to be determined.

Of note, in this study, we report that antigen-presenting DCs with multiple centrioles conduct ameliorated T cell activation capacity. This finding adds to previous work by Weier et al., who demonstrated that DCs harboring multiple centrioles bear an increased capacity to induce T cell proliferation as well as an improved directional locomotion. Together, this highlights the potential of DCs with multiple centrioles to augment immune cell activation. DCs with multiple centrioles may therefore be particularly well-suited for rapid migration to LNs and T cell activation and proliferation within a short timeframe.

In line with our findings, artificial duplication of centrioles in other APCs, such as B cells and macrophages, shows boosted cell functionality as well. In B cells, artificial centriole amplification by PLK4 overexpression, leads to augmented T cell activation which is mediated by improved antigen processing and presentation (Yuseff et al. 2011). Upon centriole amplification in microglia, which are the tissue resident macrophages of the brain, phagocytosis of dead neurons – a process termed efferocytosis – is enhanced (Möller et al. 2022). Curiously, both processes are marked by centriole polarization either to the B-T cell synapse or to the phagosome. Centriole polarization in different cell types will be discussed in chapter 6.2.1.

We primarily studied centriole amplification occurring after LPS stimulation of DCs, but other pathogenic stimuli induced a similar phenotype with slightly varying rates of amplification (Kiermaier group, unpublished data). This suggests a possible mechanism by which modifications in centriole amplification during initial DC activation could fine-tune the evolving immune response. However, this raises the question of whether DCs with multiple centrioles, which induce enhanced T cell activation, could pose a risk of excessive immune activation, indicating the need to further investigate the regulation and balance of centriole amplification in immune cells.

6.1.4.2. MTOC functionality and intracellular organization

One project aim was to understand the intracellular events associated with centriole amplification in DCs. Our results demonstrated that multiple centrioles in DCs form a single over-active MTOC characterized by increased PCM condensation at the centrosome and an elevated number of MTs.

Typically, enhanced recruitment of PCM is linked to PLK1-induced centrosome maturation in G_2/M transition of the cell cycle. PLK1 is not upregulated in DCs upon LPS stimulation, which indicates that an alternative mechanism facilitating PCM recruitment might be in place in DCs with multiple centrioles (Weier et al. 2022). Notably, in macrophages, pathogen encounter induces PLK1-independent centrosome maturation during interphase leading to PCM expansion and increased MT nucleation (Vertii et al. 2016). This atypical centrosome maturation depends on members of the mixed-lineage kinase (MLK) family, whose role in the recruitment of PCM to multiple centrioles in DCs remains to be elucidated.

It would be interesting to perform high resolution analysis of PCM composition in DCs with multiple centrioles and subsequently identify whether alternative signaling pathways might be activated, like it is the case in cancer cells. More precisely, in cancer cells amplified centrioles cause PIDDosome formation (Fava et al. 2017). The activation of this multi-protein complex induces p53-dependent and p21-mediated cell cycle arrest and apoptosis (Fava et al. 2017). Other well characterized events linked to amplified centrioles are the production of reactive oxygen species (ROS), an extra centrosome-associated secretory phenotype (ECASP) and lysosome dysfunction (Adams et al. 2021; Arnandis et al. 2018). ROS production as well as the ECASP promote invasion of surrounding cells. Strikingly, ROS are also produced in DCs upon antigen encounter but whether ROS production correlates with centriole numbers remains an open question (Vulcano et al. 2004). In macrophages, the centrosome and its maturation are crucial for cytokine production (Vertii et al. 2016). As the cytoskeleton is notoriously linked to the secretory pathway, the role of multiple centrioles and MTs for secretion will be discussed in a later paragraph (6.1.4.4). Additionally, as a future perspective, analysis of the lysosome compartment, which's proper function is important for antigen processing and presentation in DCs, will provide a deeper understanding of the intracellular organization in DCs upon centriole multiplication (Embgenbroich and Burgdorf 2018).

6.1.4.3. A computational approach to understand the role of MT numbers

To elaborate on the effects of increased MT numbers resulting from the presence of multiple centrioles, a computational modeling approach complemented our findings (model developed by collaboration partners: Apurba Sarkar, Subhendu Som, Raja Paul, Heiko Rieger). This interdisciplinary approach enables the integration of experimental data into complex simulations across multiple spatial and temporal scales, revealing insights that cannot be observed or measured experimentally. This method simulates growth and shrinkage of MTs and docking at the IS region (see also (Sarkar et al. 2019)). This additional data demonstrated that enhanced MT numbers accelerate MT docking at IS regions (**Figure 6.29**).

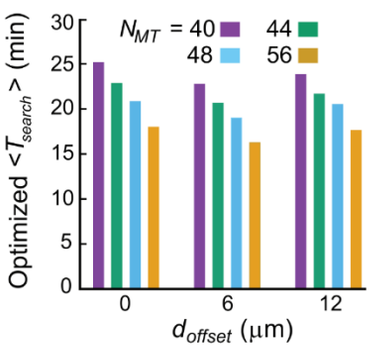

Figure 6.29 Search time of MTs for the IS region is decreased in cells with elevated numbers of MTs
d_{offset}: offset of the nucleus from the cell center; N_{MT}: MT number; T_{search}: MT search time.

To assess whether this enhancement is causal for improved T cell activation, we conducted a gain-of-function study by inducing overexpression of Nedd1-mOrange2-rCM1 in Hoxb8-derived DCs to increase MT nucleation. However, this increase did not appear to enhance T cell activation, potentially due to de-clustered centrioles and the presence of multiple MTOCs within each cell. We speculate that this altered centriole configuration perturbs MT array organization, thereby diminishing the T cell priming capacity of DCs, which is in line with results from DC treatment with the de-clustering agent PJ-34 (**Figure 5.24**). Supporting this, multiple MTOCs have been shown to perturb DC migration in both 2D and 3D environments by causing polarization defects (Homrich 2023). Moreover, elevated MT numbers alone may be insufficient to improve T cell activation, as MTs in cells with multiple centrioles could be subject to distinct posttranslational modifications that affect their properties such as stability and motor binding affinity (Janke and Magiera 2020). Thus, it remains uncertain whether increasing MT nucleation beyond the physiological level induces, in addition to centriole disengagement, other unknown and functionally adverse side effects that resulted in unimproved T cell priming. In summary, computational modeling of MT dynamics and docking at the synapse suggests a minimized search time for the synapse region in cells with enriched MT numbers such as in DCs with multiple centrioles.

6.1.4.4. IS arrangement and the secretory pathway

Mechanistically, MTs might participate in IS formation and efficient T cell priming by influencing the transport of surface molecules to the synapse region like it was shown in T cells that MTs bring endosomal TCR to the cSMAC area (Choudhuri et al. 2014; Mittelbrunn et al. 2011). It would be interesting to investigate whether the composition or structure of the synapse region varies in DCs harboring two or multiple centrioles. For example, perturbing the cytoskeletal component actin converts a multi-focal synapse structure into a mono-focal synapse in DCs, which reduces $CD4^+$ T cell priming efficiency (Leithner et al. 2021). Recent advancements in cryo-expansion microscopy can facilitate detailed analysis of synapse structure and composition. This technique has been successfully applied to visualize cytotoxic T cell synapses and enables improved nanoscale imaging of synaptic proteins, providing novel insights into IS organization (Lemaître et al. 2025).

In addition, MTs are largely involved in regulating long-distance transport of vesicles and thus facilitating directional secretion of soluble molecules to the IS, which was shown previously in T and B cells – but is contradictory reported for DCs (Huse et al. 2006; Sáez et al. 2019; Pulecio et al. 2010; Bertrand et al. 2010). In other immune cells, namely macrophages, cytokine secretion depends on the centrosome acquiring more PCM and MT filaments upon cell activation (Vertii et al. 2016). These changes in MTOC function were also observed in DCs with multiple centrioles. Based on this, we characterized the secretory phenotype of DCs in relation to their centriole numbers. Therefore, cells were sorted via flow cytometry according to their CETN2-GFP signal intensity, which correlates with centriole numbers. This method introduced by Weier et al. was advanced by establishing a stable stringency of cell selection, which aims for greater reproducibility. Secretome analysis was performed using mass spectrometry. While this technology enabled a comprehensive profiling of the variety of secreted proteins, it does not provide information on the directionality of secretion. In addition, our experimental design did not incorporate signals that DCs may receive from T cells, although, this represents a potential area for future research as T cell-derived signaling via the CD40L-CD40 axis is known to modulate IL-12 secretion by DC (Tourret et al. 2010; Miro et al. 2006). Nevertheless, our results demonstrated that extra centrioles influence the secretory phenotype of DCs which, in turn, directs the immune response as previously described in chapter 2.2.3 (**Figure 2.5**). Whether these proteins are more precisely regulated on a transcriptional level was not addressed. In previous studies, no changes in Il-6, Ccl5 and Cxcl1 mRNA but changes in Ccl17 mRNA levels were observed (Weier et al. 2022). This implies that also the production of CCL17 and not only the secretion is upregulated, while the level of regulation is unclear for other detected cytokines such as IL-12 or IL-23. As a future direction, mRNA sequencing could be employed to address this missing aspect.

At present, we speculate that enriched secretion of the chemokines CCL17 and CCL22 and the cytokine IL-12 or IL-23 by cells with multiple centrioles may enhance T cell attraction and activation. IL-12 secretion by DCs is known to induce Th1 cell differentiation of naïve $CD4^+$ T cells, thereby playing a critical role in protection against intracellular pathogens and tumors (Macatonia et al. 1995). Similarly, IL-36γ, which is found at elevated levels in supernatant of cells with two centrioles, has been described to promote Th1 differentiation (Vigne et al. 2012). Although there is no direct indication of a difference regarding Th1 cell differentiation, it would be interesting to analyze whether there are alterations in T helper cell subtype differentiation induced by DCs with different centriole numbers.

Extending the discussion of cytokine functions, IL-12 and IL-23 have therapeutic implications in the inflammatory skin disease psoriasis. Neutralizing antibodies against the p40-subunit (alternative name for IL-12β subunit), which is present in IL-12 and also IL-23 cytokine, substantially improved psoriasis pathogenesis in patients (Leonardi et al. 2008). The beneficial effects of this therapy were shown to depend on IL-23 inhibition, which prevents pathogenic Th17 cell expansion, while IL-12 has a regulatory function and limits skin inflammation (Kulig et al. 2016). IL-36γ has both protective functions and pro-inflammatory effects as well. It's expression is increased after skin injury and promotes wound healing (Jiang et al. 2017). In contrast, IL-36γ is also involved in pro-inflammatory activation of keratinocytes and macrophages, which promotes leukocyte recruitment and contributes to pathogenic inflammation during psoriasis pathogenesis (Bachmann et al. 2012; Bridgewood et al. 2017; Bridgewood et al. 2018). Targeting this axis via blocking IL-36 receptor is described and discussed as new treatment strategy for psoriasis (Maçães et al. 2022; Mullard 2022). In summary, targeting IL-12, IL-23 or IL-36γ axes could dampen the progression of inflammatory diseases, thus how their release by DCs is regulated and whether it depends on the cytoskeleton network will be an important investigation in the future.

The functions of S100a8 and S100a9, two alarmins which were increased detected in supernatant of CETN2-GFP^{low} cells, are particularly intriguing. S100a8 and S100a9 are predominantly produced by activated myeloid and endothelial cells during various inflammatory disorders and, thus, are used as a diagnostic marker for diseases such as arthritis, inflammatory bowel disease or dermatitis (Pruenster et al. 2016). Once released, S100a8/S100a9 heterodimers act on surrounding cells. Binding to TLR4 amplifies inflammation in epithelial cells, monocytes, macrophages, neutrophils or T cells (Pruenster et al. 2016). More precisely, $CD8^+$ T cells from patients with lupus erythematosus produce IL-17 in response to S100a8/S100a9, which contributes to the development of autoreactive lymphocytes (Loser et al. 2010). The same study, implementing a mouse model of systemic autoimmunity via CD40L expression in keratinocytes, demonstrates that $CD4^+$ T cells are not responding to S100a8/S100a9 by IL-17 upregulation and do not drive autoimmunity via this pathway, even though $CD4^+$ T cells also

express functional TLR4, which can contribute to autoimmune inflammation (Reynolds et al. 2012). The reason for this difference in $CD4^+$ and $CD8^+$ T cell responses remains unclear. Thus, further investigations of T cell phenotypes after priming by DCs with varying centriole numbers may shed light on these mechanisms and regulatory processes.

Of note, the response of DCs to S100a8/S100a9 was analyzed during allergic contact dermatitis (Petersen et al. 2013). Surprisingly, persistent stimulation with S100a8/S100a9 blocks DC differentiation and antigen presentation, resulting in a diminished T cell response. This suggests that while S100a8/S100a9 might initially promote inflammation, their prolonged presence dampens immune activation and limits tissue-damaging inflammation. In connection with our experiments, MHCII expression, indicative of antigen presentation, were unaltered in DCs harboring two or multiple centrioles (Weier et al. 2022). Whether the S100a8/S100a9-TLR4 axis also plays a role in our experiments, which encompass only a rather short timeframe of 20 h, was not addressed. Beyond effects via extracellular release, S100a8/S100a9 complexes also have intracellular functions. For instance, in granulocytes, they promote tubulin polymerization, which is regulated via p38 mitogen-activated protein kinases (MAPKs) and calcium-dependent signal transduction (Vogl et al. 2004). The authors also showed that cells deficient in S100a8/S100a9 complexes contain reduced MT numbers (Vogl et al. 2004). Moreover, the connection of the cytoskeleton and S100a8/S100a9 is shown by the observation that targeting S100a8/S100a9 reduces transendothelial migration of phagocytes by attenuating the activity of the small guanosine triphosphate (GTP-)ases Rac1 and Cdc42, which are involved in actin remodeling (Vogl et al. 2004; Ridley et al. 1992; Adams et al. 1990). Collectively, these findings highlight the complex intracellular and paracrine roles of S100a8/S100a9 in modulating cellular functions.

Interesting is the release of S100a8 and S100a9 per se because it does not occur via the classical ER/Golgi route, as these proteins lack signal sequences (Rammes et al. 1997). Instead, their secretion involves a protein kinase C-dependent mechanism that intriguingly requires an intact MT cytoskeleton (Rammes et al. 1997). Thus, the abundance of S100a8/S100a9 in the supernatant of CETN2-GFP^{low} cells suggests that cells with two centrioles maintain a functional MT network necessary for this secretion process. In addition, S100a8/S100a9 release can result from cellular necrosis upon tissue damage or transient gasdermin D pore formation triggered by NOD-like receptor pyrin domain-containing protein 3 (NLRP3) inflammasome activation (Voganatsi et al. 2001; Pruenster et al. 2023). In combination with enhanced IL-1β secretion by CETN2-GFP^{low} cells, inflammasome activation is likely in these cells. However, it is fundamental to verify whether the detected IL-1β is in its active (cleaved) form and to directly visualize inflammasome complex formation. In macrophages, a connection between inflammasome activation and loss of PCM proteins has been described (Bai et al. 2024). Thus,

inflammasome activation in CETN2-GFP^{low} cells could explain less PCM and less MT numbers in these cells.

These insights highlight distinct and tightly regulated pathways governing the release of inflammatory mediators, with the precise role of the MT cytoskeleton remaining unresolved. Moreover, further investigations are needed to understand the interplay between the centrosome and inflammation.

From a methodological perspective, it is interesting that for research on T cell biology the APC has been mimicked using lipid bilayers presenting peptide-MHC complexes along with integrins and co-stimulatory molecules (Dustin and Groves 2012). These bilayers provide controlled conditions allowing to study T cell intrinsic events during IS formation, while leaving the DC as complex interaction partner and activator aside. Such an approach, mimicking the T cell side, was not yet established for analyzing DCs during IS formation. However, as we have shown that the DC phenotype majorly controls T cell priming, it should be revised whether conclusions drawn from isolated analyses without cell-cell communication hold true under physiological conditions.

Taken together, both DC 'subpopulations' – containing two centrioles or multiple – secrete immunomodulatory mediators and are capable of priming T cells. However, we hypothesize that DCs with two centrioles are more specialized to induce inflammation directly at the site of infection via inflammasome activation and the secretion of alarmins, while DCs with multiple centrioles are highly migratory and superior in priming T cells by chemoattraction and cytokine stimulation.

As this hypothesis includes multiple factors and complex microenvironments, it is hard to address this question of DC centriole numbers and the outcome of the immune response in practical experiments. Possibly, modifying the performed animal experiment by injecting CETN2-GFP^{low} or CETN2-GFP^{high} cells into mice and monitoring T cell activation in the LNs could reveal the effects of the cell identity during the whole process. However, an alternative approach to address this hypothesis would be to develop a computational model, which mimics DC and T cell behavior towards and within the LN. This approach would include multiple DC properties such as migratory capacity and chemokine and cytokine secretion and could analyze their individual influence on T cell priming, possibly explaining the outcome of *in vivo* experiments.

In summary, we want to highlight the dual role of amplified centrioles in cancerous cells contributing to invasiveness and in benign cells of the immune system fostering the immune response. This emphasizes the need for cell type- and context-dependent studies.

6.2. Centrosome positioning and organization during IS formation

6.2.1. Effects of a centrally localized centrosome in DCs

Dynamic movement of the centrosome and establishment of cell polarity are important for cellular functionality, demonstrated by precise centrosome localization for example during mitosis, cell locomotion or IS formation. By analyzing antigen-specific contacts of DCs and $CD4^+$ T cells *in vitro* by live cell imaging and *in vivo* in lymphoid tissues, we could show that DC centrioles – either two or multiple – are located at the cell center near the nucleus and not polarizing to the IS contact site as it has been reported for NK, T and B cells. Moreover, computational modeling of optimal centriole positioning in DCs provided evidence that the geometrically optimal MTOC position, to minimize the MT search time for the IS, is in the DC cell center (**Figure 6.30 a** and **b**, data from Apurba Sarkar, Subhendu Som, Raja Paul, Heiko Rieger). Thus, true to its name, the centrosome remains at the center of the cell.

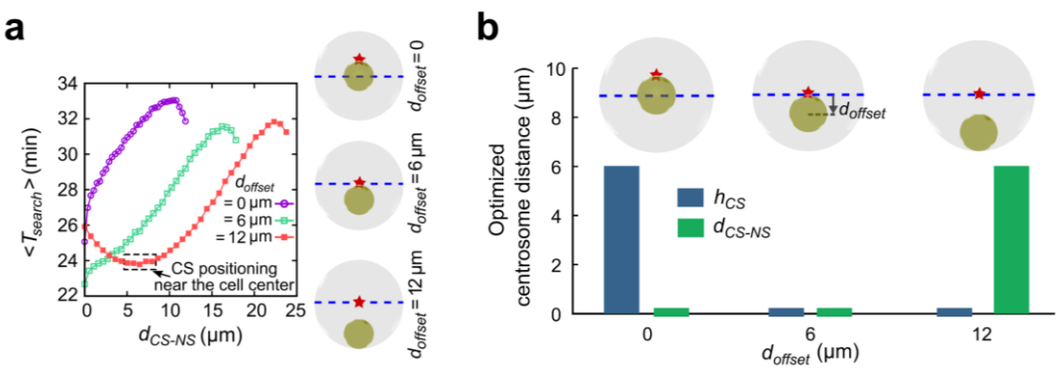

Figure 6.30 Centrosome positioning near the cell center is optimal to achieve a minimal MT search time
(**a**) Graph displays the MT search time (T_{search}) versus the distance of the centrosome to the nuclear surface (d_{CS-NS}) for different nucleus offset positions (d_{offset}). (**b**) Optimized values of the centrosome distance from the cell center (h_{CS}) and from the nuclear surface (d_{CS-NS}) for different off-centered positions of the nucleus. The optimal centrosome positions are denoted by the red stars in the schemes.

As underlying mechanism, which makes the cell center the optimal centrosome position, we postulate that especially the docking of MTs at synapse regions and thereby the supply of stimulatory molecules to T cells are improved when the MTOC is located at the cell center. From *in vitro* and *in vivo* experiments, we concluded that DCs form contacts with multiple T cells at the same time. This situation, in particular, requires a central centrosome to enable fast MT docking at all T cell contact sites. Simply the large size of DCs could contribute to binding of multiple T cells. However, B cells, which are smaller, can also form synapses with two or even four T cells at the same time (Gonzalez et al. 2015). Unfortunately, the MTOC position during this process was not analyzed in this study. For cytotoxic T cells, it is shown that binding to two antigen-specific targets simultaneously leads to oscillation of the MTOC between the two target cells and that lytic granules accumulate at both sites, which seems to enable efficient killing of multiple cells (Kuhn and Poenie 2002; Wiedemann et al.

2006). Of note, we have extensively analyzed mono- and multi-conjugate synapses and two or multiple centriole abundance to elaborate on the possibility of MTOC polarization in different scenarios.

Similar to our results, other studies imply that MTOC polarization in conventional and plasmacytoid DCs is dispensable for $CD4^+$ T cell activation (Bouma et al. 2011; Mittelbrunn et al. 2009). In contrast, DCs priming $CD8^+$ T cells were shown to reposition their centrosome towards the T cell site (Pulecio et al. 2010). In this case, MTOC polarization is important for the delivery of IL-12 to the synapse and efficient T cell activation. Of note, there is also the possibility that cytokines in DCs polarize without MTOC polarization, which was reported for IL-18 in immature DCs interacting with NK cells (Semino et al. 2005). This contact is important for NK cell activation and can lead to DC maturation or DC lysis (Piccioli et al. 2002). Cytokine localization within the DC during priming of $CD4^+$ T cells was not yet evaluated but individual tests of lysosome or Golgi staining in DCs showed major parts of these organelle compartments localized at the centrosome, which indicates a central role for the centrosome to orchestrate organelle positioning while the precise localization of cytokine-containing vesicles remains unclear (data not shown).

In $CD4^+$ T cells, two separate pathways of secretion are described: one directs cytokines such as IL-2, IFN-γ and IL-10 to the IS and the other releases proteins such as TNF, IL-4 and CCL3 in a multi-directional way (Huse et al. 2006). It is assumed that specifically targeted cytokines are meant to influence only the interacting cells while a broader release affects also bystander cells and leads to wider activation. Interestingly, IFN-γ, which is secreted in a polarized manner by cytotoxic T cells, is not restricted to the target cell and affects bystander cells (Sanderson et al. 2012). DCs presumably possess a large and diverse secretion machinery, as their functions include extensive cytokine secretion and regulating the attraction and activation of multiple immune cells.

In essence, we observed a central position of the centrosome during $CD4^+$ T cell priming and in combination with results from computational modeling we concluded that this is the optimal position in this context. It remains an open question whether this is connected to additional functions DCs fulfill simultaneously, such as recruitment and activation of other immune cells via chemokine and cytokine release, which are independent of polarized secretion. As a future perspective, visualization and tracing of cytokines within DCs during T cell priming could be assessed via high-resolution live cell microcopy. This approach would reveal insights into the spatio-temporal organization and regulation of cytokine secretion in DCs.

6.2.2. How is centrosome positioning accomplished within a cell?

As the centrosome localization is variable and might change dynamically according to cell function, one might pose the general questions: How is the centrosome positioned within a cell and particularly during IS formation? What are the key physical forces and proteins involved in this process? One part of the newly developed computational model describes that MT-generated pushing forces alone are sufficient to act on the centrosome and position it at the center near the nucleus (**Figure 6.31**, data from Apurba Sarkar, Subhendu Som, Raja Paul, Heiko Rieger). However, under complex physiological conditions centrosome positioning can be influenced by multiple factors such as pulling forces generated by dynein, interaction with other organelles like the nucleus, cytoplasmic viscosity and actomyosin contractility (Wu et al. 2011; Kimura and Kimura 2011; Schaeffer et al. 2025; Xie et al. 2022; Malone et al. 2003).

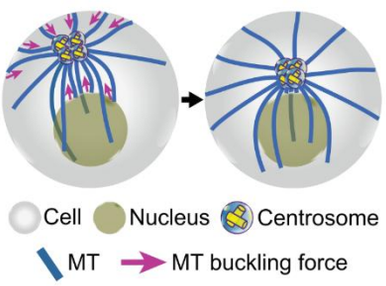

Figure 6.31 Scheme describing that MT-generated forces are sufficient to position the centrosome at the cell center

A physical association of the centrosome to the nucleus has been described in *C. elegans* during embryogenesis, which requires the proteins SUN-1 and ZYG-12 belonging to the linker of nucleoskeleton and cytoskeleton (LINC) complex (Malone et al. 2003). In murine B cells, disruption of the LINC complex or centrosomal actin allows detachment of the centrosome from the nucleus and polarization to the IS (Obino et al. 2016). This study by Obino et al. shows that the centrosome to nucleus connection is a conserved mechanism to position the centrosome in murine immune cells but it undergoes changes during the immune response. In our experiments, we observed a close association of the centrosome to the nucleus which suggests that there might be linker proteins maintained in DCs during IS formation to keep the centrosome in place. How the centrosome to nucleus connection is regulated in DCs during T cell activation is largely unstudied.

One recent approach of an image-based phenotypic siRNA-mediated knock-down screen uncovered proteins regulating centrosome and/or lysosome polarization in B cells upon B cell stimulation (Obino et al. 2023). Whether a knock-down screen could also uncover proteins, which *induce* centrosome polarization in DCs, is unclear. One might speculate that inducing DC centrosome polarization to the

DC-T cell contact site is difficult to achieve artificially because multiple proteins are required for this process in other cells. For example, T cell MTOC reorientation depends on TCR signaling, localized accumulation of diacylglycerol (DAG) and MTs docking at the pSMAC synapse region (Sedwick et al. 1999; Kuhn and Poenie 2002; Quann et al. 2009). The study by Pulecio et al., which showed DC centrosome polarization during priming of $CD8^+$ T cells, reported that the process in DCs depends on Cdc42 (Pulecio et al. 2010). Centrosome polarization to the forming phagosome in microglia is also linked to DAG recruitment (Möller et al. 2022). Deciphering localization and activation of these molecules in DCs would reveal new insights in cell type and synapse differences.

Recent work observes a great influence of non-specific actomyosin flow to position the centrosome at the cell center in immortalized human retinal pigment epithelial (RPE) cells (Schaeffer et al. 2025). In addition, during the process of centrosome centering, dynein-mediated transport along MTs drives cell shape changes leading to a redistribution of the cell mass around the centrosome. The authors discuss that the extent to which MTs contribute to the centrosome position may depend on size and shape of the cell in relation to the density of the actin network as both cytoskeletal networks are coupled and influence each other (Schaeffer et al. 2025).

During cytotoxic synapse formation, within the first minute, actin accumulates at the contact area (Ritter et al. 2015). Next, retrograde actin flow leads to a decrease in actin density and at the same time centrosome polarization begins, which highlights the interplay of both cytoskeletal components. Interestingly, in DCs, actin controls the contact time with T helper cells (Leithner et al. 2021). Optimal actin dynamics in DCs are important to form a multi-focal synapse structure and efficiently prime T cells. In the present study, actin controlling the DC centrosome positioning or organization was not studied but it would be valuable to explore this in the future.

Actin density and organization might not be the only difference between cell types. DCs and B or T cells largely differ in their size and their ratio between nucleus-to-cytoplasm size. This requires, for example, B cells to reorient their nuclear groove facing the IS to facilitate antigen extraction (Ulloa et al. 2021). Additionally, MTs bend in T cells to a higher extent than in DCs, where they can grow astrally from the centrosome. In DCs, MTs might more often touch the cell surface perpendicular leading to instant catastrophe and no MT gliding along the surface as it is proposed in T cells (Yi et al. 2013).

This highlights that specialized cells bear specialized MT and actin organization, suggesting also a cell-type-specific regulation of these cytoskeletal components. While several studies discovered the roles of individual cytoskeletal components and associated proteins during IS formation, further investigations are needed to understand centrosome positioning in DCs forming conjugates with T

cells, particularly elucidating how the interplay of multiple factors and differences to other cell types contribute to our observations of a centrally localized centrosome.

6.2.3. Significance of centriole clustering for cell functionality

A second measurement of centriole organization, which largely influences MTOC functionality and intracellular organization, includes centriole clustering. In comparison to cancer cells, which are highly proliferative and need to cope with multiple centrioles during mitosis, mature DCs are non-proliferating cells. Therefore, we sought that de-clustering and subsequent polarization might happen as part of fulfilling the specific effector function of priming multiple T cells. However, we observed *in vitro* and *in vivo* a tight clustering of multiple centrioles within DCs during antigen-specific T cell contacts. In cells with two centrioles, the intracentrosomal distance, which resembles a measurement for centrosome linker integrity, was unchanged as well. In addition, artificial de-clustering of multiple centrioles perturbed the DC efficiency to prime T cells. Further, mimicking de-clustering of multiple centrioles in computational simulations showed that an optimal MT search time for synapse regions is reached when all centrioles remain in a clustered configuration (**Figure 6.32**, data from Apurba Sarkar, Subhendu Som, Raja Paul, Heiko Rieger).

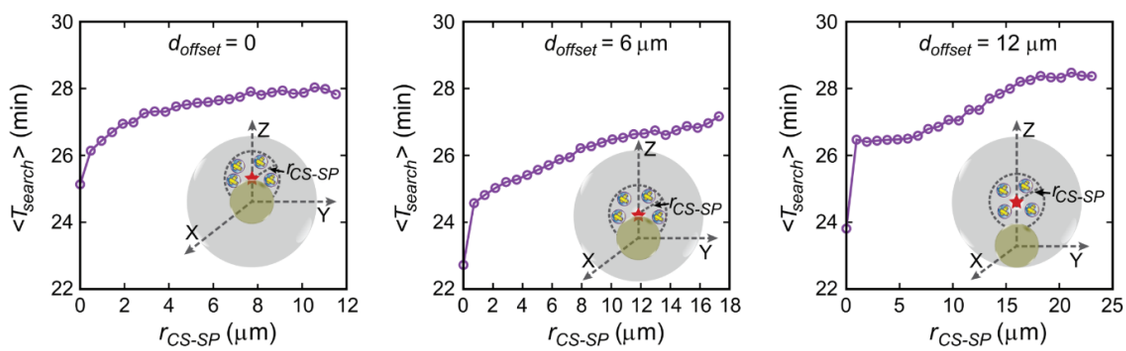

Figure 6.32 MT search time is minimized when centrioles maintain a clustered configuration
Graphs display MT search time (T_{search}) versus the radius of a cluster of multiple centrioles in cells with different nucleus offset (d_{offset}) positions. r_{CS-SP}: radius of the imaginary sphere centered at the optimal centrosome position.

Of note, DC treatment with the de-clustering agent PJ-34 had primarily an impact on cells with multiple centrioles, thus we assume that the centrosomal linker remained intact during T cell priming. Others have shown that manipulation of linker proteins leads to rupture of centrosome coherence in immune cells during migration in challenging environments (Schmitt et al. 2025). Similar perturbation experiments would reveal insights into the importance of two tightly connected centrioles in DCs for priming T cells.

De-clustering of multiple centrioles is accompanied by multiple MTOCs within one DC. As proposed earlier, in DCs a perturbed MT array organization might impair efficient delivery of molecules to the IS or to the cell periphery in general. Centriole de-clustering, which was observed as a side effect after enhancement of MT nucleation via Nedd1 overexpression, could also explain why the DC capacity to prime T cells was not improved. Effects of de-clustering agents on DC migration were analyzed before (Homrich 2023). Cells with de-clustered centrioles showed an impaired cellular polarization phenotype but in parts side effects on MT integrity were reported. However, both observations indicate that de-clustered centrioles perturb DC functions.

In cancer cells, de-clustering of centrioles leads to multi-polar spindle assembly resulting in chromosomal instability, mitosis failure or cell death. Therefore, treatment of cancer with de-clustering agents shows promising results (Pannu et al. 2014). In cardiomyocytes, which are often binucleated and contain multiple centrioles, clustering of centrioles and the assembly of pseudo-bipolar spindles have been reported and are supposed to be crucial mechanisms for enabling cell division and supporting heart regeneration (Leone and Engel 2019).

In contrast to impaired cellular functions or viability due to centriole de-clustering, in MCCs, centriole dissociation and dispersion are integral parts of multiple cilia formation. Ciliogenesis is regulated through oscillating proteins such as CDK1 and anaphase-promoting complex or cyclosome (APC/C) spatiotemporally coordinating centriole growth and disengagement, while the underlying mechanisms are unclear (Al Jord et al. 2017; Choksi et al. 2024). In this context, centriole disengagement occurrs under physiological conditions to enable multi-ciliation and cellular functionality. Additionally, in the study by Möller et al., in which the phagocytic capacity of microglia was enhanced by artificial centrosome duplication, two separated centrosomes were reported in the cells – each being able to mediate successful phagocytic engulfment (Möller et al. 2022). This represents not only an advantage of multiple centrioles but also of de-clustered centrioles.

In summary, DCs, cancer cells and cardiomyocytes rely on a proper arrangement of multiple centrioles either for cell functionality or for cell proliferation, which emphasizes the importance of elucidating the molecular mechanisms involved in maintaining a clustered centriole configuration.

6.2.4. Underlying mechanisms of centriole clustering

Mechanisms of centriole clustering or disengagement can be attributed to various mechanisms ranging from centrosomal linker integrity to cytoskeleton-dependent forces or associated proteins.

The linker proteins C-Nap1 and Rootletin are involved in centrosome coherence and upon the onset of mitosis they are phosphorylated by Nek2 kinase and thereby displaced (Bahe et al. 2005; Fry et al. 1998). Recently, C-Nap1 was also described to be important for centrosome coherence in immune cells during migration in challenging environments (Schmitt et al. 2025). In this context, also the protein dual-specificity tyrosine-(Y)-phosphorylation regulated kinase 3 (Dyrk3) was identified to protect the centrosome from splitting (Schmitt et al. 2025).

In addition to aspects of centrosome linker integrity, in cells with multiple centrioles also other mechanisms might contribute to centriole clustering. In cancer cells, a genome-wide screen uncovered multiple factors that cooperatively maintain centriole clustering during mitosis into two spindle poles (Kwon et al. 2008). These include actin and actin-based contractions, cell adhesion proteins or MT-associated proteins (Kwon et al. 2008). In more detail, dynein localization is important for centriole clustering (Quintyne et al. 2005; Mercadante et al. 2023). Different kinesin-14 family members (Kif25, KIFC1) were reported to keep multiple centrioles clustered in cancer cells or in proplatelets (Decarreau et al. 2017; Becker et al. 2024; Kwon et al. 2008). By studying CDK5RAP2-knockout cells, CDK5RAP2 was shown to be important for centriole cohesion and preventing centriole overduplication and multi-polar spindles (Barrera et al. 2010). As we observed increased levels of CDK5RAP2 in DCs with multiple centrioles, this protein might be involved in centriole clustering in immune cells as well.

Our study proposes a simplified mechanism based on MTs-pushing forces with the cell and nuclear membrane which keep centrioles clustered (**Figure 6.31**). However, additional factors, mentioned above, could not be excluded and it remains elusive which proteins contribute to centriole clustering in DCs.

The de-clustering agent PJ-34 used in this study is a PARP1 and PARP2 inhibitor (Wahlberg et al. 2012). It affects cancer cell growth by centriole de-clustering disturbing the assembly of pseudo-bipolar spindles (Pannu et al. 2014; Castiel et al. 2011). PJ-34 blocks PARP-dependent post-translational modifications of proteins, which are important for centriole clustering such as KIFC1 (Visochek et al. 2017). The de-clustering agent PJ-34 was shown to only affect the cell cycle of cancerous cells and not normal proliferating cells (Castiel et al. 2011). In cancer cells, PJ-34 also blocks proliferation via dampening PARP1-dependent NF-κB activity that normally promotes proliferation (Wang et al. 2013). In addition, PJ-34 blocks PARP1-dependent DNA repair, which causes cell death specifically in cells defective for homologous recombination repair (Bryant et al. 2005). It is interesting to note that, PJ-34 targets tankyrases 1 and 2 as well, which belong to the PARP family and are linked to the regulation of telomerase activity, DNA repair and Wnt signaling (Wahlberg et al. 2012; Smith et al. 1998; McCabe et al. 2009; Huang et al. 2009). Due to the high potency of PARP inhibitors such as PJ-34 to eradicate

human cancer cells, these molecules are interesting from a clinical perspective and individual drugs have been approved for cancer treatment already (Muzzana et al. 2025). By using a cancer drug and elaborating on the effects on immune cells, we contribute to the understanding of possible side effects on healthy cells. Whether in human patients, which are treated with PARP inhibitors or other de-clustering agents, DCs with multiple centrioles display a de-clustered centriole configuration and how this may influence the immune system and tumor eradication remains unclear.

In 2019, the new potential anti-cancer drug CCB02 was developed. CCB02 was shown to inhibit centriole clustering and enhance MT nucleation in cancer cells with extra centrosomes by preventing interaction of free tubulin with centrosomal P4.1-associated protein (CPAP), which normally negatively regulates MT nucleation (Mariappan et al. 2019; Gopalakrishnan et al. 2012). It might be useful to test the effect of the drug on the DC cytoskeleton. Whether CCB02 enhances MT numbers and induces centriole de-clustering in DCs comparable to Nedd1 overexpression, as well as the downstream effects on the T cell priming capacity, remain unclear.

All in all, comparing the process of centriole dissociation in MCCs and centriole de-clustering in cancer or immune cells might offer new insights into what keeps centrioles together and how de-clustering agents act in cancer therapy. Moreover, it highlights the importance of an optimal centriole configuration for cellular functionality in multiple cell types.

6.3. Conclusions and future perspectives

Overall, this study demonstrates the pivotal role of the DC cytoskeleton during T helper cell priming. Multiple centrioles, acquired by DCs after antigen encounter, enhance MTOC functionality. These DCs containing multiple centrioles display an altered secretory phenotype and facilitated capacity to activate T cells. During T cell priming, a tight cluster of centrioles is maintained without MTOC polarization to the IS contact site.

For the concluding part, the concept expressed by Jean-Henri Fabre is well suited: *one must observe before they can truly understand* (Fabre 1879). Our observations aimed to enlarge information available on the DC side of the IS, while most studies have focused on processes within T cells and their activation during IS formation as one has presumably noticed by referenced literature. The concept of ‘observation before understanding’ can be also extended to the fact that our findings, made by direct visualization through microscopy and other approaches, are essential both for gaining new insights and for inspiring further scientific questions.

Great remaining open questions of DC cell biology during IS formation are: How do DC 'subpopulations' with distinct centriole numbers differ in their transcriptomic profile and what individual role do the populations play for the immune response? Are DCs with multiple centrioles superior in priming T cells and thereby solely beneficial for body health? The appearance of amplified centrioles in DCs and in malignant tumor cells emphasizes the need for cell type- and context-dependent research. Moreover, further investigations are needed to understand the regulation of the MT cytoskeleton contributing to the release of inflammatory mediators. From both perspectives, it remains open how the communication of DCs and T cells influences the organization of the cytoskeleton.

Finally, this thesis contributed to the understanding of immune cell functions on a cellular level including data from *in vitro* and *in vivo* approaches. We revealed insights on the cytoskeletal processes during cell-cell communication, which hopefully will stimulate and advance the development of therapeutical interventions during disease onsets.

References

Ackerman, Anne L.; Kyritsis, Christoph; Tampé, Robert; Cresswell, Peter (2003): Early phagosomes in dendritic cells form a cellular compartment sufficient for cross presentation of exogenous antigens. In *Proceedings of the National Academy of Sciences of the United States of America* 100 (22), pp. 12889–12894. DOI: 10.1073/pnas.1735556100.

Adams, A. E.; Johnson, D. I.; Longnecker, R. M.; Sloat, B. F.; Pringle, J. R. (1990): CDC42 and CDC43, two additional genes involved in budding and the establishment of cell polarity in the yeast Saccharomyces cerevisiae. In *The Journal of cell biology* 111 (1), pp. 131–142. DOI: 10.1083/jcb.111.1.131.

Adams, Sophie D.; Csere, Judit; D'angelo, Gisela; Carter, Edward P.; Romao, Maryse; Arnandis, Teresa et al. (2021): Centrosome amplification mediates small extracellular vesicle secretion via lysosome disruption. In *Current biology : CB* 31 (7), 1403-1416.e7. DOI: 10.1016/j.cub.2021.01.028.

Aguiar, Murilo Porfírio de; Vieira, Julia Hailer (2024): Entrance to the multifaceted world of CD4+ T cell subsets. In *Explor Immunol* 4 (2), pp. 152–168. DOI: 10.37349/ei.2024.00134.

Akira, Shizuo; Uematsu, Satoshi; Takeuchi, Osamu (2006): Pathogen recognition and innate immunity. In *Cell* 124 (4), pp. 783–801. DOI: 10.1016/j.cell.2006.02.015.

Al Jord, Adel; Shihavuddin, Asm; Servignat d'Aout, Raphaël; Faucourt, Marion; Genovesio, Auguste; Karaiskou, Anthi et al. (2017): Calibrated mitotic oscillator drives motile ciliogenesis. In *Science (New York, N.Y.)* 358 (6364), pp. 803–806. DOI: 10.1126/science.aan8311.

Altmann, K. H.; Wartmann, M.; O'Reilly, T. (2000): Epothilones and related structures--a new class of microtubule inhibitors with potent in vivo antitumor activity. In *Biochimica et biophysica acta* 1470 (3), M79-91. DOI: 10.1016/s0304-419x(00)00009-3.

Anderson, R. G.; Brenner, R. M. (1971): The formation of basal bodies (centrioles) in the Rhesus monkey oviduct. In *The Journal of cell biology* 50 (1), pp. 10–34. DOI: 10.1083/jcb.50.1.10.

Arnandis, Teresa; Monteiro, Pedro; Adams, Sophie D.; Bridgeman, Victoria Louise; Rajeeve, Vinothini; Gadaleta, Emanuela et al. (2018): Oxidative Stress in Cells with Extra Centrosomes Drives Non-Cell-Autonomous Invasion. In *Developmental cell* 47 (4), 409-424.e9. DOI: 10.1016/j.devcel.2018.10.026.

Arquint, Christian; Gabryjonczyk, Anna-Maria; Nigg, Erich A. (2014): Centrosomes as signalling centres. In *Philosophical Transactions of the Royal Society B: Biological Sciences* 369 (1650). DOI: 10.1098/rstb.2013.0464.

Averill, Michelle M.; Barnhart, Shelley; Becker, Lev; Li, Xin; Heinecke, Jay W.; Leboeuf, Renee C. et al. (2011): S100A9 differentially modifies phenotypic states of neutrophils, macrophages, and dendritic cells: implications for atherosclerosis and adipose tissue inflammation. In *Circulation* 123 (11), pp. 1216–1226. DOI: 10.1161/CIRCULATIONAHA.110.985523.

Bachmann, Malte; Scheiermann, Patrick; Härdle, Lorena; Pfeilschifter, Josef; Mühl, Heiko (2012): IL-36γ/IL-1F9, an innate T-bet target in myeloid cells. In *The Journal of biological chemistry* 287 (50), pp. 41684–41696. DOI: 10.1074/jbc.M112.385443.

Bahe, Susanne; Stierhof, York-Dieter; Wilkinson, Christopher J.; Leiss, Florian; Nigg, Erich A. (2005): Rootletin forms centriole-associated filaments and functions in centrosome cohesion. In *The Journal of cell biology* 171 (1), pp. 27–33. DOI: 10.1083/jcb.200504107.

Bai, Siyi; Martin-Sanchez, Fatima; Brough, David; Lopez-Castejon, Gloria (2024): Pyroptosis leads to loss of centrosomal integrity in macrophages. In *Cell death discovery* 10 (1), p. 354. DOI: 10.1038/s41420-024-02093-1.

Baker, Brendon M.; Chen, Christopher S. (2012): Deconstructing the third dimension: how 3D culture microenvironments alter cellular cues. In *Journal of cell science* 125 (Pt 13), pp. 3015–3024. DOI: 10.1242/jcs.079509.

Banchereau, J.; Steinman, R. M. (1998): Dendritic cells and the control of immunity. In *Nature* 392 (6673), pp. 245–252. DOI: 10.1038/32588.

Barlan, Kari; Gelfand, Vladimir I. (2017): Microtubule-Based Transport and the Distribution, Tethering, and Organization of Organelles. In *Cold Spring Harbor perspectives in biology* 9 (5). DOI: 10.1101/cshperspect.a025817.

Barnden, M. J.; Allison, J.; Heath, W. R.; Carbone, F. R. (1998): Defective TCR expression in transgenic mice constructed using cDNA-based alpha- and beta-chain genes under the control of heterologous regulatory elements. In *Immunology and cell biology* 76 (1), pp. 34–40. DOI: 10.1046/j.1440-1711.1998.00709.x.

Barrera, Jose A.; Kao, Ling-Rong; Hammer, Robert E.; Seemann, Joachim; Fuchs, Jannon L.; Megraw, Timothy L. (2010): CDK5RAP2 regulates centriole engagement and cohesion in mice. In *Developmental cell* 18 (6), pp. 913–926. DOI: 10.1016/j.devcel.2010.05.017.

Basu, Roshni; Whitlock, Benjamin M.; Husson, Julien; Le Floc'h, Audrey; Jin, Weiyang; Oyler-Yaniv, Alon et al. (2016): Cytotoxic T Cells Use Mechanical Force to Potentiate Target Cell Killing. In *Cell* 165 (1), pp. 100–110. DOI: 10.1016/j.cell.2016.01.021.

Batth, Tanveer S.; Tollenaere, MaximA X.; Rüther, Patrick; Gonzalez-Franquesa, Alba; Prabhakar, Bhargav S.; Bekker-Jensen, Simon et al. (2019): Protein Aggregation Capture on Microparticles Enables Multipurpose Proteomics Sample Preparation. In *Molecular & cellular proteomics : MCP* 18 (5), pp. 1027–1035. DOI: 10.1074/mcp.TIR118.001270.

Becker, Isabelle C.; Wilkie, Adrian R.; Nikols, Emma; Carminita, Estelle; Roweth, Harvey G.; Tilburg, Julia et al. (2024): Cell cycle-dependent centrosome clustering precedes proplatelet formation. In *Science advances* 10 (25), eadl6153. DOI: 10.1126/sciadv.adl6153.

Benvenuti, Federica; Lagaudrière-Gesbert, Cecile; Grandjean, Isabelle; Jancic, Carolina; Hivroz, Claire; Trautmann, Alain et al. (2004): Dendritic cell maturation controls adhesion, synapse formation, and the duration of the interactions with naive T lymphocytes. In *Journal of immunology (Baltimore, Md. : 1950)* 172 (1), pp. 292–301. DOI: 10.4049/jimmunol.172.1.292.

Bertrand, Florie; Esquerré, Michael; Petit, Anne-Elisabeth; Rodrigues, Magda; Duchez, Sophie; Delon, Jérôme; Valitutti, Salvatore (2010): Activation of the ancestral polarity regulator protein kinase C zeta at the immunological synapse drives polarization of Th cell secretory machinery toward APCs. In *The Journal of Immunology* 185 (5), pp. 2887–2894. DOI: 10.4049/jimmunol.1000739.

Boisvert, Judie; Edmondson, Samuel; Krummel, Matthew F. (2004): Immunological synapse formation licenses CD40-CD40L accumulations at T-APC contact sites. In *Journal of immunology (Baltimore, Md. : 1950)* 173 (6), pp. 3647–3652. DOI: 10.4049/jimmunol.173.6.3647.

Bornens, M.; Paintrand, M.; Berges, J.; Marty, M. C.; Karsenti, E. (1987): Structural and chemical characterization of isolated centrosomes. In *Cell motility and the cytoskeleton* 8 (3), pp. 238–249. DOI: 10.1002/cm.970080305.

Bornens, Michel (2012): The centrosome in cells and organisms. In *Science (New York, N.Y.)* 335 (6067), pp. 422–426. DOI: 10.1126/science.1209037.

Borst, J.; Alexander, S.; Elder, J.; Terhorst, C. (1983): The T3 complex on human T lymphocytes involves four structurally distinct glycoproteins. In *The Journal of biological chemistry* 258 (8), pp. 5135–5141.

Bouma, Gerben; Mendoza-Naranjo, Ariadna; Blundell, Michael P.; Falco, Elena de; Parsley, Kathryn L.; Burns, Siobhan O.; Thrasher, Adrian J. (2011): Cytoskeletal remodeling mediated by WASp in dendritic cells is necessary for normal immune synapse formation and T-cell priming. In *Blood* 118 (9), pp. 2492–2501. DOI: 10.1182/blood-2011-03-340265.

Braig, S.; Wiedmann, R. M.; Liebl, J.; Singer, M.; Kubisch, R.; Schreiner, L. et al. (2014): Pretubulysin: a new option for the treatment of metastatic cancer. In *Cell death & disease* 5 (1), e1001. DOI: 10.1038/cddis.2013.510.

Braun, Vincent Z.; Karbon, Gerlinde; Schuler, Fabian; Schapfl, Marina A.; Weiss, Johannes G.; Petermann, Paul Y. et al. (2024): Extra centrosomes delay DNA damage-driven tumorigenesis. In *Science advances* 10 (13), eadk0564. DOI: 10.1126/sciadv.adk0564.

Breslow, David K.; Holland, Andrew J. (2019): Mechanism and Regulation of Centriole and Cilium Biogenesis. In *Annual review of biochemistry* 88, pp. 691–724. DOI: 10.1146/annurev-biochem-013118-111153.

Bridgewood, Charlie; Fearnley, Gareth W.; Berekmeri, Anna; Laws, Philip; Macleod, Tom; Ponnambalam, Sreenivasan et al. (2018): IL-36γ Is a Strong Inducer of IL-23 in Psoriatic Cells and Activates Angiogenesis. In *Frontiers in Immunology* 9, p. 200. DOI: 10.3389/fimmu.2018.00200.

Bridgewood, Charlie; Stacey, Martin; Alase, Adewonuola; Lagos, Dimitris; Graham, Anne; Wittmann, Miriam (2017): IL-36γ has proinflammatory effects on human endothelial cells. In *Experimental dermatology* 26 (5), pp. 402–408. DOI: 10.1111/exd.13228.

Brossard, Cédric; Feuillet, Vincent; Schmitt, Alain; Randriamampita, Clotilde; Romao, Maryse; Raposo, Graça; Trautmann, Alain (2005): Multifocal structure of the T cell - dendritic cell synapse. In *European journal of immunology* 35 (6), pp. 1741–1753. DOI: 10.1002/eji.200425857.

Bryant, Helen E.; Schultz, Niklas; Thomas, Huw D.; Parker, Kayan M.; Flower, Dan; Lopez, Elena et al. (2005): Specific killing of BRCA2-deficient tumours with inhibitors of poly(ADP-ribose) polymerase. In *Nature* 434 (7035), pp. 913–917. DOI: 10.1038/nature03443.

Cabeza-Cabrerizo, Mar; Cardoso, Ana; Minutti, Carlos M.; Da Pereira Costa, Mariana; Reis e Sousa, Caetano (2021): Dendritic Cells Revisited. In *Annual review of immunology* 39, pp. 131–166. DOI: 10.1146/annurev-immunol-061020-053707.

Campi, Gabriele; Varma, Rajat; Dustin, Michael L. (2005): Actin and agonist MHC-peptide complex-dependent T cell receptor microclusters as scaffolds for signaling. In *The Journal of experimental medicine* 202 (8), pp. 1031–1036. DOI: 10.1084/jem.20051182.

Castiel, Asher; Visochek, Leonid; Mittelman, Leonid; Dantzer, Françoise; Izraeli, Shai; Cohen-Armon, Malka (2011): A phenanthrene derived PARP inhibitor is an extra-centrosomes de-clustering agent exclusively eradicating human cancer cells. In *BMC cancer* 11, p. 412. DOI: 10.1186/1471-2407-11-412.

Chabin-Brion, K.; Marceiller, J.; Perez, F.; Settegrana, C.; Drechou, A.; Durand, G.; Poüs, C. (2001): The Golgi complex is a microtubule-organizing organelle. In *Molecular biology of the cell* 12 (7), pp. 2047–2060. DOI: 10.1091/mbc.12.7.2047.

Chan, Jason Yongsheng (2011): A clinical overview of centrosome amplification in human cancers. In *International journal of biological sciences* 7 (8), pp. 1122–1144. DOI: 10.7150/ijbs.7.1122.

Choksi, Semil P.; Byrnes, Lauren E.; Konjikusic, Mia J.; Tsai, Benedict W. H.; Deleon, Rachel; Lu, Quanlong et al. (2024): An alternative cell cycle coordinates multiciliated cell differentiation. In *Nature* 630 (8015), pp. 214–221. DOI: 10.1038/s41586-024-07476-z.

Choudhuri, Kaushik; Llodrá, Jaime; Roth, Eric W.; Tsai, Jones; Gordo, Susana; Wucherpfennig, Kai W. et al. (2014): Polarized release of T-cell-receptor-enriched microvesicles at the immunological synapse. In *Nature* 507 (7490), pp. 118–123. DOI: 10.1038/nature12951.

Chun, Nicholas; Ang, Rosalind L.; Chan, Mark; Fairchild, Robert L.; Baldwin, William M.; Horwitz, Julian K. et al. (2021): T cell-derived tumor necrosis factor induces cytotoxicity by activating RIPK1-dependent target cell death. In *JCI insight* 6 (24). DOI: 10.1172/jci.insight.148643.

Cizmecioglu, Onur; Warnke, Silke; Arnold, Marc; Duensing, Stefan; Hoffmann, Ingrid (2008): Plk2 regulated centriole duplication is dependent on its localization to the centrioles and a functional polo-box domain. In *Cell cycle (Georgetown, Tex.)* 7 (22), pp. 3548–3555. DOI: 10.4161/cc.7.22.7071.

Decarreau, Justin; Wagenbach, Michael; Lynch, Eric; Halpern, Aaron R.; Vaughan, Joshua C.; Kollman, Justin; Wordeman, Linda (2017): The tetrameric kinesin Kif25 suppresses pre-mitotic centrosome separation to establish proper spindle orientation. In *Nature cell biology* 19 (4), pp. 384–390. DOI: 10.1038/ncb3486.

Delon, J.; Kaibuchi, K.; Germain, R. N. (2001): Exclusion of CD43 from the immunological synapse is mediated by phosphorylation-regulated relocation of the cytoskeletal adaptor moesin. In *Immunity* 15 (5), pp. 691–701. DOI: 10.1016/s1074-7613(01)00231-x.

Denu, Ryan A.; Shabbir, Maria; Nihal, Minakshi; Singh, Chandra K.; Longley, B. Jack; Burkard, Mark E.; Ahmad, Nihal (2018): Centriole Overduplication is the Predominant Mechanism Leading to Centrosome Amplification in Melanoma. In *Molecular cancer research : MCR* 16 (3), pp. 517–527. DOI: 10.1158/1541-7786.MCR-17-0197.

Detmar, M.; Imcke, E.; Ruszczak, Z.; Orfanos, C. E. (1990): Effects of recombinant tumor necrosis factor-alpha on cultured microvascular endothelial cells derived from human dermis. In *The Journal of investigative dermatology* 95 (6 Suppl), 219S-222S. DOI: 10.1111/1523-1747.ep12875807.

Dienz, Oliver; Rincon, Mercedes (2009): The effects of IL-6 on CD4 T cell responses. In *Clinical immunology (Orlando, Fla.)* 130 (1), pp. 27–33. DOI: 10.1016/j.clim.2008.08.018.

Dieu, M. C.; Vanbervliet, B.; Vicari, A.; Bridon, J. M.; Oldham, E.; Aït-Yahia, S. et al. (1998): Selective recruitment of immature and mature dendritic cells by distinct chemokines expressed in different anatomic sites. In *The Journal of experimental medicine* 188 (2), pp. 373–386. DOI: 10.1084/jem.188.2.373.

Dirksen, E. R.; Satir, P. (1972): Ciliary activity in the mouse oviduct as studied by transmission and scanning electron microscopy. In *Tissue and Cell* 4 (3), pp. 389–403. DOI: 10.1016/s0040-8166(72)80017-x.

Douanne, Tiphaine; Stinchcombe, Jane C.; Griffiths, Gillian M. (2021): Teasing out function from morphology: Similarities between primary cilia and immune synapses. In *The Journal of cell biology* 220 (6). DOI: 10.1083/jcb.202102089.

Dubois, B.; Vanbervliet, B.; Fayette, J.; Massacrier, C.; van Kooten, C.; Brière, F. et al. (1997): Dendritic cells enhance growth and differentiation of CD40-activated B lymphocytes. In *The Journal of experimental medicine* 185 (5), pp. 941–951. DOI: 10.1084/jem.185.5.941.

Dustin, M. L.; Cooper, J. A. (2000): The immunological synapse and the actin cytoskeleton: molecular hardware for T cell signaling. In *Nature immunology* 1 (1), pp. 23–29. DOI: 10.1038/76877.

Dustin, Michael L.; Colman, David R. (2002): Neural and immunological synaptic relations. In *Science (New York, N.Y.)* 298 (5594), pp. 785–789. DOI: 10.1126/science.1076386.

Dustin, Michael L.; Groves, Jay T. (2012): Receptor signaling clusters in the immune synapse. In *Annual review of biophysics* 41, pp. 543–556. DOI: 10.1146/annurev-biophys-042910-155238.

Dwivedi, Devashish; Harry, Daniela; Meraldi, Patrick (2023): Mild replication stress causes premature centriole disengagement via a sub-critical Plk1 activity under the control of ATR-Chk1. In *Nature communications* 14 (1), p. 6088. DOI: 10.1038/s41467-023-41753-1.

Dzhindzhev, Nikola S.; Yu, Quan D.; Weiskopf, Kipp; Tzolovsky, George; Cunha-Ferreira, Ines; Riparbelli, Maria et al. (2010): Asterless is a scaffold for the onset of centriole assembly. In *Nature* 467 (7316), pp. 714–718. DOI: 10.1038/nature09445.

Embgenbroich, Maria; Burgdorf, Sven (2018): Current Concepts of Antigen Cross-Presentation. In *Frontiers in Immunology* 9, p. 1643. DOI: 10.3389/fimmu.2018.01643.

Fabre, Jean-Henri (1879): Erinnerungen eines Insektenforschers. With assistance of Heide Lipecky, Christian Thanhäuser. Sechste Auflage 2018. Berlin: Matthes & Seitz.

Faragher, Alison J.; Fry, Andrew M. (2003): Nek2A kinase stimulates centrosome disjunction and is required for formation of bipolar mitotic spindles. In *Molecular biology of the cell* 14 (7), pp. 2876–2889. DOI: 10.1091/mbc.e03-02-0108.

Fava, Luca L.; Schuler, Fabian; Sladky, Valentina; Haschka, Manuel D.; Soratroi, Claudia; Eiterer, Lisa et al. (2017): The PIDDosome activates p53 in response to supernumerary centrosomes. In *Genes & development* 31 (1), pp. 34–45. DOI: 10.1101/gad.289728.116.

Fawcett, Don W.; Porter, Keith R. (1954): A study of the fine structure of ciliated epithelia. In *Journal of Morphology* 94 (2), pp. 221–281. DOI: 10.1002/jmor.1050940202.

Ferrer, Ivana R.; Liu, Danya; Pinelli, David F.; Koehn, Brent H.; Stempora, Linda L.; Ford, Mandy L. (2012): CD40/CD154 blockade inhibits dendritic cell expression of inflammatory cytokines but not costimulatory molecules. In *The Journal of Immunology* 189 (9), pp. 4387–4395. DOI: 10.4049/jimmunol.1201757.

Finetti, Francesca; Paccani, Silvia Rossi; Riparbelli, Maria Giovanna; Giacomello, Emiliana; Perinetti, Giuseppe; Pazour, Gregory J. et al. (2009): Intraflagellar transport is required for polarized recycling of the TCR/CD3 complex to the immune synapse. In *Nature cell biology* 11 (11), pp. 1332–1339. DOI: 10.1038/ncb1977.

Fırat-Karalar, Elif Nur; Stearns, Tim (2014): The centriole duplication cycle. In *Philosophical Transactions of the Royal Society B: Biological Sciences* 369 (1650). DOI: 10.1098/rstb.2013.0460.

Follit, John A.; Tuft, Richard A.; Fogarty, Kevin E.; Pazour, Gregory J. (2006): The intraflagellar transport protein IFT20 is associated with the Golgi complex and is required for cilia assembly. In *Molecular biology of the cell* 17 (9), pp. 3781–3792. DOI: 10.1091/mbc.e06-02-0133.

Fong, Chii Shyang; Mazo, Gregory; Das, Tuhin; Goodman, Joshua; Kim, Minhee; O'Rourke, Brian P. et al. (2016): 53BP1 and USP28 mediate p53-dependent cell cycle arrest in response to centrosome loss and prolonged mitosis. In *eLife* 5. DOI: 10.7554/eLife.16270.

Förster, R.; Schubel, A.; Breitfeld, D.; Kremmer, E.; Renner-Müller, I.; Wolf, E.; Lipp, M. (1999): CCR7 coordinates the primary immune response by establishing functional microenvironments in secondary lymphoid organs. In *Cell* 99 (1), pp. 23–33. DOI: 10.1016/s0092-8674(00)80059-8.

Frosch, Michael; Strey, Anke; Vogl, Thomas; Wulffraat, Nico M.; Kuis, Wietse; Sunderkötter, Cord et al. (2000): Myeloid-related proteins 8 and 14 are specifically secreted during interaction of phagocytes and activated endothelium and are useful markers for monitoring disease activity in pauciarticular-onset juvenile rheumatoid arthritis. In *Arthritis & Rheumatism* 43 (3), p. 628. DOI: 10.1002/1529-0131(200003)43:3<628::AID-ANR20>3.0.CO;2-X.

Fry, A. M.; Mayor, T.; Meraldi, P.; Stierhof, Y. D.; Tanaka, K.; Nigg, E. A. (1998): C-Nap1, a novel centrosomal coiled-coil protein and candidate substrate of the cell cycle-regulated protein kinase Nek2. In *The Journal of cell biology* 141 (7), pp. 1563–1574. DOI: 10.1083/jcb.141.7.1563.

Ganem, Neil J.; Godinho, Susana A.; Pellman, David (2009): A mechanism linking extra centrosomes to chromosomal instability. In *Nature* 460 (7252), pp. 278–282. DOI: 10.1038/nature08136.

Gao, Qi; Hofer, Florian W.; Filbeck, Sebastian; Vermeulen, Bram J. A.; Würtz, Martin; Neuner, Annett et al. (2025): Structural mechanisms for centrosomal recruitment and organization of the microtubule nucleator γ-TuRC. In *Nature communications* 16 (1), p. 2453. DOI: 10.1038/s41467-025-57729-2.

Garcia-Carpio, Irmina; Braun, Vincent Z.; Weiler, Elias S.; Leone, Marina; Niñerola, Sergio; Barco, Angel et al. (2023): Extra centrosomes induce PIDD1-mediated inflammation and immunosurveillance. In *The EMBO journal* 42 (20), e113510. DOI: 10.15252/embj.2023113510.

Geiger, B.; Rosen, D.; Berke, G. (1982): Spatial relationships of microtubule-organizing centers and the contact area of cytotoxic T lymphocytes and target cells. In *The Journal of cell biology* 95 (1), pp. 137–143. DOI: 10.1083/jcb.95.1.137.

Godinho, Susana A.; Kwon, Mijung; Pellman, David (2009): Centrosomes and cancer: how cancer cells divide with too many centrosomes. In *Cancer metastasis reviews* 28 (1-2), pp. 85–98. DOI: 10.1007/s10555-008-9163-6.

Godinho, Susana A.; Picone, Remigio; Burute, Mithila; Dagher, Regina; Su, Ying; Leung, Cheuk T. et al. (2014): Oncogene-like induction of cellular invasion from centrosome amplification. In *Nature* 510 (7503), pp. 167–171. DOI: 10.1038/nature13277.

Gonzalez, Nela Klein; Wennhold, Kerstin; Balkow, Sandra; Kondo, Eisei; Bölck, Birgit; Weber, Tanja et al. (2015): In vitro and in vivo imaging of initial B-T-cell interactions in the setting of B-cell based cancer immunotherapy. In *Oncoimmunology* 4 (9), e1038684. DOI: 10.1080/2162402X.2015.1038684.

González-Navajas, José M.; Lee, Jongdae; David, Michael; Raz, Eyal (2012): Immunomodulatory functions of type I interferons. In *Nature Reviews Immunology* 12 (2), pp. 125–135. DOI: 10.1038/nri3133.

Goodson, Holly V.; Jonasson, Erin M. (2018): Microtubules and Microtubule-Associated Proteins. In *Cold Spring Harbor perspectives in biology* 10 (6). DOI: 10.1101/cshperspect.a022608.

Gopalakrishnan, Jayachandran; Chim, Yiu-Cheung Frederick; Ha, Andrew; Basiri, Marcus L.; Lerit, Dorothy A.; Rusan, Nasser M.; Avidor-Reiss, Tomer (2012): Tubulin nucleotide status controls Sas-4-

dependent pericentriolar material recruitment. In *Nature cell biology* 14 (8), pp. 865–873. DOI: 10.1038/ncb2527.

Gossen, M.; Freundlieb, S.; Bender, G.; Müller, G.; Hillen, W.; Bujard, H. (1995): Transcriptional activation by tetracyclines in mammalian cells. In *Science (New York, N.Y.)* 268 (5218), pp. 1766–1769. DOI: 10.1126/science.7792603.

Grakoui, A.; Bromley, S. K.; Sumen, C.; Davis, M. M.; Shaw, A. S.; Allen, P. M.; Dustin, M. L. (1999): The immunological synapse: a molecular machine controlling T cell activation. In *Science (New York, N.Y.)* 285 (5425), pp. 221–227. DOI: 10.1126/science.285.5425.221.

Gramaglia, I.; Weinberg, A. D.; Lemon, M.; Croft, M. (1998): Ox-40 ligand: a potent costimulatory molecule for sustaining primary CD4 T cell responses. In *Journal of immunology (Baltimore, Md. : 1950)* 161 (12), pp. 6510–6517.

Graser, Susanne; Stierhof, York-Dieter; Nigg, Erich A. (2007): Cep68 and Cep215 (Cdk5rap2) are required for centrosome cohesion. In *Journal of cell science* 120 (Pt 24), pp. 4321–4331. DOI: 10.1242/jcs.020248.

Green, J. M.; Noel, P. J.; Sperling, A. I.; Walunas, T. L.; Gray, G. S.; Bluestone, J. A.; Thompson, C. B. (1994): Absence of B7-dependent responses in CD28-deficient mice. In *Immunity* 1 (6), pp. 501–508. DOI: 10.1016/1074-7613(94)90092-2.

Guidotti, Jacques-Emmanuel; Brégerie, Olivier; Robert, Aude; Debey, Pascale; Brechot, Christian; Desdouets, Chantal (2003): Liver cell polyploidization: a pivotal role for binuclear hepatocytes. In *The Journal of biological chemistry* 278 (21), pp. 19095–19101. DOI: 10.1074/jbc.M300982200.

Habedanck, Robert; Stierhof, York-Dieter; Wilkinson, Christopher J.; Nigg, Erich A. (2005): The Polo kinase Plk4 functions in centriole duplication. In *Nature cell biology* 7 (11), pp. 1140–1146. DOI: 10.1038/ncb1320.

Harding, F. A.; McArthur, J. G.; Gross, J. A.; Raulet, D. H.; Allison, J. P. (1992): CD28-mediated signalling co-stimulates murine T cells and prevents induction of anergy in T-cell clones. In *Nature* 356 (6370), pp. 607–609. DOI: 10.1038/356607a0.

Haren, Laurence; Remy, Marie-Hélène; Bazin, Ingrid; Callebaut, Isabelle; Wright, Michel; Merdes, Andreas (2006): NEDD1-dependent recruitment of the gamma-tubulin ring complex to the centrosome is necessary for centriole duplication and spindle assembly. In *The Journal of cell biology* 172 (4), pp. 505–515. DOI: 10.1083/jcb.200510028.

Hessian, Paul A.; Edgeworth, Jonathan; Hogg, Nancy (1993): MRP-8 and MRP-14, two abundant Ca2+-binding proteins of neutrophils and monocytes. In *Journal of Leukocyte Biology* 53 (2), pp. 197–204. DOI: 10.1002/jlb.53.2.197.

Higginbotham, Holden; Bielas, Stephanie; Tanaka, Teruyuki; Gleeson, Joseph G. (2004): Transgenic mouse line with green-fluorescent protein-labeled Centrin 2 allows visualization of the centrosome in living cells. In *Transgenic research* 13 (2), pp. 155–164. DOI: 10.1023/b:trag.0000026071.41735.8e.

Homrich, Mirka (2023): Elucidation of multinumerous centrosomes and their impact on migration in dendritic cells. Doctoral dissertation. University of Bonn.

Hsieh, C. S.; Macatonia, S. E.; Tripp, C. S.; Wolf, S. F.; O'Garra, A.; Murphy, K. M. (1993): Development of TH1 CD4+ T cells through IL-12 produced by Listeria-induced macrophages. In *Science (New York, N.Y.)* 260 (5107), pp. 547–549. DOI: 10.1126/science.8097338.

Huang, Shih-Min A.; Mishina, Yuji M.; Liu, Shanming; Cheung, Atwood; Stegmeier, Frank; Michaud, Gregory A. et al. (2009): Tankyrase inhibition stabilizes axin and antagonizes Wnt signalling. In *Nature* 461 (7264), pp. 614–620. DOI: 10.1038/nature08356.

Hunter, M. J.; Chazin, W. J. (1998): High level expression and dimer characterization of the S100 EF-hand proteins, migration inhibitory factor-related proteins 8 and 14. In *Journal of Biological Chemistry* 273 (20), pp. 12427–12435. DOI: 10.1074/jbc.273.20.12427.

Huse, Morgan; Lillemeier, Björn F.; Kuhns, Michael S.; Chen, Daniel S.; Davis, Mark M. (2006): T cells use two directionally distinct pathways for cytokine secretion. In *Nature immunology* 7 (3), pp. 247–255. DOI: 10.1038/ni1304.

Imai, T.; Nagira, M.; Takagi, S.; Kakizaki, M.; Nishimura, M.; Wang, J. et al. (1999): Selective recruitment of CCR4-bearing Th2 cells toward antigen-presenting cells by the CC chemokines thymus and activation-regulated chemokine and macrophage-derived chemokine. In *International immunology* 11 (1), pp. 81–88. DOI: 10.1093/intimm/11.1.81.

Imai, Toshio; Chantry, David; Raport, Carol J.; Wood, Christi L.; Nishimura, Miyuki; Godiska, Ronald et al. (1998): Macrophage-derived Chemokine Is a Functional Ligand for the CC Chemokine Receptor 4. In *Journal of Biological Chemistry* 273 (3), pp. 1764–1768. DOI: 10.1074/jbc.273.3.1764.

Inaba, K.; Steinman, R. M. (1987): Monoclonal antibodies to LFA-1 and to CD4 inhibit the mixed leukocyte reaction after the antigen-dependent clustering of dendritic cells and T lymphocytes. In *The Journal of experimental medicine* 165 (5), pp. 1403–1417. DOI: 10.1084/jem.165.5.1403.

Ito, Daisuke; Zitouni, Sihem; Jana, Swadhin Chandra; Duarte, Paulo; Surkont, Jaroslaw; Carvalho-Santos, Zita et al. (2019): Pericentrin-mediated SAS-6 recruitment promotes centriole assembly. In *eLife* 8. DOI: 10.7554/eLife.41418.

Janeway, C. A.; Goodnow, C. C.; Medzhitov, R. (1996): Danger - pathogen on the premises! Immunological tolerance. In *Current biology : CB* 6 (5), pp. 519–522. DOI: 10.1016/s0960-9822(02)00531-6.

Janke, Carsten; Magiera, Maria M. (2020): The tubulin code and its role in controlling microtubule properties and functions. In *Nature reviews. Molecular cell biology* 21 (6), pp. 307–326. DOI: 10.1038/s41580-020-0214-3.

Jiang, Ziwei; Liu, Yuanqi; Li, Changwei; Chang, Leilei; Wang, Wang; Wang, Zhenhua et al. (2017): IL-36γ Induced by the TLR3-SLUG-VDR Axis Promotes Wound Healing via REG3A. In *The Journal of investigative dermatology* 137 (12), pp. 2620–2629. DOI: 10.1016/j.jid.2017.07.820.

Joshi, H. C.; Palacios, M. J.; McNamara, L.; Cleveland, D. W. (1992): Gamma-tubulin is a centrosomal protein required for cell cycle-dependent microtubule nucleation. In *Nature* 356 (6364), pp. 80–83. DOI: 10.1038/356080a0.

Kaizuka, Yoshihisa; Douglass, Adam D.; Varma, Rajat; Dustin, Michael L.; Vale, Ronald D. (2007): Mechanisms for segregating T cell receptor and adhesion molecules during immunological synapse formation in Jurkat T cells. In *Proceedings of the National Academy of Sciences of the United States of America* 104 (51), pp. 20296–20301. DOI: 10.1073/pnas.0710258105.

Kim, Joon; Lee, Ji Eun; Heynen-Genel, Susanne; Suyama, Eigo; Ono, Keiichiro; Lee, Kiyoung et al. (2010): Functional genomic screen for modulators of ciliogenesis and cilium length. In *Nature* 464 (7291), pp. 1048–1051. DOI: 10.1038/nature08895.

Kim, Tae-Sung; Park, Jung-Eun; Shukla, Anil; Choi, Sunho; Murugan, Ravichandran N.; Lee, Jin H. et al. (2013): Hierarchical recruitment of Plk4 and regulation of centriole biogenesis by two centrosomal scaffolds, Cep192 and Cep152. In *Proceedings of the National Academy of Sciences of the United States of America* 110 (50), E4849-57. DOI: 10.1073/pnas.1319656110.

Kimura, Kenji; Kimura, Akatsuki (2011): Intracellular organelles mediate cytoplasmic pulling force for centrosome centration in the Caenorhabditis elegans early embryo. In *Proceedings of the National Academy of Sciences of the United States of America* 108 (1), pp. 137–142. DOI: 10.1073/pnas.1013275108.

Klausner, R. D.; Lippincott-Schwartz, J.; Bonifacino, J. S. (1990): The T cell antigen receptor: insights into organelle biology. In *Annual review of cell biology* 6, pp. 403–431. DOI: 10.1146/annurev.cb.06.110190.002155.

Kleylein-Sohn, Julia; Westendorf, Jens; Le Clech, Mikael; Habedanck, Robert; Stierhof, York-Dieter; Nigg, Erich A. (2007): Plk4-induced centriole biogenesis in human cells. In *Developmental cell* 13 (2), pp. 190–202. DOI: 10.1016/j.devcel.2007.07.002.

Klos Dehring, Deborah A.; Vladar, Eszter K.; Werner, Michael E.; Mitchell, Jennifer W.; Hwang, Peter; Mitchell, Brian J. (2013): Deuterosome-mediated centriole biogenesis. In *Developmental cell* 27 (1), pp. 103–112. DOI: 10.1016/j.devcel.2013.08.021.

Kopf, Aglaja; Kiermaier, Eva (2021): Dynamic Microtubule Arrays in Leukocytes and Their Role in Cell Migration and Immune Synapse Formation. In *Frontiers in cell and developmental biology* 9, p. 635511. DOI: 10.3389/fcell.2021.635511.

Kopf, Aglaja; Renkawitz, Jörg; Hauschild, Robert; Girkontaite, Irute; Tedford, Kerry; Merrin, Jack et al. (2020): Microtubules control cellular shape and coherence in amoeboid migrating cells. In *The Journal of cell biology* 219 (6). DOI: 10.1083/jcb.201907154.

Korbecki, Jan; Barczak, Katarzyna; Gutowska, Izabela; Chlubek, Dariusz; Baranowska-Bosiacka, Irena (2022): CXCL1: Gene, Promoter, Regulation of Expression, mRNA Stability, Regulation of Activity in the Intercellular Space. In *International journal of molecular sciences* 23 (2), p. 792. DOI: 10.3390/ijms23020792.

Kovacsovics-Bankowski, M.; Rock, K. L. (1995): A phagosome-to-cytosol pathway for exogenous antigens presented on MHC class I molecules. In *Science (New York, N.Y.)* 267 (5195), pp. 243–246. DOI: 10.1126/science.7809629.

Kuhn, Jeffrey R.; Poenie, Martin (2002): Dynamic polarization of the microtubule cytoskeleton during CTL-mediated killing. In *Immunity* 16 (1), pp. 111–121. DOI: 10.1016/s1074-7613(02)00262-5.

Kulig, Paulina; Musiol, Stephanie; Freiberger, Sandra Nicole; Schreiner, Bettina; Gyülveszi, Gabor; Russo, Giancarlo et al. (2016): IL-12 protects from psoriasiform skin inflammation. In *Nature communications* 7, p. 13466. DOI: 10.1038/ncomms13466.

Kupfer, A.; Dennert, G. (1984a): Reorientation of the microtubule-organizing center and the Golgi apparatus in cloned cytotoxic lymphocytes triggered by binding to lysable target cells. In *Journal of immunology (Baltimore, Md. : 1950)* 133 (5), pp. 2762–2766.

Kupfer, A.; Dennert, G. (1984b): Reorientation of the microtubule-organizing center and the Golgi apparatus in cloned cytotoxic lymphocytes triggered by binding to lysable target cells. In *The Journal of Immunology* 133 (5), pp. 2762–2766. DOI: 10.4049/jimmunol.133.5.2762.

Kupfer, A.; Dennert, G.; Singer, S. J. (1985): The reorientation of the Golgi apparatus and the microtubule-organizing center in the cytotoxic effector cell is a prerequisite in the lysis of bound target cells. In *The Journal of molecular and cellular immunology : JMCI* 2 (1), pp. 37–49.

Kupfer, A.; Singer, S. J. (1989): The specific interaction of helper T cells and antigen-presenting B cells. IV. Membrane and cytoskeletal reorganizations in the bound T cell as a function of antigen dose. In *The Journal of experimental medicine* 170 (5), pp. 1697–1713. DOI: 10.1084/jem.170.5.1697.

Kwon, Mijung; Godinho, Susana A.; Chandhok, Namrata S.; Ganem, Neil J.; Azioune, Ammar; Thery, Manuel; Pellman, David (2008): Mechanisms to suppress multipolar divisions in cancer cells with extra centrosomes. In *Genes & development* 22 (16), pp. 2189–2203. DOI: 10.1101/gad.1700908.

Lambrus, Bramwell G.; Daggubati, Vikas; Uetake, Yumi; Scott, Phillip M.; Clutario, Kevin M.; Sluder, Greenfield; Holland, Andrew J. (2016): A USP28-53BP1-p53-p21 signaling axis arrests growth after centrosome loss or prolonged mitosis. In *The Journal of cell biology* 214 (2), pp. 143–153. DOI: 10.1083/jcb.201604054.

Lane, H. A.; Nigg, E. A. (1996): Antibody microinjection reveals an essential role for human polo-like kinase 1 (Plk1) in the functional maturation of mitotic centrosomes. In *The Journal of cell biology* 135 (6 Pt 2), pp. 1701–1713. DOI: 10.1083/jcb.135.6.1701.

Lasek, R. J.; Brady, S. T. (1985): Attachment of transported vesicles to microtubules in axoplasm is facilitated by AMP-PNP. In *Nature* 316 (6029), pp. 645–647. DOI: 10.1038/316645a0.

Lawo, Steffen; Hasegan, Monica; Gupta, Gagan D.; Pelletier, Laurence (2012): Subdiffraction imaging of centrosomes reveals higher-order organizational features of pericentriolar material. In *Nature cell biology* 14 (11), pp. 1148–1158. DOI: 10.1038/ncb2591.

Leithner, Alexander; Altenburger, Lukas M.; Hauschild, Robert; Assen, Frank P.; Rottner, Klemens; Stradal, Theresia E. B. et al. (2021): Dendritic cell actin dynamics control contact duration and priming efficiency at the immunological synapse. In *The Journal of cell biology* 220 (4). DOI: 10.1083/jcb.202006081.

Lemaître, Florent; Mercey, Olivier; Mean, Isabelle; Paulin, Elise; Dutoit, Valérie; Rath, Jan et al. (2025): Unveiling the Molecular Architecture of T Cells and Immune Synapses with Cryo-Expansion Microscopy.

Leonardi, Craig L.; Kimball, Alexa B.; Papp, Kim A.; Yeilding, Newman; Guzzo, Cynthia; Wang, Yuhua et al. (2008): Efficacy and safety of ustekinumab, a human interleukin-12/23 monoclonal antibody, in patients with psoriasis: 76-week results from a randomised, double-blind, placebo-controlled trial (PHOENIX 1). In *Lancet (London, England)* 371 (9625), pp. 1665–1674. DOI: 10.1016/S0140-6736(08)60725-4.

Leone, Marina; Engel, Felix B. (2019): Pseudo-bipolar spindle formation and cell division in postnatal binucleated cardiomyocytes. In *Journal of molecular and cellular cardiology* 134, pp. 69–73. DOI: 10.1016/j.yjmcc.2019.07.005.

Leupin, O.; Zaru, R.; Laroche, T.; Müller, S.; Valitutti, S. (2000): Exclusion of CD45 from the T-cell receptor signaling area in antigen-stimulated T lymphocytes. In *Current biology : CB* 10 (5), pp. 277–280. DOI: 10.1016/s0960-9822(00)00362-6.

Levine, Michelle S.; Bakker, Bjorn; Boeckx, Bram; Moyett, Julia; Lu, James; Vitre, Benjamin et al. (2017): Centrosome Amplification Is Sufficient to Promote Spontaneous Tumorigenesis in Mammals. In *Developmental cell* 40 (3), 313-322.e5. DOI: 10.1016/j.devcel.2016.12.022.

Li, Yan; Yu, Qing; Zhang, Zhengguo; Wang, Jian; Li, Simin; Zhang, Jiangyuan; Liu, Guangwei (2016): TH9 cell differentiation, transcriptional control and function in inflammation, autoimmune diseases and cancer. In *Oncotarget* 7 (43), pp. 71001–71012. DOI: 10.18632/oncotarget.11681.

Lieberam, Ivo; Förster, Irmgard (1999): The murine β-chemokine TARC is expressed by subsets of dendritic cells and attracts primed CD4+ T cells. In *European journal of immunology* 29 (9), pp. 2684–2694. DOI: 10.1002/(SICI)1521-4141(199909)29:09<2684::AID-IMMU2684>3.0.CO;2-Y.

Liu, Z. G.; Smith, S. W.; McLaughlin, K. A.; Schwartz, L. M.; Osborne, B. A. (1994): Apoptotic signals delivered through the T-cell receptor of a T-cell hybrid require the immediate-early gene nur77. In *Nature* 367 (6460), pp. 281–284. DOI: 10.1038/367281a0.

Liu, Zhenzhen; Roche, Paul A. (2015): Macropinocytosis in phagocytes: regulation of MHC class-II-restricted antigen presentation in dendritic cells. In *Frontiers in Physiology* 6, p. 1. DOI: 10.3389/fphys.2015.00001.

LoMastro, Gina M.; Holland, Andrew J. (2019): The Emerging Link between Centrosome Aberrations and Metastasis. In *Developmental cell* 49 (3), pp. 325–331. DOI: 10.1016/j.devcel.2019.04.002.

Loncarek, Jadranka; Hergert, Polla; Khodjakov, Alexey (2010): Centriole reduplication during prolonged interphase requires procentriole maturation governed by Plk1. In *Current biology : CB* 20 (14), pp. 1277–1282. DOI: 10.1016/j.cub.2010.05.050.

Loncarek, Jadranka; Hergert, Polla; Magidson, Valentin; Khodjakov, Alexey (2008): Control of daughter centriole formation by the pericentriolar material. In *Nature cell biology* 10 (3), pp. 322–328. DOI: 10.1038/ncb1694.

Loser, Karin; Vogl, Thomas; Voskort, Maik; Lueken, Aloys; Kupas, Verena; Nacken, Wolfgang et al. (2010): The Toll-like receptor 4 ligands Mrp8 and Mrp14 are crucial in the development of autoreactive CD8+ T cells. In *Nature medicine* 16 (6), pp. 713–717. DOI: 10.1038/nm.2150.

Lüders, Jens; Patel, Urvashi K.; Stearns, Tim (2006): GCP-WD is a gamma-tubulin targeting factor required for centrosomal and chromatin-mediated microtubule nucleation. In *Nature cell biology* 8 (2), pp. 137–147. DOI: 10.1038/ncb1349.

Mações, Cláudia Oliveira; Lé, Ana Maria; Torres, Tiago (2022): Generalized pustular psoriasis: the new era of treatment with IL-36 receptor inhibitors. In *The Journal of dermatological treatment* 33 (7), pp. 2911–2918. DOI: 10.1080/09546634.2022.2089335.

Macatonia, S. E.; Hosken, N. A.; Litton, M.; Vieira, P.; Hsieh, C. S.; Culpepper, J. A. et al. (1995): Dendritic cells produce IL-12 and direct the development of Th1 cells from naive CD4+ T cells. In *The Journal of Immunology* 154 (10), pp. 5071–5079. DOI: 10.4049/jimmunol.154.10.5071.

Madden, D. R. (1995): The three-dimensional structure of peptide-MHC complexes. In *Annual review of immunology* 13, pp. 587–622. DOI: 10.1146/annurev.iy.13.040195.003103.

Magupalli, Venkat Giri; Negro, Roberto; Tian, Yuzi; Hauenstein, Arthur V.; Di Caprio, Giuseppe; Skillern, Wesley et al. (2020): HDAC6 mediates an aggresome-like mechanism for NLRP3 and pyrin inflammasome activation. In *Science (New York, N.Y.)* 369 (6510). DOI: 10.1126/science.aas8995.

Malone, Christian J.; Misner, Lisa; Le Bot, Nathalie; Tsai, Miao-Chih; Campbell, Jay M.; Ahringer, Julie; White, John G. (2003): The C. elegans hook protein, ZYG-12, mediates the essential attachment between the centrosome and nucleus. In *Cell* 115 (7), pp. 825–836. DOI: 10.1016/s0092-8674(03)00985-1.

Mariappan, Aruljothi; Soni, Komal; Schorpp, Kenji; Zhao, Fan; Minakar, Amin; Zheng, Xiangdong et al. (2019): Inhibition of CPAP-tubulin interaction prevents proliferation of centrosome-amplified cancer cells. In *The EMBO journal* 38 (2). DOI: 10.15252/embj.201899876.

Martín-Cófreces, Noa B.; Robles-Valero, Javier; Cabrero, J. Román; Mittelbrunn, María; Gordón-Alonso, Mónica; Sung, Ching-Hwa et al. (2008): MTOC translocation modulates IS formation and controls sustained T cell signaling. In *The Journal of cell biology* 182 (5), pp. 951–962. DOI: 10.1083/jcb.200801014.

Martinon, Fabio; Burns, Kimberly; Tschopp, Jürg (2002): The inflammasome: a molecular platform triggering activation of inflammatory caspases and processing of proIL-beta. In *Molecular cell* 10 (2), pp. 417–426. DOI: 10.1016/s1097-2765(02)00599-3.

Matzinger, Polly (2002): The danger model: a renewed sense of self. In *Science (New York, N.Y.)* 296 (5566), pp. 301–305. DOI: 10.1126/science.1071059.

McCabe, N.; Cerone, M. A.; Ohishi, T.; Seimiya, H.; Lord, C. J.; Ashworth, A. (2009): Targeting Tankyrase 1 as a therapeutic strategy for BRCA-associated cancer. In *Oncogene* 28 (11), pp. 1465–1470. DOI: 10.1038/onc.2008.483.

McCoy, K. L.; Miller, J.; Jenkins, M.; Ronchese, F.; Germain, R. N.; Schwartz, R. H. (1989): Diminished antigen processing by endosomal acidification mutant antigen-presenting cells. In *The Journal of Immunology* 143 (1), pp. 29–38. DOI: 10.4049/jimmunol.143.1.29.

Medzhitov, R. (2001): Toll-like receptors and innate immunity. In *Nature reviews. Immunology* 1 (2), pp. 135–145. DOI: 10.1038/35100529.

Meitinger, Franz; Anzola, John V.; Kaulich, Manuel; Richardson, Amelia; Stender, Joshua D.; Benner, Christopher et al. (2016): 53BP1 and USP28 mediate p53 activation and G1 arrest after centrosome loss or extended mitotic duration. In *The Journal of cell biology* 214 (2), pp. 155–166. DOI: 10.1083/jcb.201604081.

Mennella, V.; Keszthelyi, B.; McDonald, K. L.; Chhun, B.; Kan, F.; Rogers, G. C. et al. (2012): Subdiffraction-resolution fluorescence microscopy reveals a domain of the centrosome critical for pericentriolar material organization. In *Nature cell biology* 14 (11), pp. 1159–1168. DOI: 10.1038/ncb2597.

Mercadante, Dayna L.; Aaron, William A.; Olson, Sarah D.; Manning, Amity L. (2023): Cortical dynein drives centrosome clustering in cells with centrosome amplification. In *Molecular biology of the cell* 34 (6), ar63. DOI: 10.1091/mbc.E22-07-0296.

Meuer, S. C.; Schlossman, S. F.; Reinherz, E. L. (1982): Clonal analysis of human cytotoxic T lymphocytes: T4+ and T8+ effector T cells recognize products of different major histocompatibility complex regions. In *Proceedings of the National Academy of Sciences of the United States of America* 79 (14), pp. 4395–4399. DOI: 10.1073/pnas.79.14.4395.

Meyer-Gerards, Charlotte; Bazzi, Hisham (2025): Developmental and tissue-specific roles of mammalian centrosomes. In *The FEBS journal* 292 (4), pp. 709–726. DOI: 10.1111/febs.17212.

Miga, Amy J.; Masters, Sally R.; Durell, Brigit G.; Gonzalez, Mercedes; Jenkins, Marc K.; Maliszewski, Charles et al. (2001): Dendritic cell longevity and T cell persistence is controlled by CD154-CD40 interactions. In *European journal of immunology* 31 (3), pp. 959–965. DOI: 10.1002/1521-4141(200103)31:3<959::aid-immu959>3.0.co;2-a.

Miller, J. F.; Mitchell, G. F. (1968): Cell to cell interaction in the immune response. I. Hemolysin-forming cells in neonatally thymectomized mice reconstituted with thymus or thoracic duct lymphocytes. In *The Journal of experimental medicine* 128 (4), pp. 801–820. DOI: 10.1084/jem.128.4.801.

Miller, Mark J.; Safrina, Olga; Parker, Ian; Cahalan, Michael D. (2004): Imaging the single cell dynamics of CD4+ T cell activation by dendritic cells in lymph nodes. In *The Journal of experimental medicine* 200 (7), pp. 847–856. DOI: 10.1084/jem.20041236.

Miro, Francesc; Nobile, Cinzia; Blanchard, Nicolas; Lind, Marianne; Filipe-Santos, Orchidée; Fieschi, Claire et al. (2006): T cell-dependent activation of dendritic cells requires IL-12 and IFN-gamma signaling in T cells. In *Journal of immunology (Baltimore, Md. : 1950)* 177 (6), pp. 3625–3634. DOI: 10.4049/jimmunol.177.6.3625.

Mitchison, T.; Kirschner, M. (1984): Dynamic instability of microtubule growth. In *Nature* 312 (5991), pp. 237–242. DOI: 10.1038/312237a0.

Mittelbrunn, María; Del Martínez Hoyo, Gloria; López-Bravo, María; Martín-Cofreces, Noa B.; Scholer, Alix; Hugues, Stéphanie et al. (2009): Imaging of plasmacytoid dendritic cell interactions with T cells. In *Blood* 113 (1), pp. 75–84. DOI: 10.1182/blood-2008-02-139865.

Mittelbrunn, María; Gutiérrez-Vázquez, Cristina; Villarroya-Beltri, Carolina; González, Susana; Sánchez-Cabo, Fátima; González, Manuel Ángel et al. (2011): Unidirectional transfer of microRNA-loaded exosomes from T cells to antigen-presenting cells. In *Nature communications* 2, p. 282. DOI: 10.1038/ncomms1285.

Möller, Katrin; Brambach, Max; Villani, Ambra; Gallo, Elisa; Gilmour, Darren; Peri, Francesca (2022): A role for the centrosome in regulating the rate of neuronal efferocytosis by microglia in vivo. In *eLife* 11. DOI: 10.7554/eLife.82094.

Monks, C. R.; Freiberg, B. A.; Kupfer, H.; Sciaky, N.; Kupfer, A. (1998): Three-dimensional segregation of supramolecular activation clusters in T cells. In *Nature* 395 (6697), pp. 82–86. DOI: 10.1038/25764.

Monteiro, Pedro; Yeon, Bongwhan; Wallis, Samuel S.; Godinho, Susana A. (2023): Centrosome amplification fine tunes tubulin acetylation to differentially control intracellular organization. In *The EMBO journal* 42 (16), e112812. DOI: 10.15252/embj.2022112812.

Moran, Amy E.; Holzapfel, Keli L.; Xing, Yan; Cunningham, Nicole R.; Maltzman, Jonathan S.; Punt, Jennifer; Hogquist, Kristin A. (2011): T cell receptor signal strength in Treg and iNKT cell development demonstrated by a novel fluorescent reporter mouse. In *The Journal of experimental medicine* 208 (6), pp. 1279–1289. DOI: 10.1084/jem.20110308.

Moritz, Michelle; Braunfeld, Michael B.; Sedat, John W.; Alberts, Bruce; Agard, David A. (1995): Microtubule nucleation by γ-tubulin-containing rings in the centrosome. In *Nature* 378 (6557), pp. 638–640. DOI: 10.1038/378638a0.

Mullard, Asher (2022): FDA approves first anti-IL-36 receptor antibody for rare skin disease. In *Nature reviews. Drug discovery* 21 (11), p. 786. DOI: 10.1038/d41573-022-00172-5.

Muzzana, Marta; Broggini, Massimo; Damia, Giovanna (2025): The Landscape of PARP Inhibitors in Solid Cancers. In *OncoTargets and therapy* 18, pp. 297–317. DOI: 10.2147/OTT.S499226.

Mylvaganam, Sivakami; Freeman, Spencer A.; Grinstein, Sergio (2021): The cytoskeleton in phagocytosis and macropinocytosis. In *Current biology : CB* 31 (10), R619-R632. DOI: 10.1016/j.cub.2021.01.036.

Nakazawa, Yuki; Hiraki, Madoka; Kamiya, Ritsu; Hirono, Masafumi (2007): SAS-6 is a cartwheel protein that establishes the 9-fold symmetry of the centriole. In *Current biology : CB* 17 (24), pp. 2169–2174. DOI: 10.1016/j.cub.2007.11.046.

Nathan, C. F.; Murray, H. W.; Wiebe, M. E.; Rubin, B. Y. (1983): Identification of interferon-gamma as the lymphokine that activates human macrophage oxidative metabolism and antimicrobial activity. In *The Journal of experimental medicine* 158 (3), pp. 670–689. DOI: 10.1084/jem.158.3.670.

Nigg, Erich A.; Holland, Andrew J. (2018): Once and only once: mechanisms of centriole duplication and their deregulation in disease. In *Nature reviews. Molecular cell biology* 19 (5), pp. 297–312. DOI: 10.1038/nrm.2017.127.

Norbury, C. C.; Chambers, B. J.; Prescott, A. R.; Ljunggren, H. G.; Watts, C. (1997): Constitutive macropinocytosis allows TAP-dependent major histocompatibility complex class I presentation of exogenous soluble antigen by bone marrow-derived dendritic cells. In *European journal of immunology* 27 (1), pp. 280–288. DOI: 10.1002/eji.1830270141.

Novy, Patricia; Quigley, Michael; Huang, Xiaopei; Yang, Yiping (2007): CD4 T cells are required for CD8 T cell survival during both primary and memory recall responses. In *Journal of immunology (Baltimore, Md. : 1950)* 179 (12), pp. 8243–8251. DOI: 10.4049/jimmunol.179.12.8243.

Obino, Dorian; Farina, Francesca; Malbec, Odile; Sáez, Pablo J.; Maurin, Mathieu; Gaillard, Jérémie et al. (2016): Actin nucleation at the centrosome controls lymphocyte polarity. In *Nature communications* 7, p. 10969. DOI: 10.1038/ncomms10969.

Obino, Dorian; Maurin, Mathieu; Dingli, Florent; Loew, Damarys; Lescure, Aurianne; Terriac, Emmanuel et al. (2023): Medium-throughput image-based phenotypic siRNA screen to unveil the molecular basis of B cell polarization. In *Scientific data* 10 (1), p. 401. DOI: 10.1038/s41597-023-02301-0.

Okoye, Isobel S.; Coomes, Stephanie M.; Pelly, Victoria S.; Czieso, Stephanie; Papayannopoulos, Venizelos; Tolmachova, Tanya et al. (2014): MicroRNA-containing T-regulatory-cell-derived exosomes suppress pathogenic T helper 1 cells. In *Immunity* 41 (1), pp. 89–103. DOI: 10.1016/j.immuni.2014.05.019.

Oppmann, B.; Lesley, R.; Blom, B.; Timans, J. C.; Xu, Y.; Hunte, B. et al. (2000): Novel p19 protein engages IL-12p40 to form a cytokine, IL-23, with biological activities similar as well as distinct from IL-12. In *Immunity* 13 (5), pp. 715–725. DOI: 10.1016/s1074-7613(00)00070-4.

Ori-McKenney, Kassandra M.; Jan, Lily Yeh; Jan, Yuh-Nung (2012): Golgi outposts shape dendrite morphology by functioning as sites of acentrosomal microtubule nucleation in neurons. In *Neuron* 76 (5), pp. 921–930. DOI: 10.1016/j.neuron.2012.10.008.

Paintrand, M.; Moudjou, M.; Delacroix, H.; Bornens, M. (1992): Centrosome organization and centriole architecture: their sensitivity to divalent cations. In *Journal of structural biology* 108 (2), pp. 107–128. DOI: 10.1016/1047-8477(92)90011-x.

Palmowski, Michael J.; Gileadi, Uzi; Salio, Mariolina; Gallimore, Awen; Millrain, Maggie; James, Edward et al. (2006): Role of immunoproteasomes in cross-presentation. In *Journal of immunology (Baltimore, Md. : 1950)* 177 (2), pp. 983–990. DOI: 10.4049/jimmunol.177.2.983.

Pannu, V.; Rida, P. C. G.; Celik, B.; Turaga, R. C.; Ogden, A.; Cantuaria, G. et al. (2014): Centrosome-declustering drugs mediate a two-pronged attack on interphase and mitosis in supercentrosomal cancer cells. In *Cell death & disease* 5 (11), e1538. DOI: 10.1038/cddis.2014.505.

Peel, Nina; Stevens, Naomi R.; Basto, Renata; Raff, Jordan W. (2007): Overexpressing centriole-replication proteins in vivo induces centriole overduplication and de novo formation. In *Current Biology* 17 (10), pp. 834–843. DOI: 10.1016/j.cub.2007.04.036.

Perez, Edith A. (2009): Microtubule inhibitors: Differentiating tubulin-inhibiting agents based on mechanisms of action, clinical activity, and resistance. In *Molecular cancer therapeutics* 8 (8), pp. 2086–2095. DOI: 10.1158/1535-7163.MCT-09-0366.

Petersen, Beatrix; Wolf, Marc; Austermann, Judith; van Lent, Peter; Foell, Dirk; Ahlmann, Martina et al. (2013): The alarmin Mrp8/14 as regulator of the adaptive immune response during allergic contact dermatitis. In *The EMBO journal* 32 (1), pp. 100–111. DOI: 10.1038/emboj.2012.309.

Philip, Reuben; Fiorino, Cara; Harrison, Rene E. (2022): Terminally differentiated osteoclasts organize centrosomes into large clusters for microtubule nucleation and bone resorption. In *Molecular biology of the cell* 33 (8), ar68. DOI: 10.1091/mbc.E22-03-0098.

Piccioli, Diego; Sbrana, Silverio; Melandri, Emiliano; Valiante, Nicholas M. (2002): Contact-dependent stimulation and inhibition of dendritic cells by natural killer cells. In *The Journal of experimental medicine* 195 (3), pp. 335–341. DOI: 10.1084/jem.20010934.

Piel, M.; Meyer, P.; Khodjakov, A.; Rieder, C. L.; Bornens, M. (2000): The respective contributions of the mother and daughter centrioles to centrosome activity and behavior in vertebrate cells. In *The Journal of cell biology* 149 (2), pp. 317–330. DOI: 10.1083/jcb.149.2.317.

Pihan, German A.; Purohit, Aruna; Wallace, Janice; Malhotra, Raji; Liotta, Lance; Doxsey, Stephen J. (2001): Centrosome Defects Can Account for Cellular and Genetic Changes That Characterize Prostate Cancer Progression. In *Cancer Res* 61 (5), pp. 2212–2219.

Pihan, German A.; Wallace, Jan; Zhou, Yening; Doxsey, Stephen J. (2003): Centrosome abnormalities and chromosome instability occur together in pre-invasive carcinomas. In *Cancer research* 63 (6), pp. 1398–1404.

Pineau, Judith; Pinon, Léa; Mesdjian, Olivier; Fattaccioli, Jacques; Lennon Duménil, Ana-Maria; Pierobon, Paolo (2022): Microtubules restrict F-actin polymerization to the immune synapse via GEF-H1 to maintain polarity in lymphocytes. In *eLife* 11. DOI: 10.7554/eLife.78330.

Prosser, Suzanna L.; Morrison, Ciaran G. (2015): Centrin2 regulates CP110 removal in primary cilium formation. In *The Journal of cell biology* 208 (6), pp. 693–701. DOI: 10.1083/jcb.201411070.

Pruenster, Monika; Immler, Roland; Roth, Jonas; Kuchler, Tim; Bromberger, Thomas; Napoli, Matteo et al. (2023): E-selectin-mediated rapid NLRP3 inflammasome activation regulates S100A8/S100A9 release from neutrophils via transient gasdermin D pore formation. In *Nature immunology* 24 (12), pp. 2021–2031. DOI: 10.1038/s41590-023-01656-1.

Pruenster, Monika; Vogl, Thomas; Roth, Johannes; Sperandio, Markus (2016): S100A8/A9: From basic science to clinical application. In *Pharmacology & therapeutics* 167, pp. 120–131. DOI: 10.1016/j.pharmthera.2016.07.015.

Pulecio, Julian; Petrovic, Jelena; Prete, Francesca; Chiaruttini, Giulia; Lennon-Dumenil, Ana-Maria; Desdouets, Chantal et al. (2010): Cdc42-mediated MTOC polarization in dendritic cells controls targeted delivery of cytokines at the immune synapse. In *The Journal of experimental medicine* 207 (12), pp. 2719–2732. DOI: 10.1084/jem.20100007.

Quah, Ben J. C.; Warren, Hilary S.; Parish, Christopher R. (2007): Monitoring lymphocyte proliferation in vitro and in vivo with the intracellular fluorescent dye carboxyfluorescein diacetate succinimidyl ester. In *Nature protocols* 2 (9), pp. 2049–2056. DOI: 10.1038/nprot.2007.296.

Quann, Emily J.; Merino, Ernesto; Furuta, Toshiaki; Huse, Morgan (2009): Localized diacylglycerol drives the polarization of the microtubule-organizing center in T cells. In *Nature immunology* 10 (6), pp. 627–635. DOI: 10.1038/ni.1734.

Queen, Dawn; Ediriweera, Chathumadavi; Liu, Liang (2019): Function and Regulation of IL-36 Signaling in Inflammatory Diseases and Cancer Development. In *Frontiers in cell and developmental biology* 7, p. 317. DOI: 10.3389/fcell.2019.00317.

Quintyne, Nicholas J.; Reing, Janet E.; Hoffelder, Diane R.; Gollin, Susanne M.; Saunders, William S. (2005): Spindle multipolarity is prevented by centrosomal clustering. In *Science (New York, N.Y.)* 307 (5706), pp. 127–129. DOI: 10.1126/science.1104905.

Raab, Marc S.; Breitkreutz, Iris; Anderhub, Simon; Rønnest, Mads H.; Leber, Blanka; Larsen, Thomas O. et al. (2012): GF-15, a novel inhibitor of centrosomal clustering, suppresses tumor cell growth in vitro and in vivo. In *Cancer research* 72 (20), pp. 5374–5385. DOI: 10.1158/0008-5472.CAN-12-2026.

Rammes, A.; Roth, J.; Goebeler, M.; Klempt, M.; Hartmann, M.; Sorg, C. (1997): Myeloid-related protein (MRP) 8 and MRP14, calcium-binding proteins of the S100 family, are secreted by activated monocytes via a novel, tubulin-dependent pathway. In *The Journal of biological chemistry* 272 (14), pp. 9496–9502. DOI: 10.1074/jbc.272.14.9496.

Redecke, Vanessa; Wu, Ruiqiong; Zhou, Jingran; Finkelstein, David; Chaturvedi, Vandana; High, Anthony A.; Häcker, Hans (2013): Hematopoietic progenitor cell lines with myeloid and lymphoid potential. In *Nature methods* 10 (8), pp. 795–803. DOI: 10.1038/nmeth.2510.

Remo, Andrea; Li, Xue; Schiebel, Elmar; Pancione, Massimo (2020): The Centrosome Linker and Its Role in Cancer and Genetic Disorders. In *Trends in molecular medicine* 26 (4), pp. 380–393. DOI: 10.1016/j.molmed.2020.01.011.

Reth, M. (1989): Antigen receptor tail clue. In *Nature* 338 (6214), pp. 383–384. DOI: 10.1038/338383b0.

Reynolds, Joseph M.; Martinez, Gustavo J.; Chung, Yeonseok; Dong, Chen (2012): Toll-like receptor 4 signaling in T cells promotes autoimmune inflammation. In *Proceedings of the National Academy of Sciences of the United States of America* 109 (32), pp. 13064–13069. DOI: 10.1073/pnas.1120585109.

Ridley, A. J.; Paterson, H. F.; Johnston, C. L.; Diekmann, D.; Hall, A. (1992): The small GTP-binding protein rac regulates growth factor-induced membrane ruffling. In *Cell* 70 (3), pp. 401–410. DOI: 10.1016/0092-8674(92)90164-8.

Ring, D.; Hubble, R.; Kirschner, M. (1982): Mitosis in a cell with multiple centrioles. In *The Journal of cell biology* 94 (3), pp. 549–556. DOI: 10.1083/jcb.94.3.549.

Riol-Blanco, Lorena; Delgado-Martín, Cristina; Sánchez-Sánchez, Noelia; Alonso-C, Luis M.; Gutiérrez-López, María Dolores; Del Hoyo, Gloria Martínez et al. (2009): Immunological synapse formation inhibits, via NF-kappaB and FOXO1, the apoptosis of dendritic cells. In *Nature immunology* 10 (7), pp. 753–760. DOI: 10.1038/ni.1750.

Ritter, Alex T.; Asano, Yukako; Stinchcombe, Jane C.; Dieckmann, N. M. G.; Chen, Bi-Chang; Gawden-Bone, C. et al. (2015): Actin depletion initiates events leading to granule secretion at the immunological synapse. In *Immunity* 42 (5), pp. 864–876. DOI: 10.1016/j.immuni.2015.04.013.

Roche, Paul A.; Furuta, Kazuyuki (2015): The ins and outs of MHC class II-mediated antigen processing and presentation. In *Nature Reviews Immunology* 15 (4), pp. 203–216. DOI: 10.1038/nri3818.

Rouvier, E.; Luciani, M. F.; Golstein, P. (1993): Fas involvement in Ca(2+)-independent T cell-mediated cytotoxicity. In *The Journal of experimental medicine* 177 (1), pp. 195–200. DOI: 10.1084/jem.177.1.195.

Rowley, Donald A.; Fitch, Frank W. (2012): The road to the discovery of dendritic cells, a tribute to Ralph Steinman. In *Cellular immunology* 273 (2), pp. 95–98. DOI: 10.1016/j.cellimm.2012.01.002.

Sáez, Juan José; Diaz, Jheimmy; Ibañez, Jorge; Bozo, Juan Pablo; Cabrera Reyes, Fernanda; Alamo, Martina et al. (2019): The exocyst controls lysosome secretion and antigen extraction at the immune synapse of B cells. In *The Journal of cell biology* 218 (7), pp. 2247–2264. DOI: 10.1083/jcb.201811131.

Sallusto, F.; Cella, M.; Danieli, C.; Lanzavecchia, A. (1995): Dendritic cells use macropinocytosis and the mannose receptor to concentrate macromolecules in the major histocompatibility complex class II compartment: downregulation by cytokines and bacterial products. In *The Journal of experimental medicine* 182 (2), pp. 389–400. DOI: 10.1084/jem.182.2.389.

Sallusto, Federica; Schaerli, Patrick; Loetscher, Pius; Schaniel, Christoph; Lenig, Danielle; Mackay, Charles R. et al. (1998): Rapid and coordinated switch in chemokine receptor expression during dendritic cell maturation. In *European journal of immunology* 28 (9), pp. 2760–2769. DOI: 10.1002/(SICI)1521-4141(199809)28:09<2760::AID-IMMU2760>3.0.CO;2-N.

Sanderson, Nicholas Stephen Rennie; Puntel, Mariana; Kroeger, Kurt M.; Bondale, Niyati S.; Swerdlow, Mark; Iranmanesh, Niloufar et al. (2012): Cytotoxic immunological synapses do not restrict the action of interferon-γ to antigenic target cells. In *Proceedings of the National Academy of Sciences of the United States of America* 109 (20), pp. 7835–7840. DOI: 10.1073/pnas.1116058109.

Sarkar, Apurba; Rieger, Heiko; Paul, Raja (2019): Search and Capture Efficiency of Dynamic Microtubules for Centrosome Relocation during IS Formation. In *Biophysical journal* 116 (11), pp. 2079–2091. DOI: 10.1016/j.bpj.2019.04.008.

Schaeffer, Alexandre; Buracco, Simona; Gazzola, Morgan; Gelin, Matthieu; Vianay, Benoit; Pascalis, Chiara de et al. (2025): Microtubule-driven cell shape changes and actomyosin flow synergize to position the centrosome. In *The Journal of cell biology* 224 (7). DOI: 10.1083/jcb.202405126.

Schapfl, Marina A.; LoMastro, Gina M.; Braun, Vincent Z.; Hirai, Maretoshi; Levine, Michelle S.; Kiermaier, Eva et al. (2024): Centrioles are frequently amplified in early B cell development but dispensable for humoral immunity. In *Nature communications* 15 (1), p. 8890. DOI: 10.1038/s41467-024-53222-4.

Schmitt, Madeleine T.; Kroll, Janina; Ruiz-Fernandez, Mauricio J. A.; Hauschild, Robert; Ghosh, Shaunak; Kameritsch, Petra et al. (2025): Protecting centrosomes from fracturing enables efficient cell navigation. In *Science advances* 11 (17), eadx4047. DOI: 10.1126/sciadv.adx4047.

Schmoranzer, Jan; Simon, Sanford M. (2003): Role of microtubules in fusion of post-Golgi vesicles to the plasma membrane. In *Molecular biology of the cell* 14 (4), pp. 1558–1569. DOI: 10.1091/mbc.e02-08-0500.

Seder, R. A.; Gazzinelli, R.; Sher, A.; Paul, W. E. (1993): Interleukin 12 acts directly on CD4+ T cells to enhance priming for interferon gamma production and diminishes interleukin 4 inhibition of such priming. In *Proceedings of the National Academy of Sciences of the United States of America* 90 (21), pp. 10188–10192. DOI: 10.1073/pnas.90.21.10188.

Sedwick, Caitlin E.; Morgan, Margaret M.; Jusino, Lismaida; Cannon, Judy L.; Miller, Jim; Burkhardt, Janis K. (1999): TCR, LFA-1, and CD28 Play Unique and Complementary Roles in Signaling T Cell Cytoskeletal Reorganization. In *The Journal of Immunology* 162 (3), pp. 1367–1375. DOI: 10.4049/jimmunol.162.3.1367.

Semino, Claudia; Angelini, Giovanna; Poggi, Alessandro; Rubartelli, Anna (2005): NK/iDC interaction results in IL-18 secretion by DCs at the synaptic cleft followed by NK cell activation and release of the DC maturation factor HMGB1. In *Blood* 106 (2), pp. 609–616. DOI: 10.1182/blood-2004-10-3906.

Shahid, Umama; Singh, Priyanka (2018): Emerging Picture of Deuterosome-Dependent Centriole Amplification in MCCs. In *Cells* 7 (10). DOI: 10.3390/cells7100152.

Shen, Lianjun; Sigal, Luis J.; Boes, Marianne; Rock, Kenneth L. (2004): Important role of cathepsin S in generating peptides for TAP-independent MHC class I crosspresentation in vivo. In *Immunity* 21 (2), pp. 155–165. DOI: 10.1016/j.immuni.2004.07.004.

Skowronek, Patricia; Thielert, Marvin; Voytik, Eugenia; Tanzer, Maria C.; Hansen, Fynn M.; Willems, Sander et al. (2022): Rapid and In-Depth Coverage of the (Phospho-)Proteome With Deep Libraries and Optimal Window Design for dia-PASEF. In *Molecular & cellular proteomics : MCP* 21 (9), p. 100279. DOI: 10.1016/j.mcpro.2022.100279.

Sluder, Greenfield (2014): One to only two: a short history of the centrosome and its duplication. In *Philosophical Transactions of the Royal Society B: Biological Sciences* 369 (1650). DOI: 10.1098/rstb.2013.0455.

Smith, K. A. (1988): Interleukin-2: inception, impact, and implications. In *Science (New York, N.Y.)* 240 (4856), pp. 1169–1176. DOI: 10.1126/science.3131876.

Smith, S.; Giriat, I.; Schmitt, A.; Lange, T. de (1998): Tankyrase, a poly(ADP-ribose) polymerase at human telomeres. In *Science (New York, N.Y.)* 282 (5393), pp. 1484–1487. DOI: 10.1126/science.282.5393.1484.

Sonnen, Katharina F.; Schermelleh, Lothar; Leonhardt, Heinrich; Nigg, Erich A. (2012): 3D-structured illumination microscopy provides novel insight into architecture of human centrosomes. In *Biology open* 1 (10), pp. 965–976. DOI: 10.1242/bio.20122337.

Steinman, R. M. (1991): The dendritic cell system and its role in immunogenicity. In *Annual review of immunology* 9, pp. 271–296. DOI: 10.1146/annurev.iy.09.040191.001415.

Steinman, R. M.; Cohn, Z. A. (1973): Identification of a novel cell type in peripheral lymphoid organs of mice. I. Morphology, quantitation, tissue distribution. In *The Journal of experimental medicine* 137 (5), pp. 1142–1162. DOI: 10.1084/jem.137.5.1142.

Stern, L. J.; Wiley, D. C. (1994): Antigenic peptide binding by class I and class II histocompatibility proteins. In *Structure (London, England : 1993)* 2 (4), pp. 245–251. DOI: 10.1016/s0969-2126(00)00026-5.

Stinchcombe, Jane C.; Randzavola, Lyra O.; Angus, Karen L.; Mantell, Judith M.; Verkade, Paul; Griffiths, Gillian M. (2015): Mother Centriole Distal Appendages Mediate Centrosome Docking at the Immunological Synapse and Reveal Mechanistic Parallels with Ciliogenesis. In *Current biology : CB* 25 (24), pp. 3239–3244. DOI: 10.1016/j.cub.2015.10.028.

Suda, T.; Takahashi, T.; Golstein, P.; Nagata, S. (1993): Molecular cloning and expression of the Fas ligand, a novel member of the tumor necrosis factor family. In *Cell* 75 (6), pp. 1169–1178. DOI: 10.1016/0092-8674(93)90326-l.

Sun, Lina; Su, Yanhong; Jiao, Anjun; Wang, Xin; Zhang, Baojun (2023): T cells in health and disease. In *Signal transduction and targeted therapy* 8 (1), p. 235. DOI: 10.1038/s41392-023-01471-y.

Tamzalit, Fella; Tran, Diana; Jin, Weiyang; Boyko, Vitaly; Bazzi, Hisham; Kepecs, Ariella et al. (2020): Centrioles control the capacity, but not the specificity, of cytotoxic T cell killing. In *Proceedings of the National Academy of Sciences of the United States of America* 117 (8), pp. 4310–4319. DOI: 10.1073/pnas.1913220117.

Tanos, Barbara E.; Yang, Hui-Ju; Soni, Rajesh; Wang, Won-Jing; Macaluso, Frank P.; Asara, John M.; Tsou, Meng-Fu Bryan (2013): Centriole distal appendages promote membrane docking, leading to cilia initiation. In *Genes & development* 27 (2), pp. 163–168. DOI: 10.1101/gad.207043.112.

Tassin, A. M.; Maro, B.; Bornens, M. (1985): Fate of microtubule-organizing centers during myogenesis in vitro. In *The Journal of cell biology* 100 (1), pp. 35–46. DOI: 10.1083/jcb.100.1.35.

Thauland, Timothy J.; Koguchi, Yoshinobu; Wetzel, Scott A.; Dustin, Michael L.; Parker, David C. (2008): Th1 and Th2 cells form morphologically distinct immunological synapses. In *Journal of immunology (Baltimore, Md. : 1950)* 181 (1), pp. 393–399. DOI: 10.4049/jimmunol.181.1.393.

Thauland, Timothy J.; Parker, David C. (2010): Diversity in immunological synapse structure. In *Immunology* 131 (4), pp. 466–472. DOI: 10.1111/j.1365-2567.2010.03366.x.

Theile, Laura; Li, Xue; Dang, Hairuo; Mersch, Dorothee; Anders, Simon; Schiebel, Elmar (2023): Centrosome linker diversity and its function in centrosome clustering and mitotic spindle formation. In *The EMBO journal* 42 (17), e109738. DOI: 10.15252/embj.2021109738.

Théry, C.; Amigorena, S. (2001): The cell biology of antigen presentation in dendritic cells. In *Current opinion in immunology* 13 (1), pp. 45–51. DOI: 10.1016/s0952-7915(00)00180-1.

Tourret, Marie; Guégan, Sarah; Chemin, Karine; Dogniaux, Stéphanie; Miro, Francesc; Bohineust, Armelle; Hivroz, Claire (2010): T cell polarity at the immunological synapse is required for CD154-dependent IL-12 secretion by dendritic cells. In *The Journal of Immunology* 185 (11), pp. 6809–6818. DOI: 10.4049/jimmunol.1001501.

Trinchieri, Giorgio (2003): Interleukin-12 and the regulation of innate resistance and adaptive immunity. In *Nature reviews. Immunology* 3 (2), pp. 133–146. DOI: 10.1038/nri1001.

Tschopp, J.; Nabholz, M. (1990): Perforin-mediated target cell lysis by cytolytic T lymphocytes. In *Annual review of immunology* 8, pp. 279–302. DOI: 10.1146/annurev.iy.08.040190.001431.

Tseng, Su-Yi; Waite, Janelle C.; Liu, Mengling; Vardhana, Santosha; Dustin, Michael L. (2008): T cell-dendritic cell immunological synapses contain TCR-dependent CD28-CD80 clusters that recruit protein kinase C theta. In *The Journal of Immunology* 181 (7), pp. 4852–4863. DOI: 10.4049/jimmunol.181.7.4852.

Tsou, Meng-Fu Bryan; Stearns, Tim (2006): Mechanism limiting centrosome duplication to once per cell cycle. In *Nature* 442 (7105), pp. 947–951. DOI: 10.1038/nature04985.

Tyanova, Stefka; Temu, Tikira; Sinitcyn, Pavel; Carlson, Arthur; Hein, Marco Y.; Geiger, Tamar et al. (2016): The Perseus computational platform for comprehensive analysis of (prote)omics data. In *Nature methods* 13 (9), pp. 731–740. DOI: 10.1038/nmeth.3901.

Ueda, Hironori; Morphew, Mary K.; McIntosh, J. Richard; Davis, Mark M. (2011): CD4+ T-cell synapses involve multiple distinct stages. In *Proceedings of the National Academy of Sciences of the United States of America* 108 (41), pp. 17099–17104. DOI: 10.1073/pnas.1113703108.

Ulloa, Romina; Corrales, Oreste; Cabrera-Reyes, Fernanda; Jara-Wilde, Jorge; Saez, Juan José; Rivas, Christopher et al. (2021): B Cells Adapt Their Nuclear Morphology to Organize the Immune Synapse and Facilitate Antigen Extraction. In *Frontiers in Immunology* 12, p. 801164. DOI: 10.3389/fimmu.2021.801164.

Ullrich, Angelika; Chai, Yi; Pistorius, Dominik; Elnakady, Yasser A.; Herrmann, Jennifer E.; Weissman, Kira J. et al. (2009): Pretubulysin, a potent and chemically accessible tubulysin precursor from Angiococcus disciformis. In *Angewandte Chemie (International ed. in English)* 48 (24), pp. 4422–4425. DOI: 10.1002/anie.200900406.

Vallée, Frédéric; Casás-Selves, Matias; Bubenik, Monica; Duplessis, Martin; Sow, Boubacar; Suarez, Catalina et al. (2025): Discovery of RP-1664: A First-in-Class Orally Bioavailable, Selective PLK4 Inhibitor. In *Journal of medicinal chemistry* 68 (11), pp. 10631–10647. DOI: 10.1021/acs.jmedchem.5c00529.

Veldhoen, Marc; Uyttenhove, Catherine; van Snick, Jacques; Helmby, Helena; Westendorf, Astrid; Buer, Jan et al. (2008): Transforming growth factor-beta 'reprograms' the differentiation of T helper 2 cells and promotes an interleukin 9-producing subset. In *Nature immunology* 9 (12), pp. 1341–1346. DOI: 10.1038/ni.1659.

Verboogen, Danielle R. J.; Dingjan, Ilse; Revelo, Natalia H.; Visser, Linda J.; Beest, Martin ter; van den Bogaart, Geert (2016): The dendritic cell side of the immunological synapse. In *Biomolecular concepts* 7 (1), pp. 17–28. DOI: 10.1515/bmc-2015-0028.

Vertii, Anastassiia; Ivshina, Maria; Zimmerman, Wendy; Hehnly, Heidi; Kant, Shashi; Doxsey, Stephen (2016): The Centrosome Undergoes Plk1-Independent Interphase Maturation during Inflammation and Mediates Cytokine Release. In *Developmental cell* 37 (4), pp. 377–386. DOI: 10.1016/j.devcel.2016.04.023.

Vigne, Solenne; Palmer, Gaby; Martin, Praxedis; Lamacchia, Céline; Strebel, Deborah; Rodriguez, Emiliana et al. (2012): IL-36 signaling amplifies Th1 responses by enhancing proliferation and Th1 polarization of naive CD4+ T cells. In *Blood* 120 (17), pp. 3478–3487. DOI: 10.1182/blood-2012-06-439026.

Vinopal, Stanislav; Dupraz, Sebastian; Alfadil, Eissa; Pietralla, Thorben; Bendre, Shweta; Stiess, Michael et al. (2023): Centrosomal microtubule nucleation regulates radial migration of projection neurons independently of polarization in the developing brain. In *Neuron* 111 (8), 1241-1263.e16. DOI: 10.1016/j.neuron.2023.01.020.

Visochek, Leonid; Castiel, Asher; Mittelman, Leonid; Elkin, Michael; Atias, Dikla; Golan, Talia et al. (2017): Exclusive destruction of mitotic spindles in human cancer cells. In *Oncotarget* 8 (13), pp. 20813–20824. DOI: 10.18632/oncotarget.15343.

Vivar, Omar I.; Masi, Giulia; Carpier, Jean-Marie; Magalhaes, Joao G.; Galgano, Donatella; Pazour, Gregory J. et al. (2016): IFT20 controls LAT recruitment to the immune synapse and T-cell activation in vivo. In *Proceedings of the National Academy of Sciences of the United States of America* 113 (2), pp. 386–391. DOI: 10.1073/pnas.1513601113.

Voganatsi, Alexandra; Panyutich, Alexander; Miyasaki, Kenneth T.; Murthy, Rekha K. (2001): Mechanism of extracellular release of human neutrophil calprotectin complex. In *Journal of Leukocyte Biology* 70 (1), pp. 130–134. DOI: 10.1189/jlb.70.1.130.

Vogl, Thomas; Ludwig, Stephan; Goebeler, Matthias; Strey, Anke; Thorey, Irmgard S.; Reichelt, Rudolf et al. (2004): MRP8 and MRP14 control microtubule reorganization during transendothelial migration of phagocytes. In *Blood* 104 (13), pp. 4260–4268. DOI: 10.1182/blood-2004-02-0446.

Vulcano, Marisa; Dusi, Stefano; Lissandrini, Daniele; Badolato, Raffaele; Mazzi, Paola; Riboldi, Elena et al. (2004): Toll receptor-mediated regulation of NADPH oxidase in human dendritic cells. In *Journal of immunology (Baltimore, Md. : 1950)* 173 (9), pp. 5749–5756. DOI: 10.4049/jimmunol.173.9.5749.

Wahlberg, Elisabet; Karlberg, Tobias; Kouznetsova, Ekaterina; Markova, Natalia; Macchiarulo, Antonio; Thorsell, Ann-Gerd et al. (2012): Family-wide chemical profiling and structural analysis of PARP and tankyrase inhibitors. In *Nature biotechnology* 30 (3), pp. 283–288. DOI: 10.1038/nbt.2121.

Wang, Zhe; Li, Yan; Lv, Shuqing; Tian, Yongjie (2013): Inhibition of proliferation and invasiveness of ovarian cancer C13* cells by a poly(ADP-ribose) polymerase inhibitor and the role of nuclear factor-κB. In *The Journal of international medical research* 41 (5), pp. 1577–1585. DOI: 10.1177/0300060513480913.

Weier, Ann-Kathrin; Homrich, Mirka; Ebbinghaus, Stephanie; Juda, Pavel; Miková, Eliška; Hauschild, Robert et al. (2022): Multiple centrosomes enhance migration and immune cell effector functions of mature dendritic cells. In *The Journal of cell biology* 221 (12). DOI: 10.1083/jcb.202107134.

Wiedemann, Aurelie; Depoil, David; Faroudi, Mustapha; Valitutti, Salvatore (2006): Cytotoxic T lymphocytes kill multiple targets simultaneously via spatiotemporal uncoupling of lytic and stimulatory synapses. In *Proceedings of the National Academy of Sciences of the United States of America* 103 (29), pp. 10985–10990. DOI: 10.1073/pnas.0600651103.

Wong, Yao Liang; Anzola, John V.; Davis, Robert L.; Yoon, Michelle; Motamedi, Amir; Kroll, Ashley et al. (2015): Cell biology. Reversible centriole depletion with an inhibitor of Polo-like kinase 4. In *Science (New York, N.Y.)* 348 (6239), pp. 1155–1160. DOI: 10.1126/science.aaa5111.

Wu, Jun; Misra, Gaurav; Russell, Robert J.; Ladd, Anthony J. C.; Lele, Tanmay P.; Dickinson, Richard B. (2011): Effects of dynein on microtubule mechanics and centrosome positioning. In *Molecular biology of the cell* 22 (24), pp. 4834–4841. DOI: 10.1091/mbc.E11-07-0611.

Xie, Jing; Najafi, Javad; Le Borgne, Rémi; Verbavatz, Jean-Marc; Durieu, Catherine; Sallé, Jeremy; Minc, Nicolas (2022): Contribution of cytoplasm viscoelastic properties to mitotic spindle positioning. In *Proceedings of the National Academy of Sciences of the United States of America* 119 (8). DOI: 10.1073/pnas.2115593119.

Xu, Yixin; Muñoz-Hernández, Hugo; Krutyhołowa, Rościsław; Marxer, Florina; Cetin, Ferdane; Wieczorek, Michal (2024): Partial closure of the γ-tubulin ring complex by CDK5RAP2 activates microtubule nucleation. In *Developmental cell* 59 (23), 3161-3174.e15. DOI: 10.1016/j.devcel.2024.09.002.

Yaffe, M. P.; Harata, D.; Verde, F.; Eddison, M.; Toda, T.; Nurse, P. (1996): Microtubules mediate mitochondrial distribution in fission yeast. In *Proceedings of the National Academy of Sciences of the United States of America* 93 (21), pp. 11664–11668. DOI: 10.1073/pnas.93.21.11664.

Yi, Jason; Wu, Xufeng; Chung, Andrew H.; Chen, James K.; Kapoor, Tarun M.; Hammer, John A. (2013): Centrosome repositioning in T cells is biphasic and driven by microtubule end-on capture-shrinkage. In *The Journal of cell biology* 202 (5), pp. 779–792. DOI: 10.1083/jcb.201301004.

Yokosuka, Tadashi; Sakata-Sogawa, Kumiko; Kobayashi, Wakana; Hiroshima, Michio; Hashimoto-Tane, Akiko; Tokunaga, Makio et al. (2005): Newly generated T cell receptor microclusters initiate and

sustain T cell activation by recruitment of Zap70 and SLP-76. In *Nature immunology* 6 (12), pp. 1253–1262. DOI: 10.1038/ni1272.

You, Fa-Ping; Zhang, Jian; Cui, Tao; Zhu, Rui; Lv, Chong-Qing; Tang, Hai-Tao; Sun, Di-Wen (2017): Th9 cells promote antitumor immunity via IL-9 and IL-21 and demonstrate atypical cytokine expression in breast cancer. In *International immunopharmacology* 52, pp. 163–167. DOI: 10.1016/j.intimp.2017.08.031.

Yuseff, Maria-Isabel; Reversat, Anne; Lankar, Danielle; Diaz, Jheimmy; Fanget, Isabelle; Pierobon, Paolo et al. (2011): Polarized secretion of lysosomes at the B cell synapse couples antigen extraction to processing and presentation. In *Immunity* 35 (3), pp. 361–374. DOI: 10.1016/j.immuni.2011.07.008.

Zebrowski, David C.; Vergarajauregui, Silvia; Wu, Chi-Chung; Piatkowski, Tanja; Becker, Robert; Leone, Marina et al. (2015): Developmental alterations in centrosome integrity contribute to the post-mitotic state of mammalian cardiomyocytes. In *eLife* 4. DOI: 10.7554/eLife.05563.

Zeng, Zhen; Lan, Tianxia; Wei, Yuquan; Wei, Xiawei (2022): CCL5/CCR5 axis in human diseases and related treatments. In *Genes & diseases* 9 (1), pp. 12–27. DOI: 10.1016/j.gendis.2021.08.004.

Zhao, Huijie; Zhu, Lei; Zhu, Yunlu; Cao, Jingli; Li, Shanshan; Huang, Qiongping et al. (2013): The Cep63 paralogue Deup1 enables massive de novo centriole biogenesis for vertebrate multiciliogenesis. In *Nature cell biology* 15 (12), pp. 1434–1444. DOI: 10.1038/ncb2880.

Zwadlo, G.; Brüggen, J.; Gerhards, G.; Schlegel, R.; Sorg, C. (1988): Two calcium-binding proteins associated with specific stages of myeloid cell differentiation are expressed by subsets of macrophages in inflammatory tissues. In *Clinical and experimental immunology* 72 (3), pp. 510–515.

List of Publications

Research article
(Preprint, under revision)

Stötzel I, Weier A, Sarkar A, Som S, Konopka P, Miková E, Böthling J, Homrich M, Schaedel L, Kazmaier U, Symeonidis K, Abdullah Z, Uderhardt S, Hons M, Paul R, Rieger H, Kiermaier E. Multiple clustered centrosomes in antigen-presenting cells foster T cell activation without MTOC polarization. *bioRxiv* 18.07.24 doi: 10.1101/2024.07.18.604057.

Research article

Schlautmann L, Burgdorf D, Ghosh S, Schieren A, Klümpen L, **Stötzel I**, Bremser J, Doengi M, Mass E, Stein V, Quast T, Kolanus W, Lang T, Kiermaier E, Simon MC, Burgdorf S. Glucose tasting depletes intracellular calcium stores and impairs macrophage functionality. Accepted for publication in *iScience*.

Research article

Wurnig SL, Huber ME, Weiler C, Baltrukevich H, Merten N, **Stötzel I**, Steffen T, Chang Y, Klammer R, Baumjohann D, Kiermaier E, Kolb P, Kostenis E, Schiedel M, Hansen F. A fluorescent probe enables the discovery of improved antagonists targeting the intracellular allosteric site of the chemokine receptor CCR7. *J Med Chem.* 2025 Feb 27;68(4):4308-4333. doi: 10.1021/acs.jmedchem.4c02102. Epub 2025 Feb 12. PMID: 39937529; PMCID: PMC11873976.

Review

Kiermaier E, **Stötzel I**, Schapfl MA, Villunger A. Amplified centrosomes – more than just a threat. *EMBO Rep*. 2024 Oct;25(10):4153-4167. doi: 10.1038/s44319-024-00260-0. Epub 2024 Sep 16. PMID: 39285247; PMCID: PMC11467336.

Editorial

Stötzel I, Kiermaier E. The central role of the centrosome. *Elife*. 2022 Dec 12; 11:e84659. doi: 10.7554/eLife.84659. PMID: 36508246; PMCID: PMC9744438.

Research article

Embgenbroich M, van der Zande HJP, Hussaarts L, Schulte-Schrepping J, Pelgrom LR, García-Tardón N, Schlautmann L, **Stoetzel I**, Händler K, Lambooij JM, Zawistowska-Deniziak A, Hoving L, de Ruiter K, Wijngaarden MA, Pijl H, Willems van Dijk K, Everts B, van Harmelen V, Yazdanbakhsh M, Schultze JL, Guigas B, Burgdorf S. Soluble mannose receptor induces proinflammatory macrophage activation and metaflammation. *Proc Natl Acad Sci* USA. 2021 Aug 3;118(31):e2103304118. doi: 10.1073/pnas.2103304118. PMID: 34326259; PMCID: PMC8346872.

Acknowledgements

First of all, I would like to thank Evi for giving me the opportunity to work on this exciting project in her group. I am truly grateful for your constant support and guidance. Over the past years, no matter how busy or stressful the situation, you always made time to discuss not only scientific questions but also personal matters concerning my future career. You continuously encouraged me to participate in conferences or workshops, which surely contributed to my personal and professional development. Thank you for your trust in me and for all your help throughout this fantastic PhD journey!

Furthermore, I would like to thank my thesis committee for the evaluation of my work: Prof. Dr. Sven Burgdorf as second examiner, PD Dr. Heike Weighardt and Prof. Dr. Felix Meissner as members of the examination board.

Moreover, I am grateful for all the past and present members of the Kiermaier group. Anni, Mirka and Steffi, you welcomed me warmly and taught me a lot. Shaunak, Henrietta, Tina, Minh and Saumya, who joined during my PhD: Your contributions either by experimental help, discussions or simply by providing social support were essential to the success of the whole project. Many thanks especially to Shaunak and Henrietta, with whom I spent most of the time; your constant support and encouragement have been truly exceptional and deeply appreciated. Together with many students in the lab, we created a great (and sometimes funny) working atmosphere that was very enjoyable. I am in particular thankful that I had the chance to meet and supervise Annika, Lea, Jan and Viktoria, who each helped with parts of the project.

Furthermore, I will never forget the daily lunch breaks together with the group of Prof. Kolanus and other colleagues from LIMES, nor the many enjoyable activities we shared. I highly appreciated your help with reagents, technical support and scientific advice. I would also like to thank non-LIMES groups in Bonn and beyond for their valuable input during different occasions.

Having such great colleagues at work was already wonderful, but I was also very lucky to always have the support and encouragement of my family and my friends. They listened patiently to my scientific talks and showed interest even without being related to the subject, while also helping me find balance outside of science.

Thank you all!